The Influence of Diabatic Heating on the Development of Two North American Jet Superposition Events

Andrew C. Winters

Department of Atmospheric and Oceanic Sciences (ATOC)

University of Colorado Boulder

2019 AGU Fall Meeting

San Francisco, CA

10 December 2019

This work was funded by an NSF-PRF (AGS-1624316)

Jet Superposition Conceptual Model

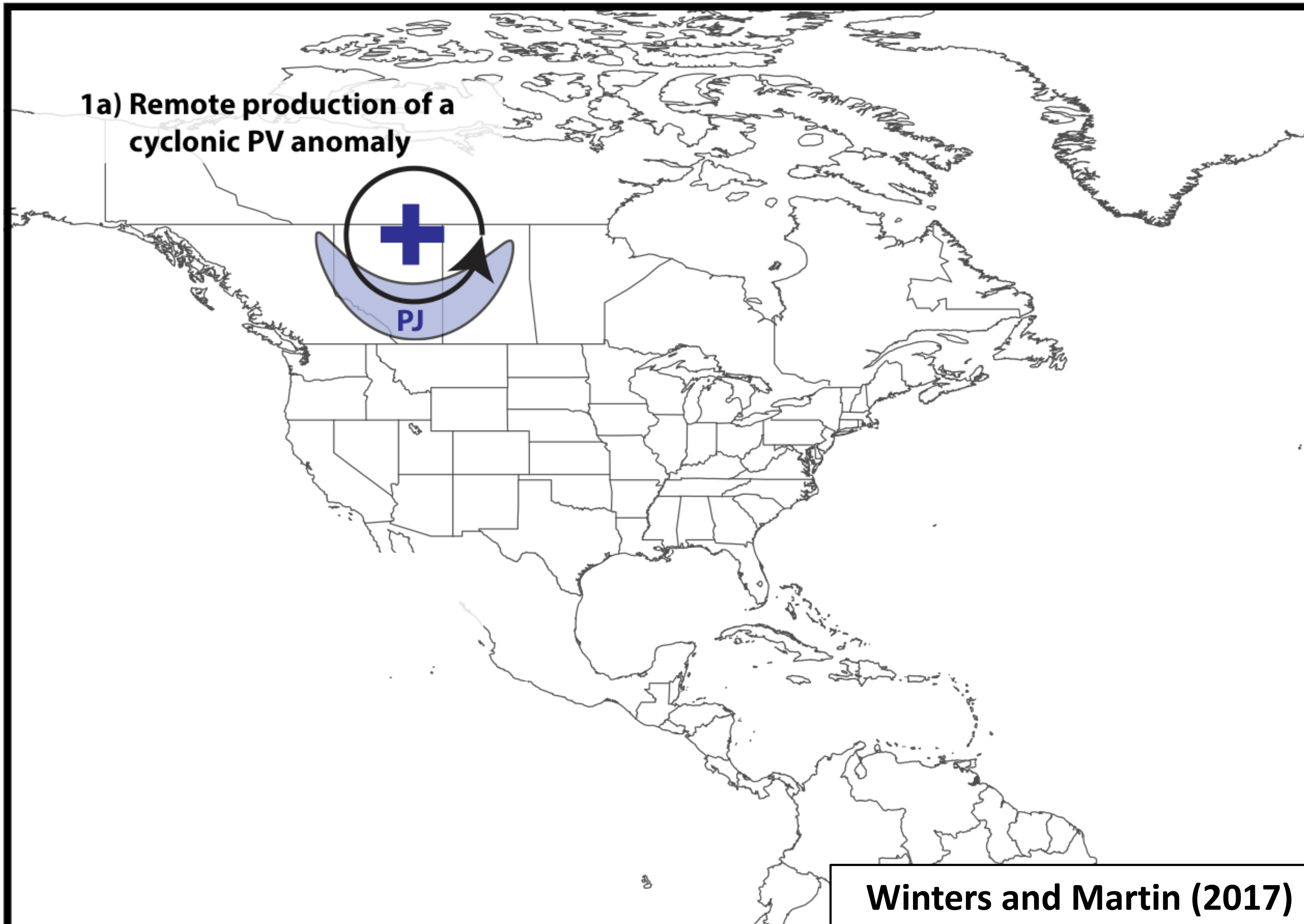

Jet Superposition Conceptual Model

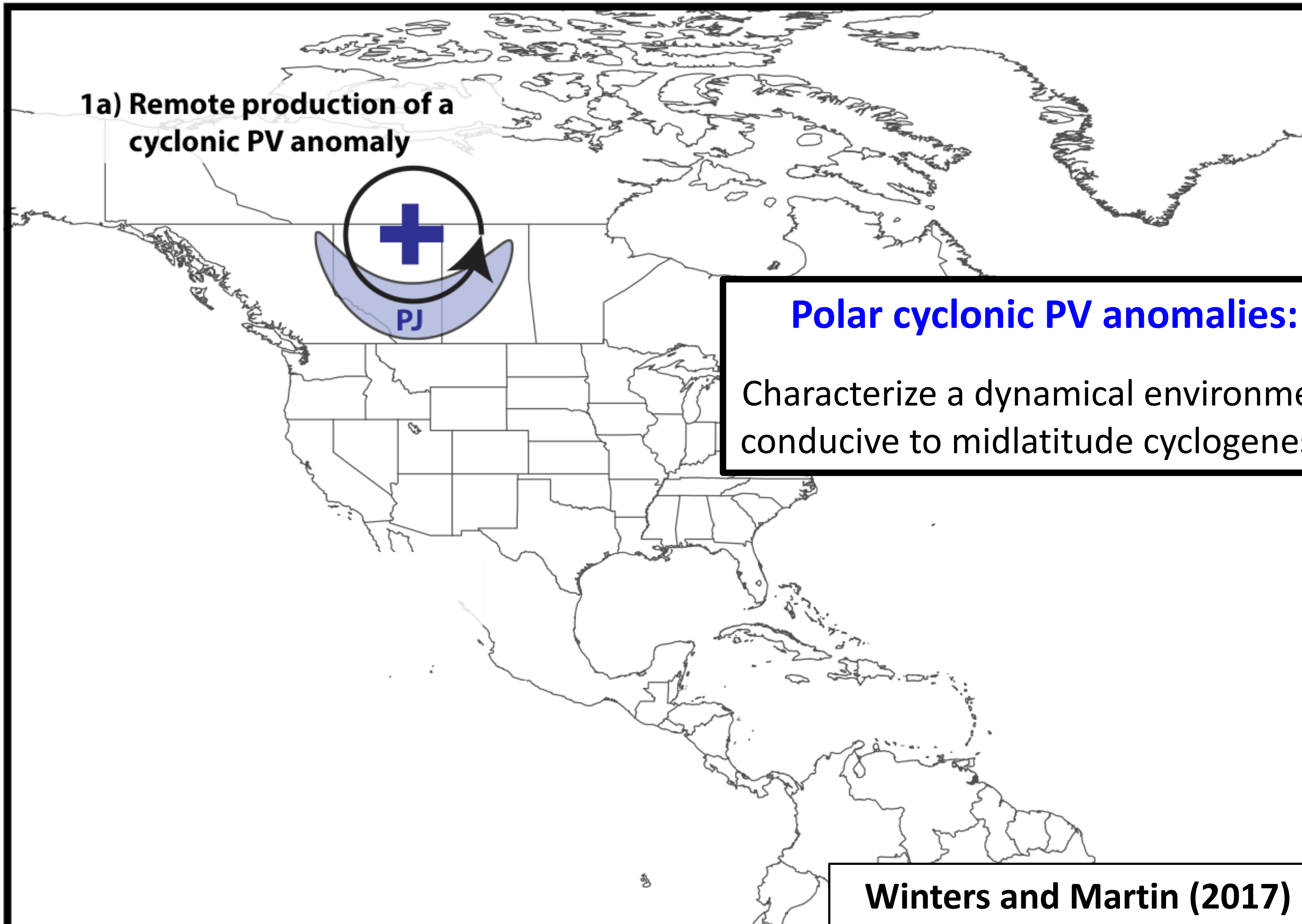

Polar cyclonic PV anomalies:

Characterize a dynamical environment conducive to midlatitude cyclogenesis.

Winters and Martin (2017)

Jet Superposition Conceptual Model

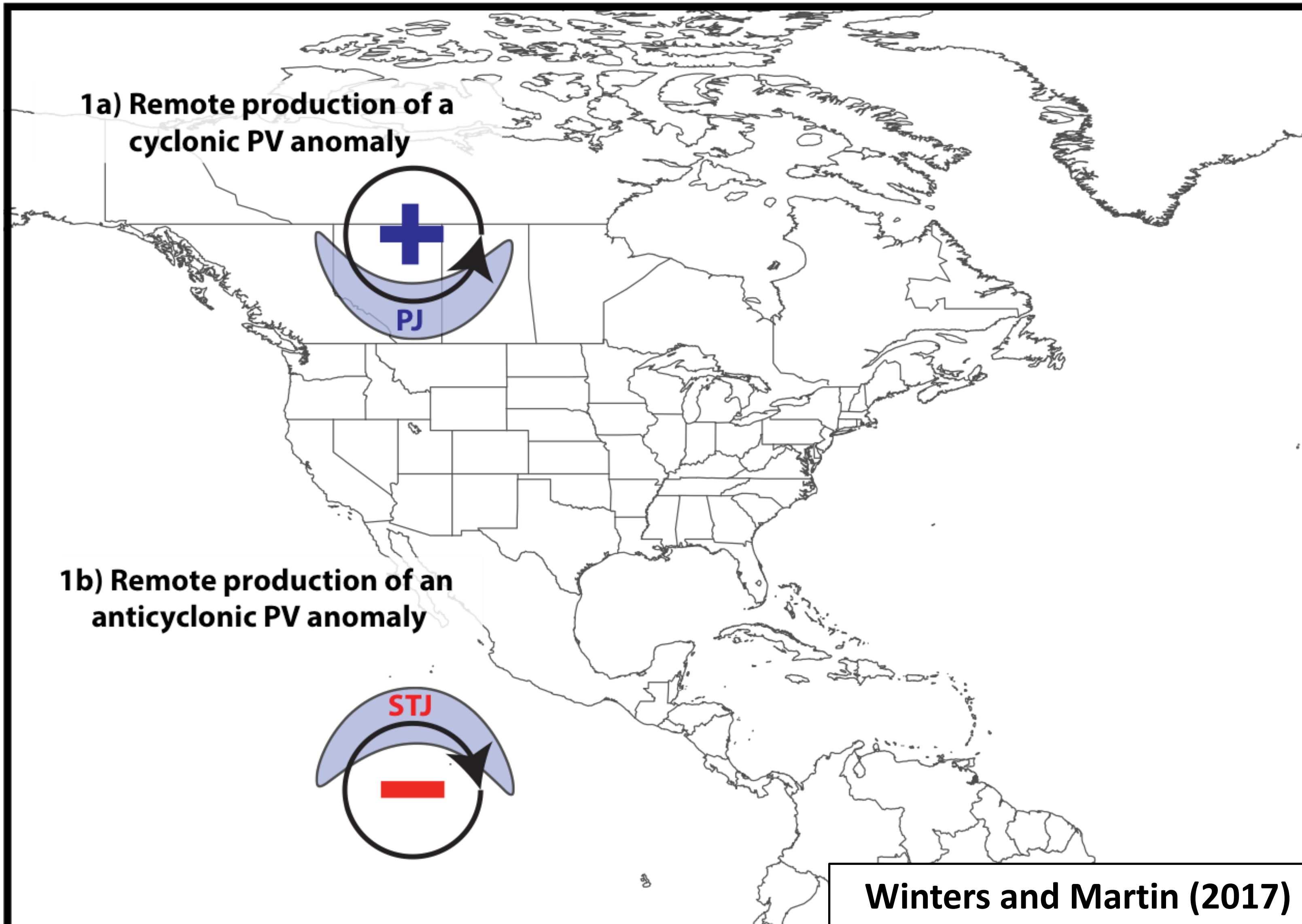

Jet Superposition Conceptual Model

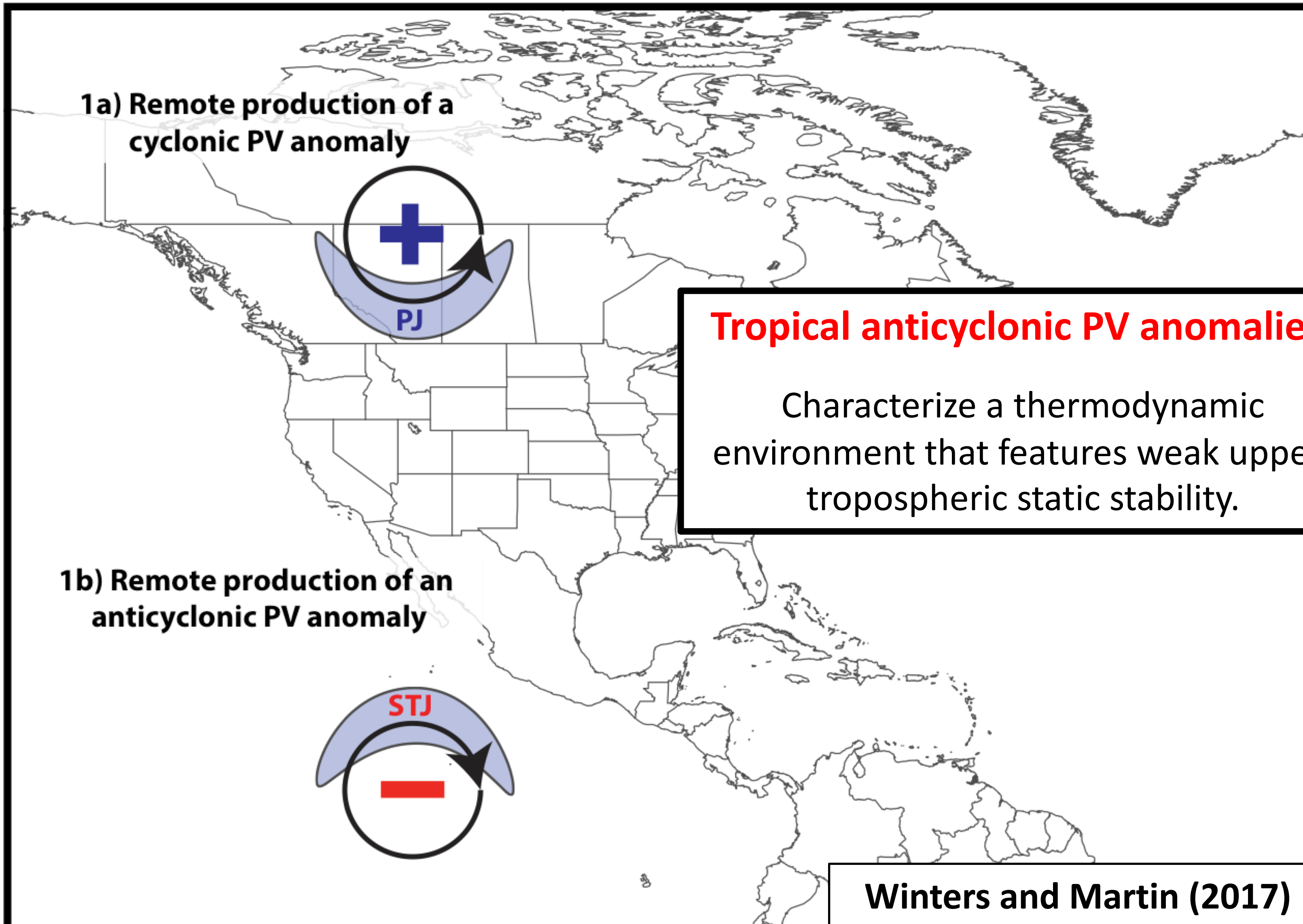

Tropical anticyclonic PV anomalies:

Characterize a thermodynamic environment that features weak upper-tropospheric static stability.

Winters and Martin (2017)

Jet Superposition Conceptual Model

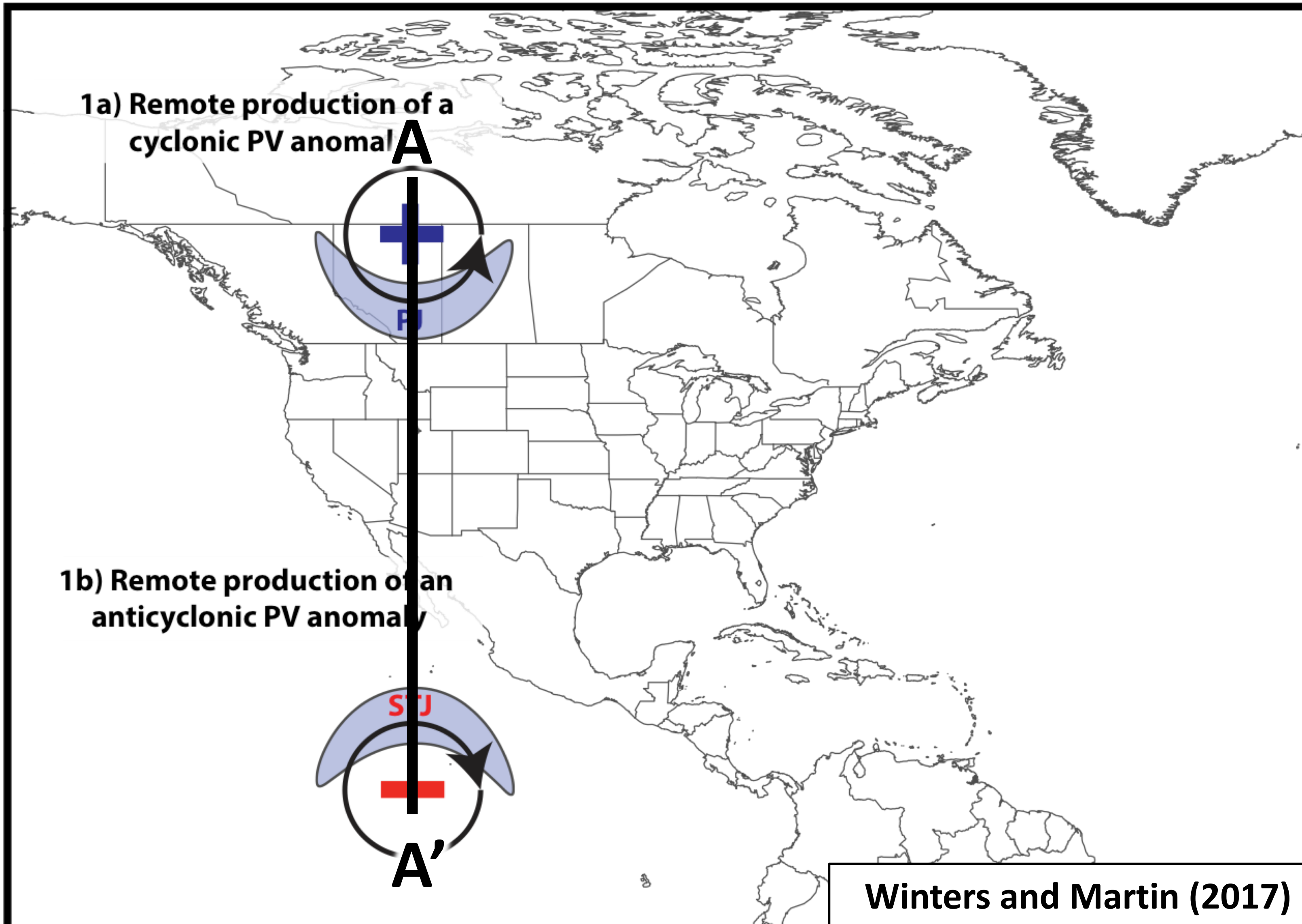

Jet Superposition Conceptual Model

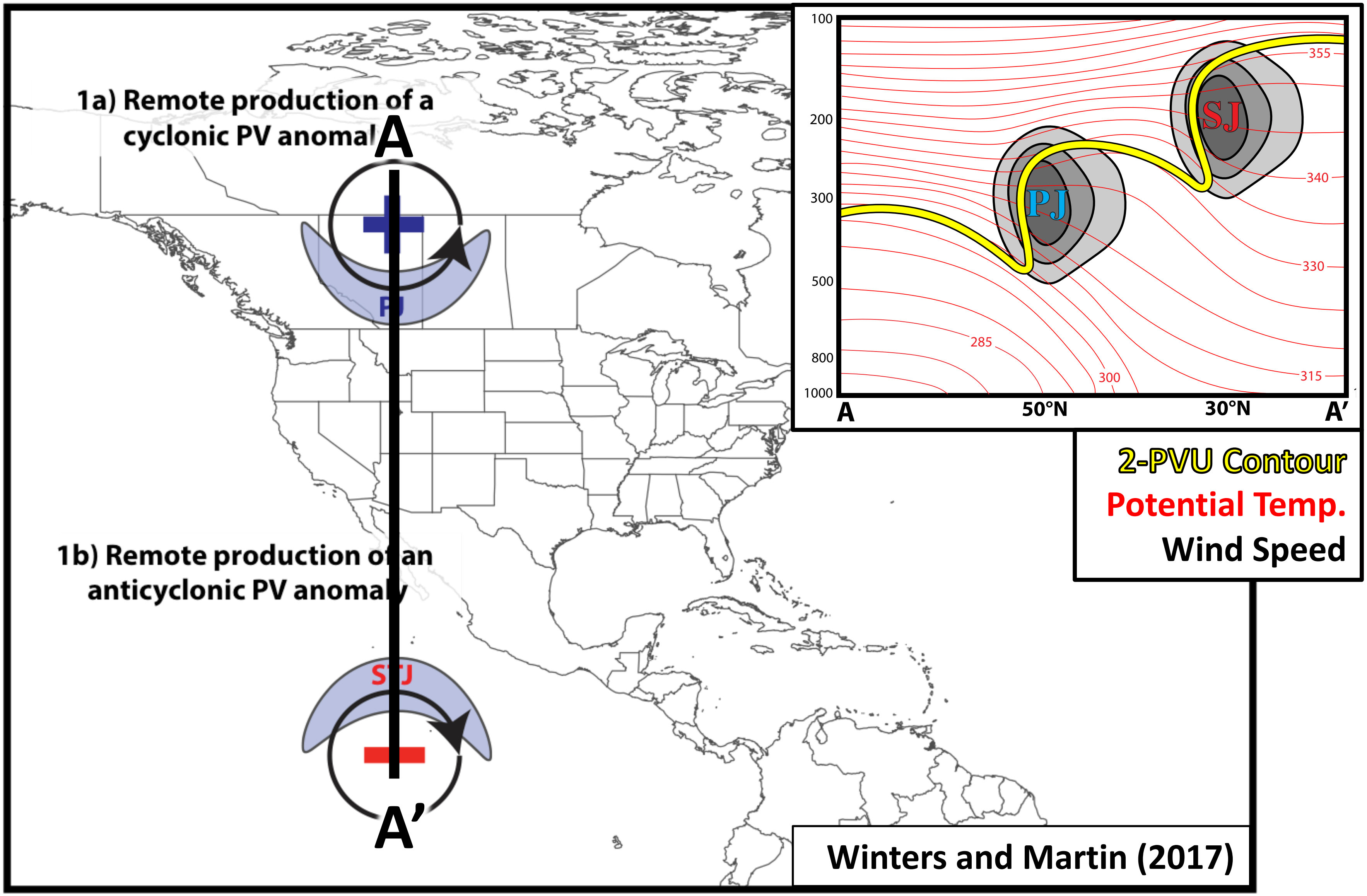

Jet Superposition Conceptual Model

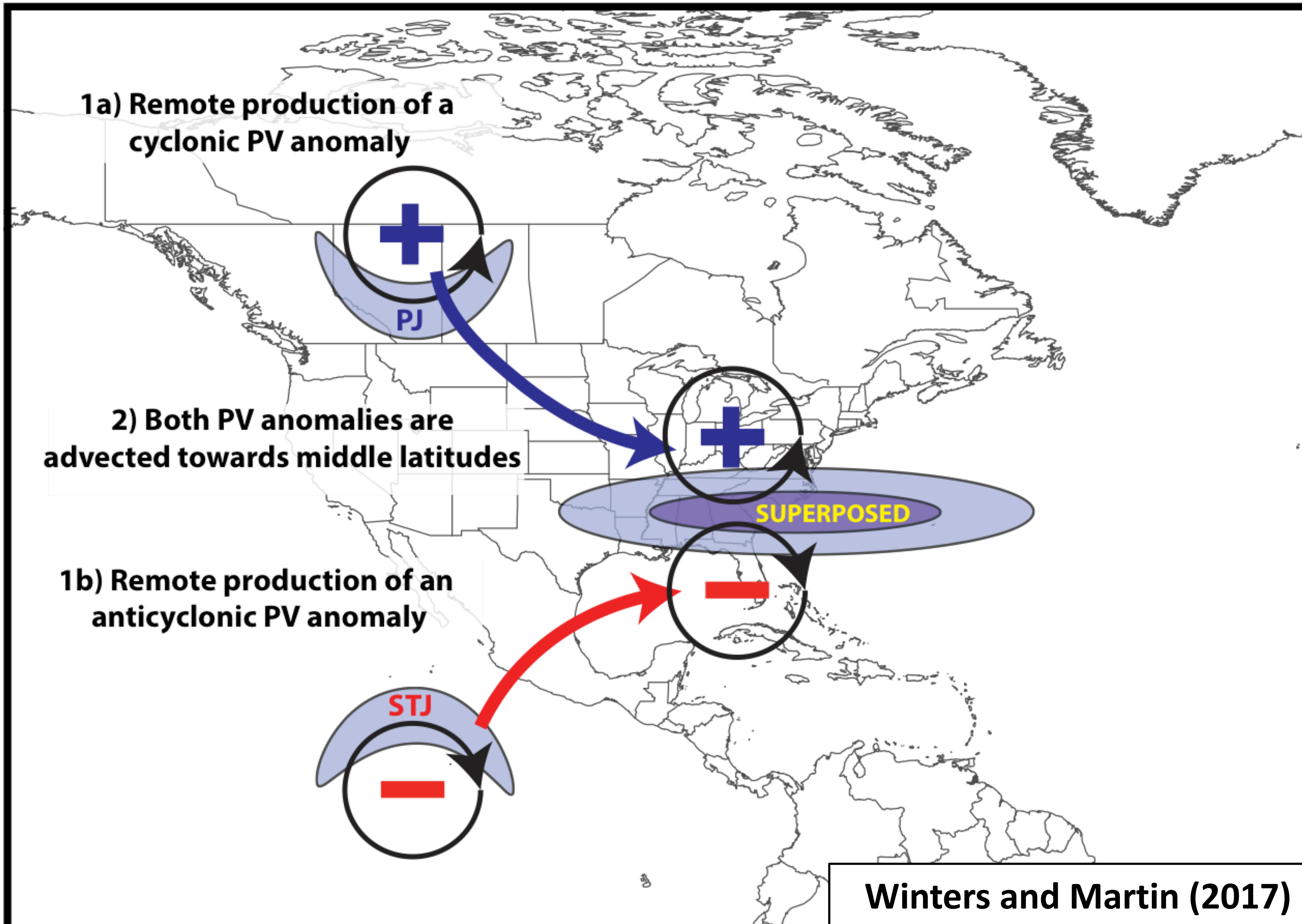

Jet Superposition Conceptual Model

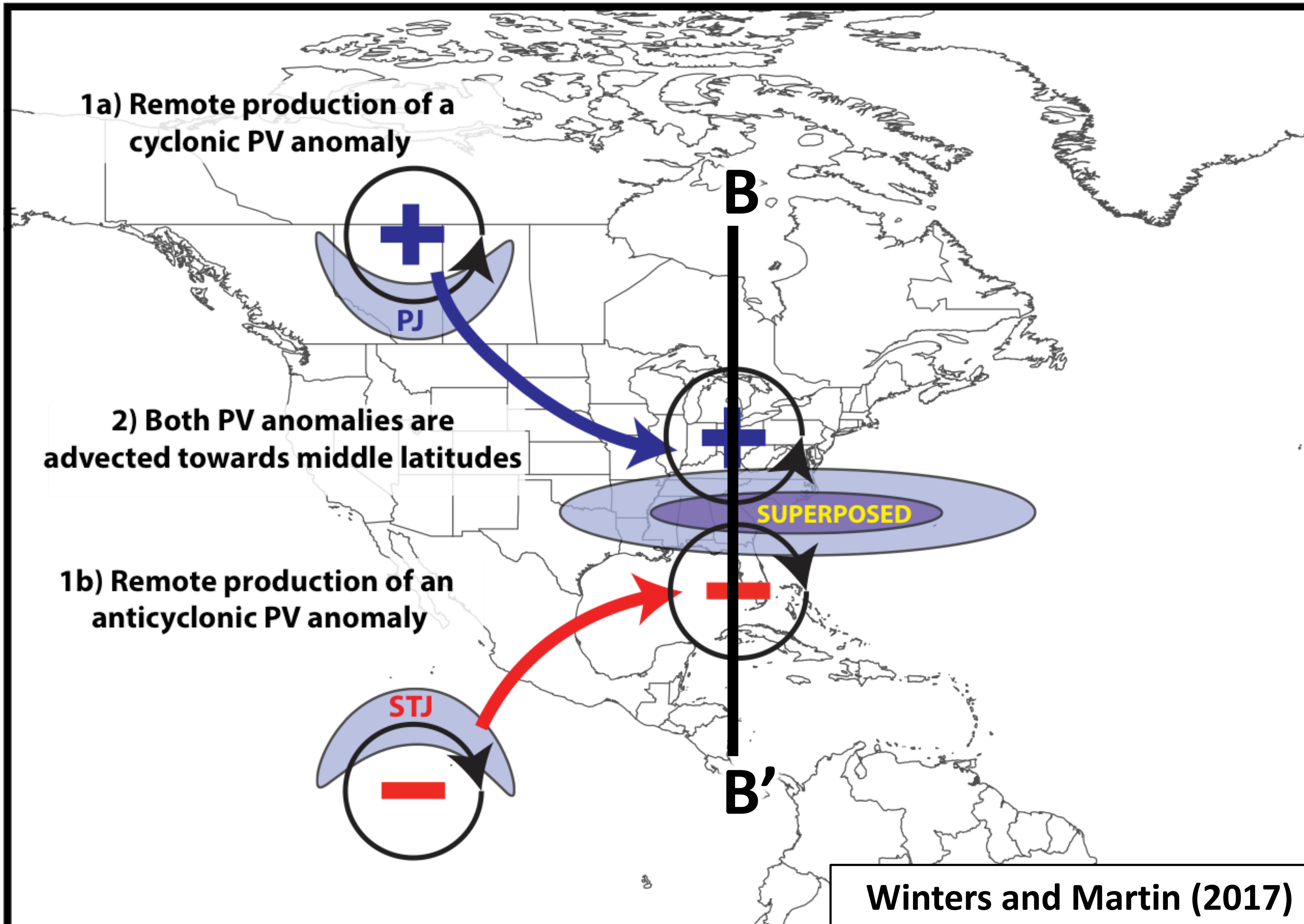

Jet Superposition Conceptual Model

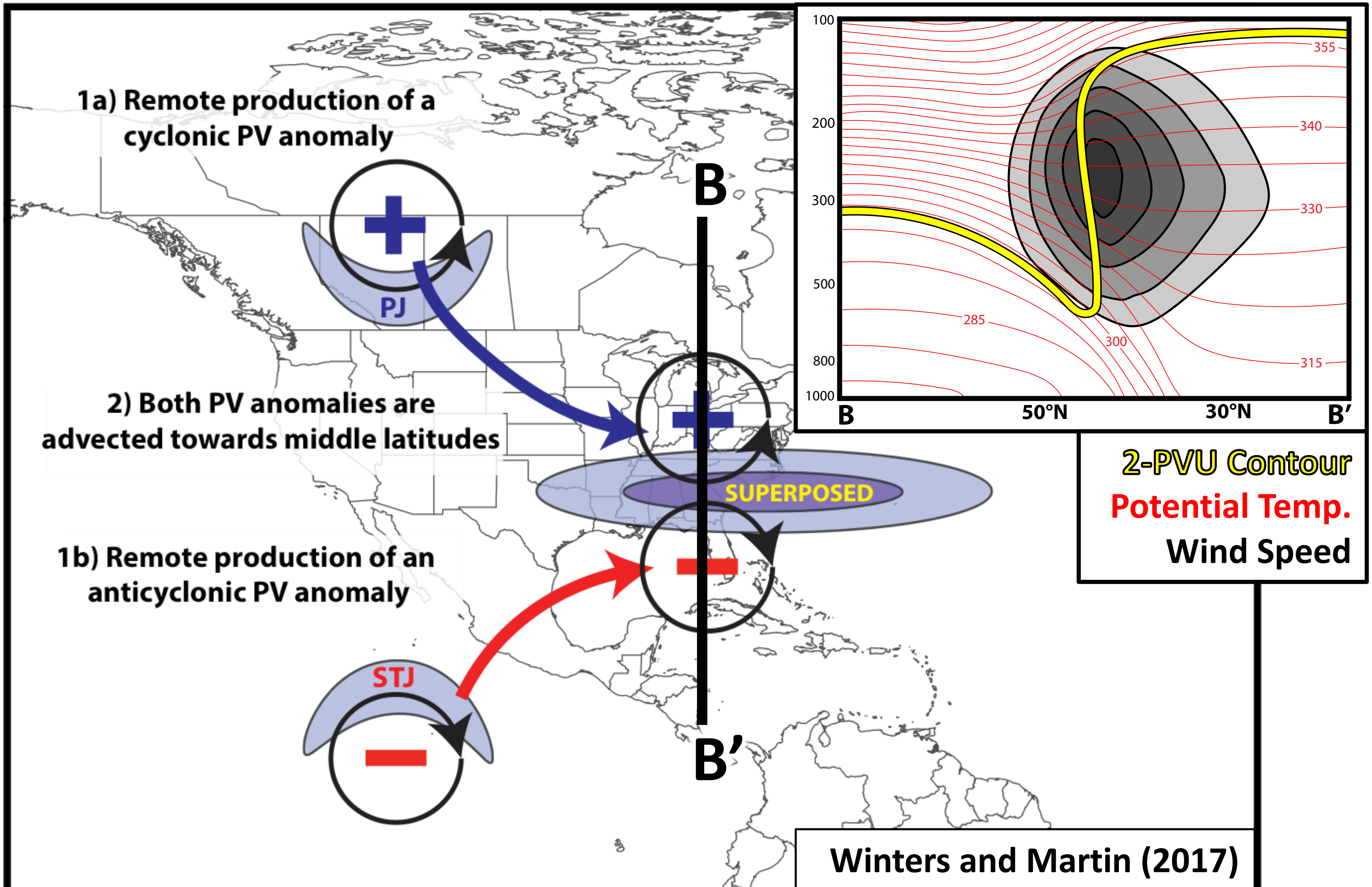

Jet Superposition Conceptual Model

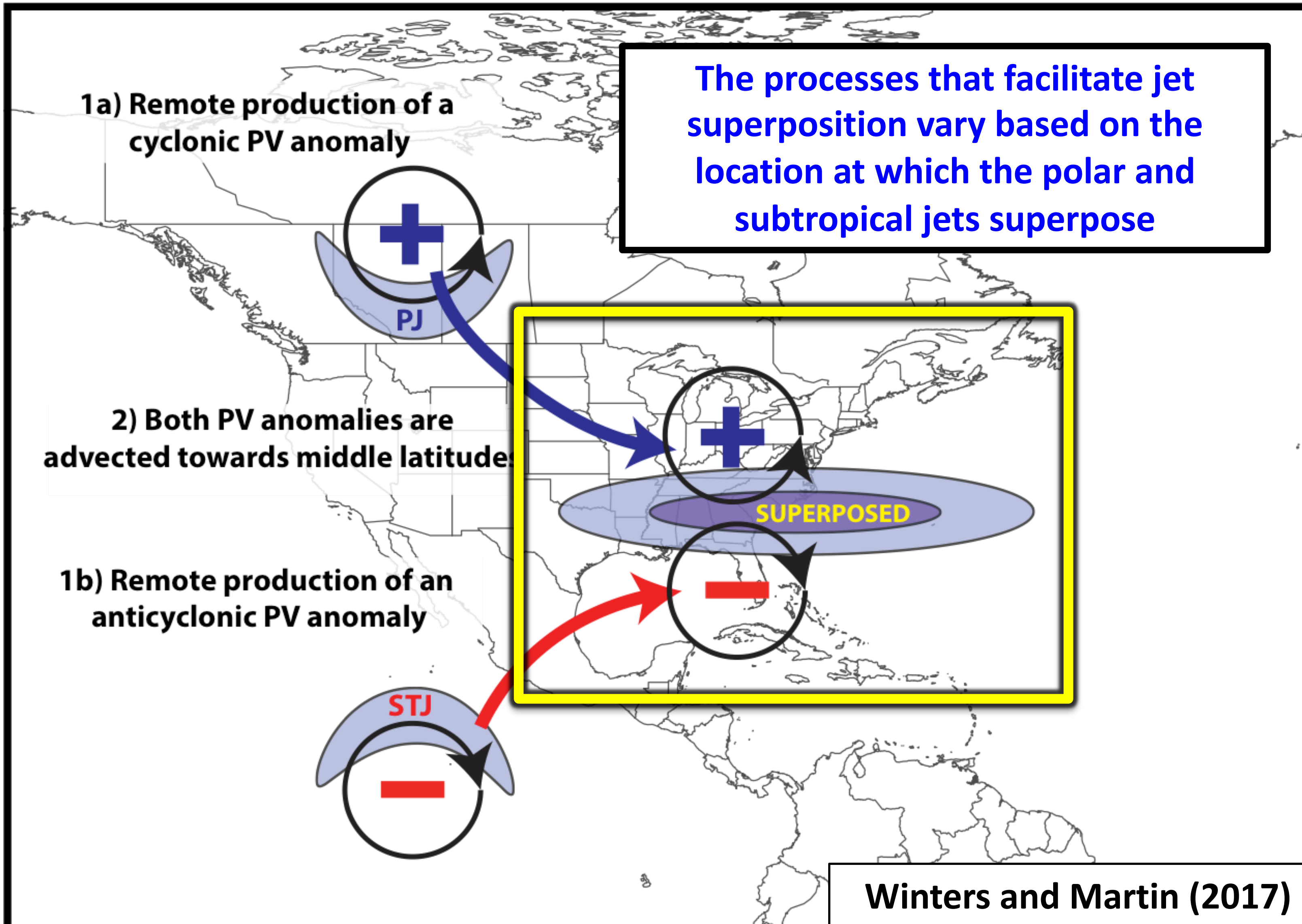

Jet Superposition Conceptual Model

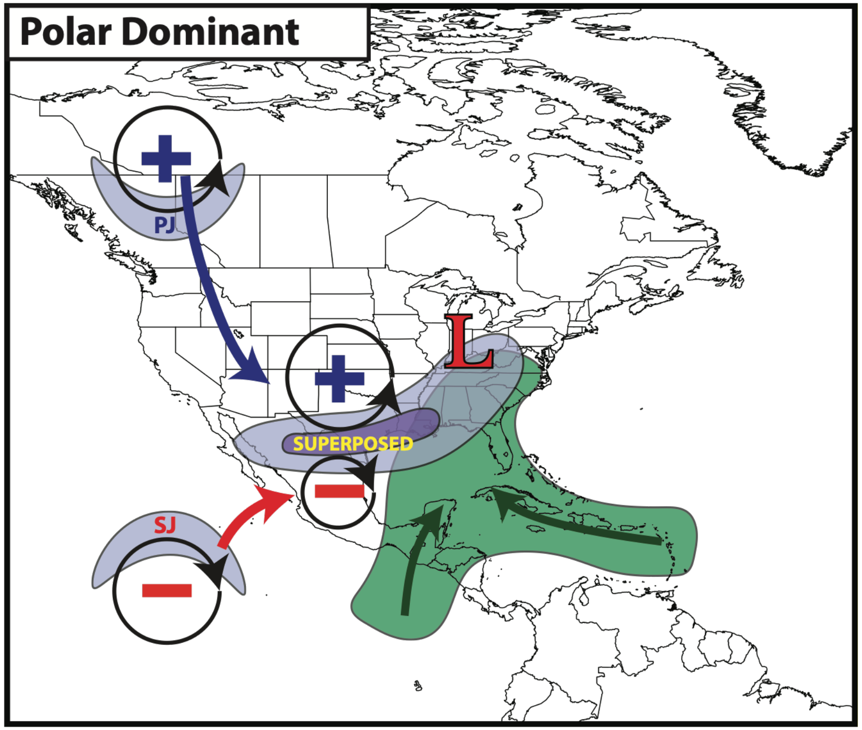

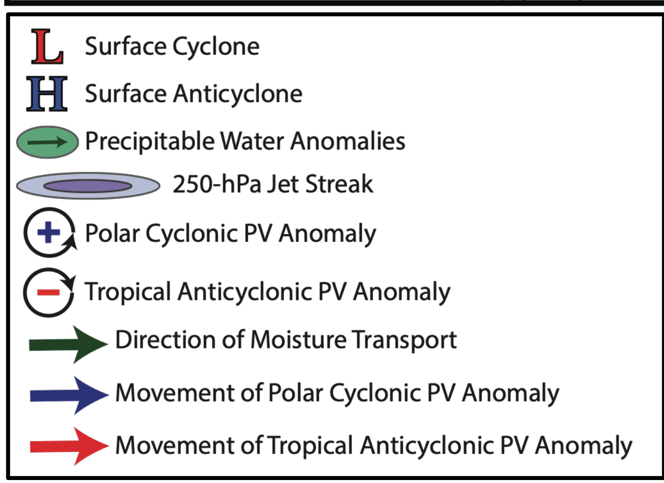

During polar dominant events, diabatic processes do not directly contribute to the formation of a steep, tropopause wall

Winters et al., *in revision*

Jet Superposition Conceptual Model

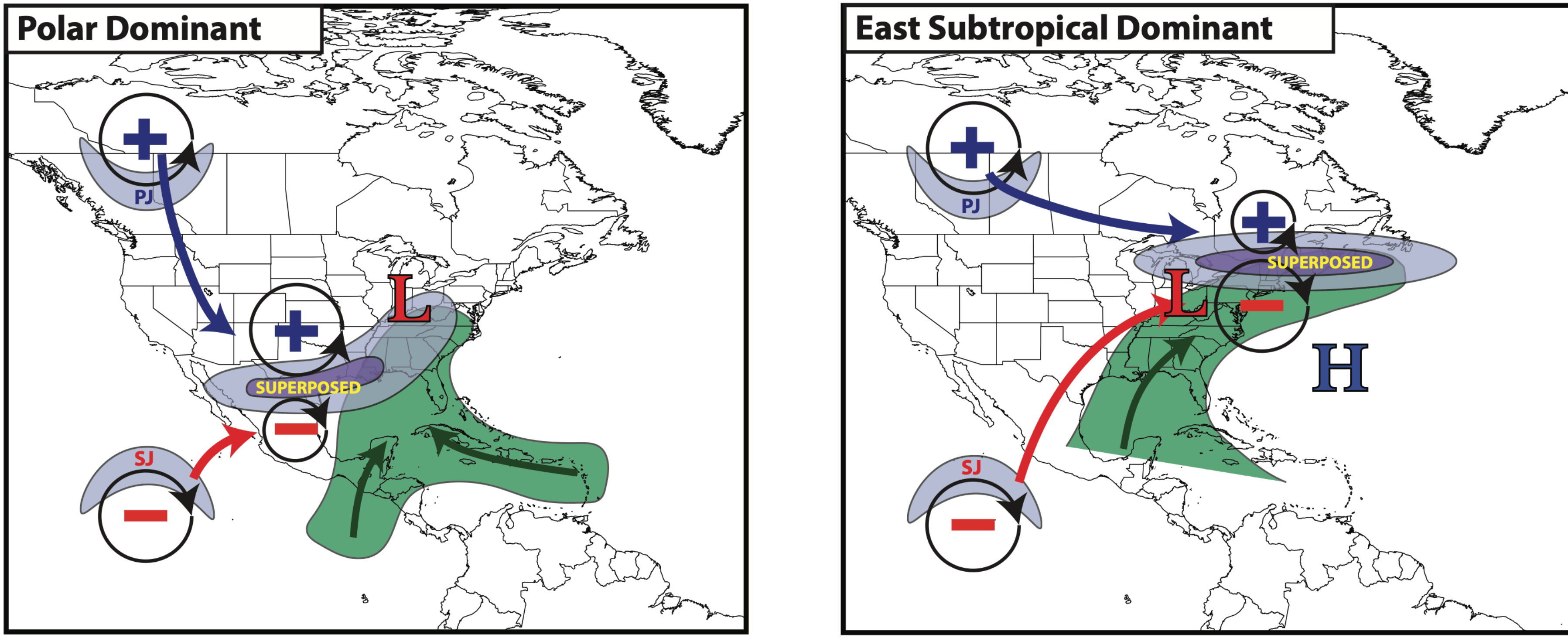

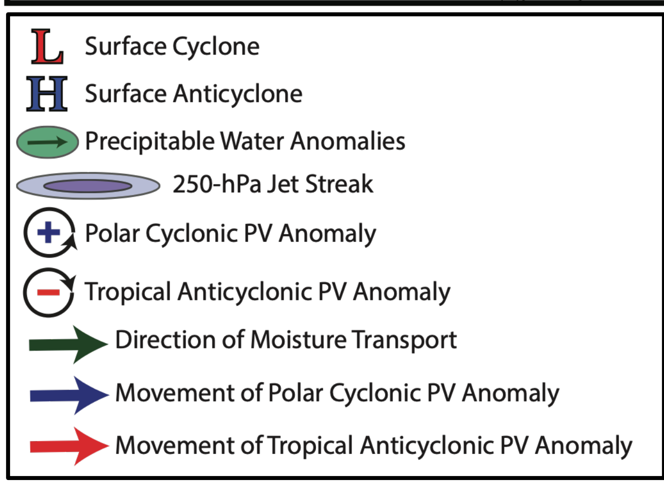

During subtropical dominant events, diabatic processes directly contribute to the formation of a steep, tropopause wall

Winters et al., *in revision*

Jet Superposition Conceptual Model

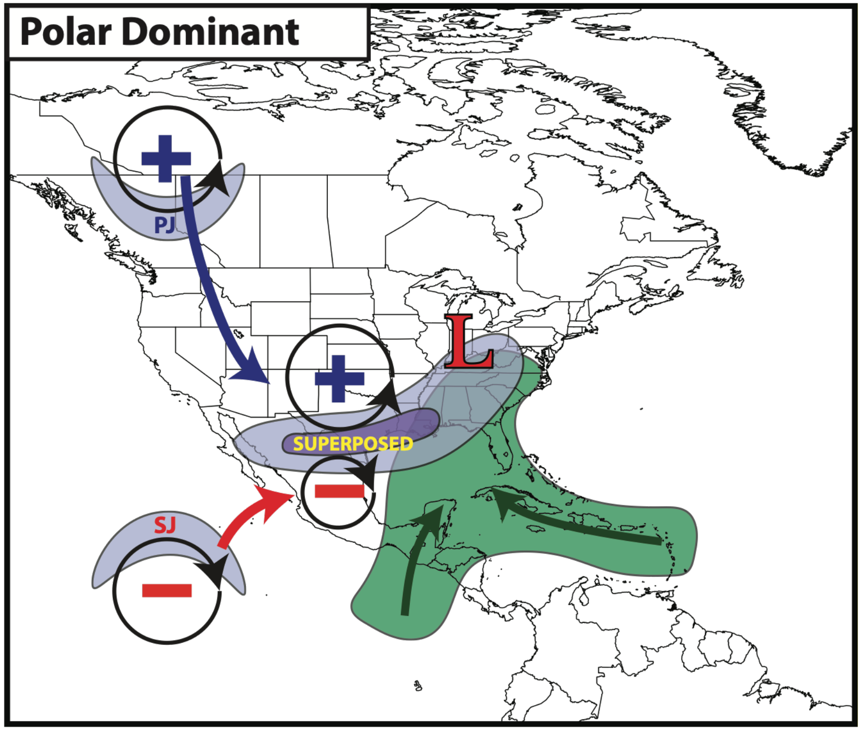

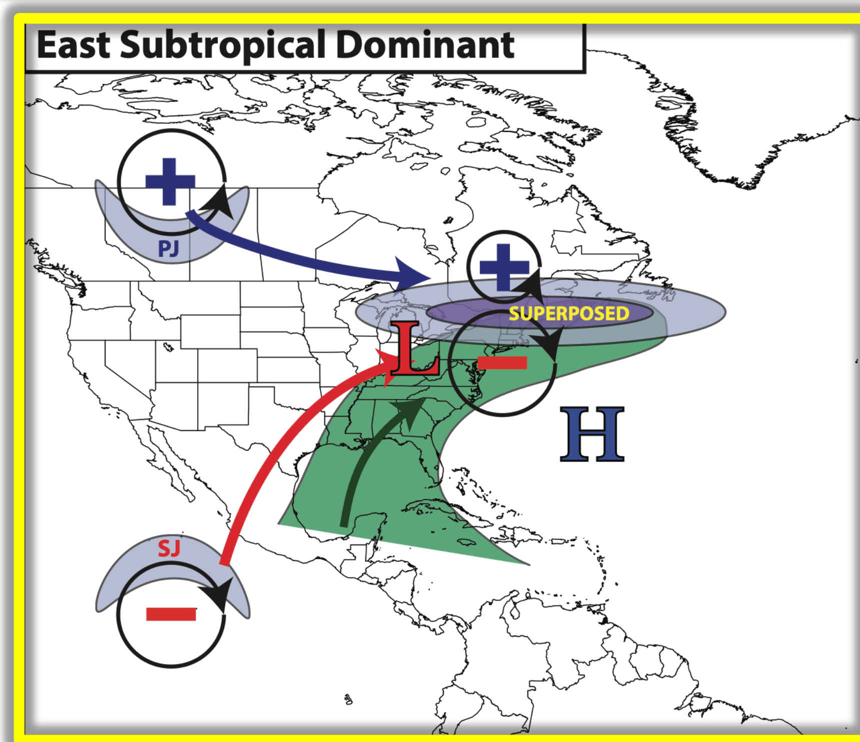

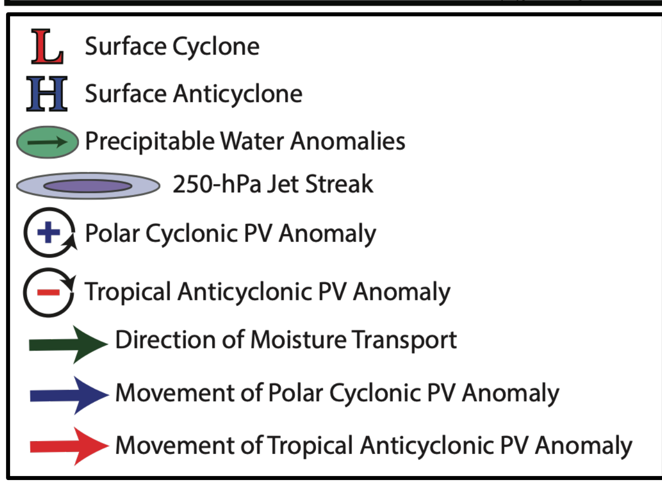

If latent heating is omitted during subtropical dominant events, do the polar and subtropical jets still superpose?

Recent Subtropical Dominant Jet Superposition Events

Recent Subtropical Dominant Superpositions

1200 UTC 22 December 2013

CFSR Analysis (Saha et al. 2014)

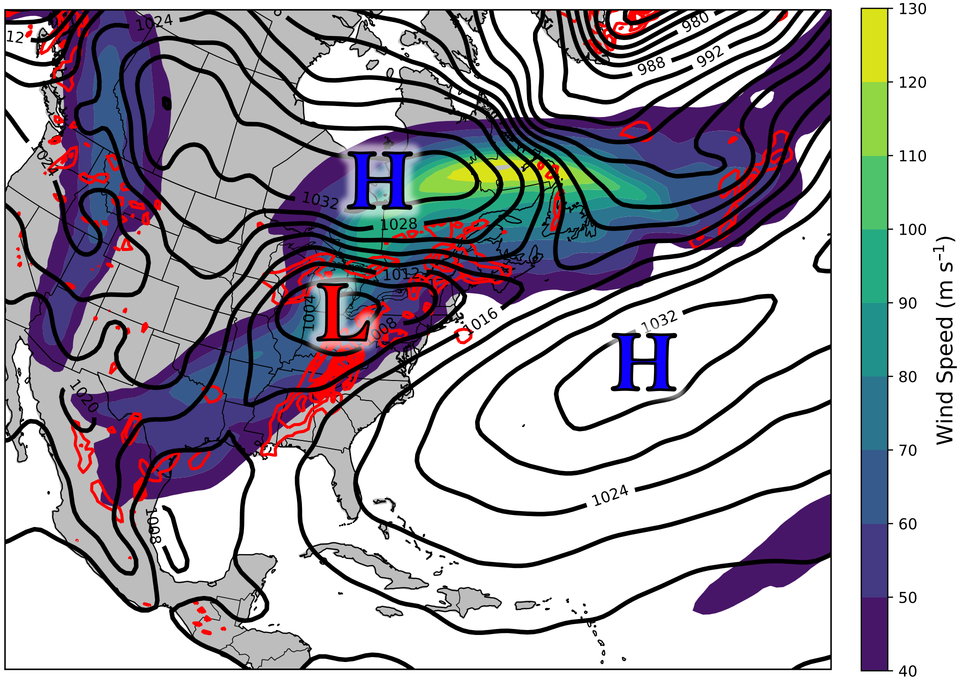

Mean Sea Level Pressure

500-hPa Ascent (Pa s^{-1})

The December 2013 case featured:

- A tornado outbreak in the southeastern U.S.
- Up to 1 in. of total ice accumulation near Toronto, ON
- Maximum jet wind speeds in excess of 110 m s^{-1}

Recent Subtropical Dominant Superpositions

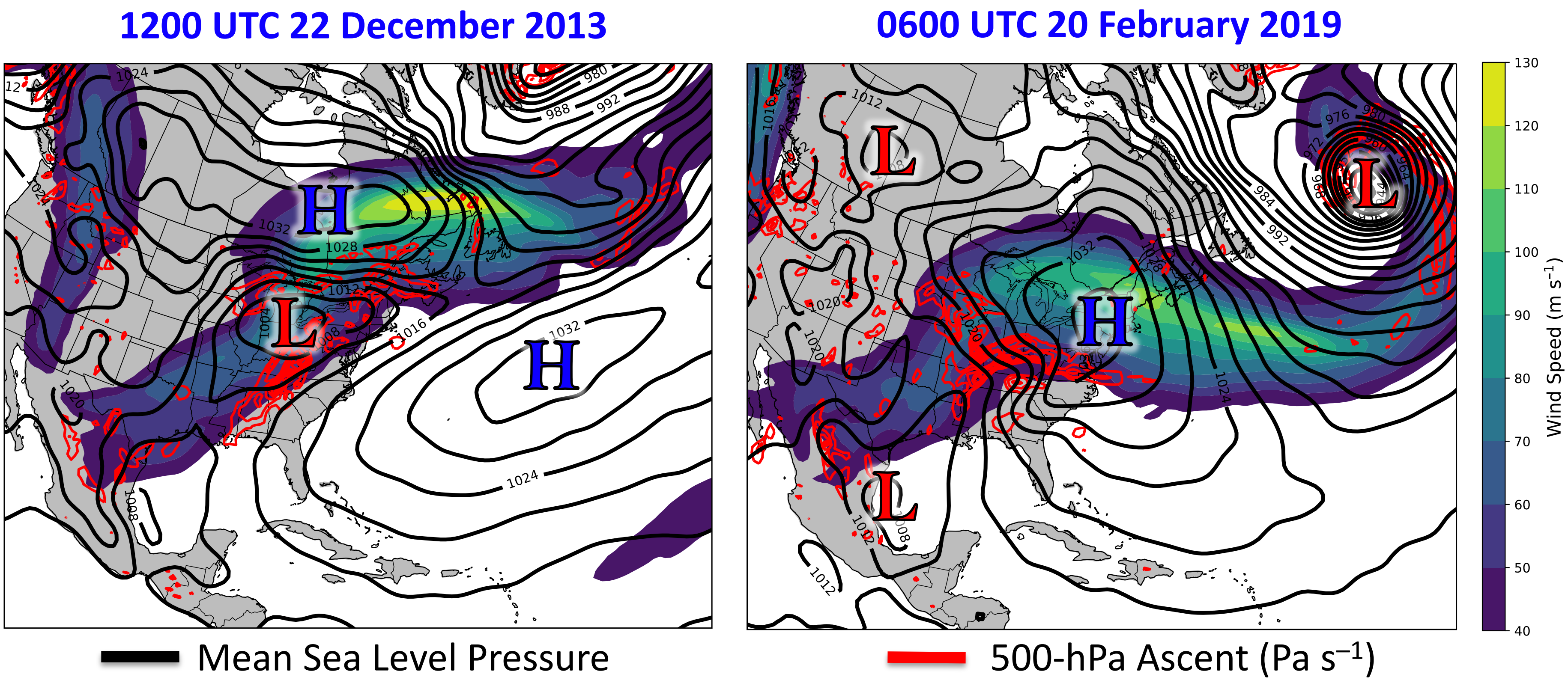

The February 2019 case featured:

- Up to 1 foot of snow accumulation in the northern Plains
- An Atlantic cyclone with a central pressure below 944 hPa
- Maximum jet wind speeds in excess of 110 m s^{-1}

Recent Subtropical Dominant Superpositions

1200 UTC 22 December 2013

0600 UTC 20 February 2019

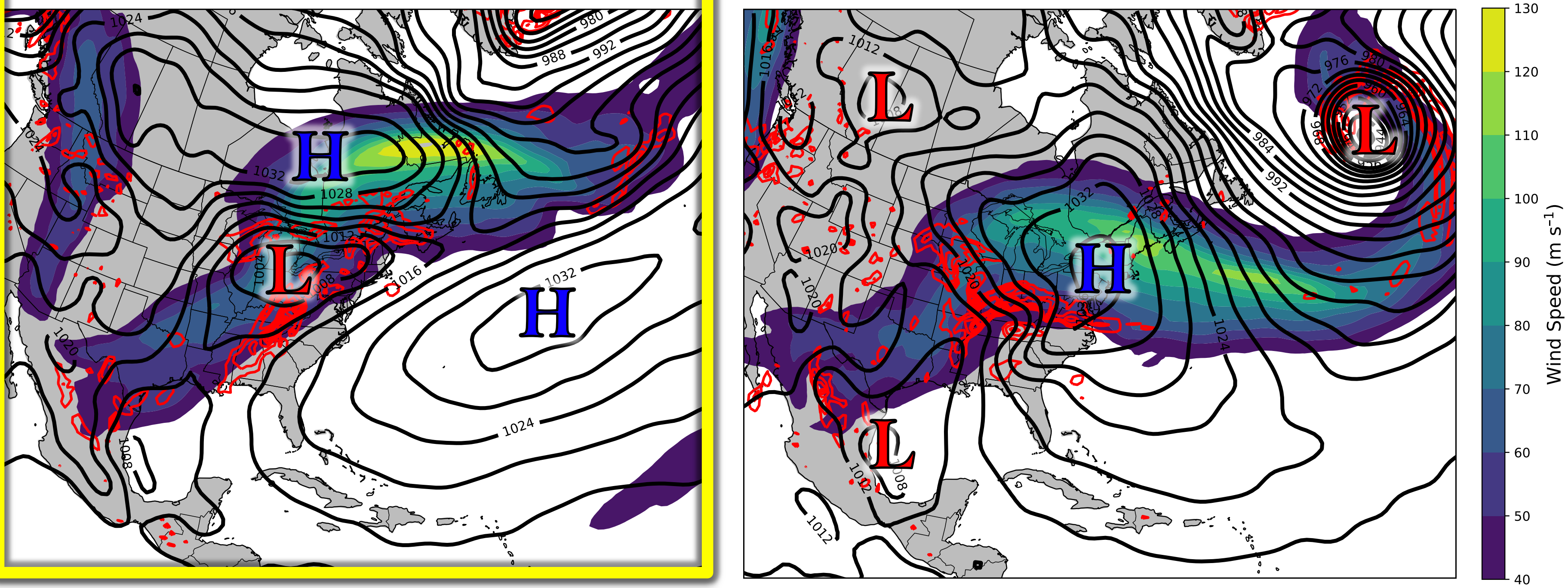

Mean Sea Level Pressure

500-hPa Ascent (Pa s^{-1})

WRF Simulations:
December 2013 Case

WRF Simulations

- 2 single-domain simulations (“FULL”, “NOLH”)
- WRF Version 3.9.1 (Skamarock et al. 2008)
- 6-day run time initialized at 0000 UTC 19 December 2013
- 90-second timestep
- 30-km horizontal resolution + 50 vertical levels (model top=50 hPa)
- Initial and boundary conditions provided by the GFS Analysis
- Thompson microphysics
- Kain-Fritsch cumulus parameterization
- MYJ PBL scheme
- RRTMG radiation scheme
- Noah land-surface model
- **No latent heating from microphysics in “NOLH” simulation**

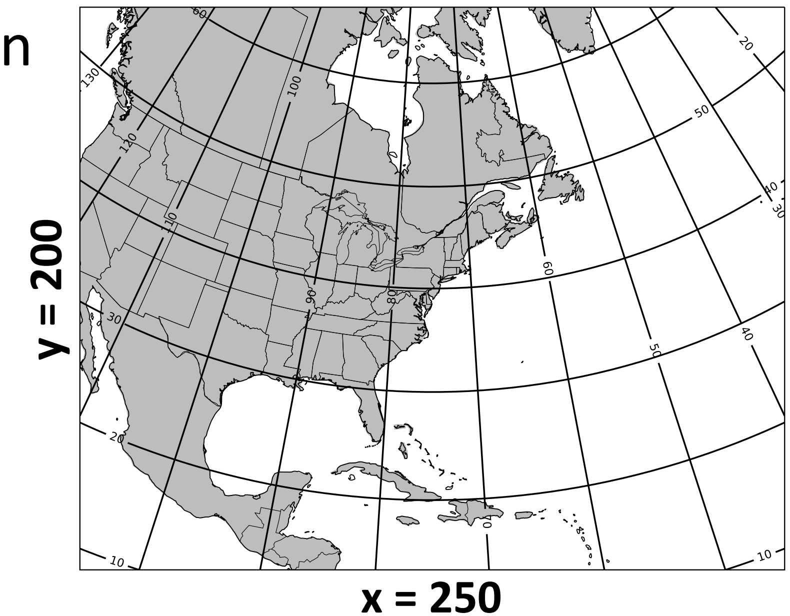

WRF Simulations

1200 UTC 22 December 2013

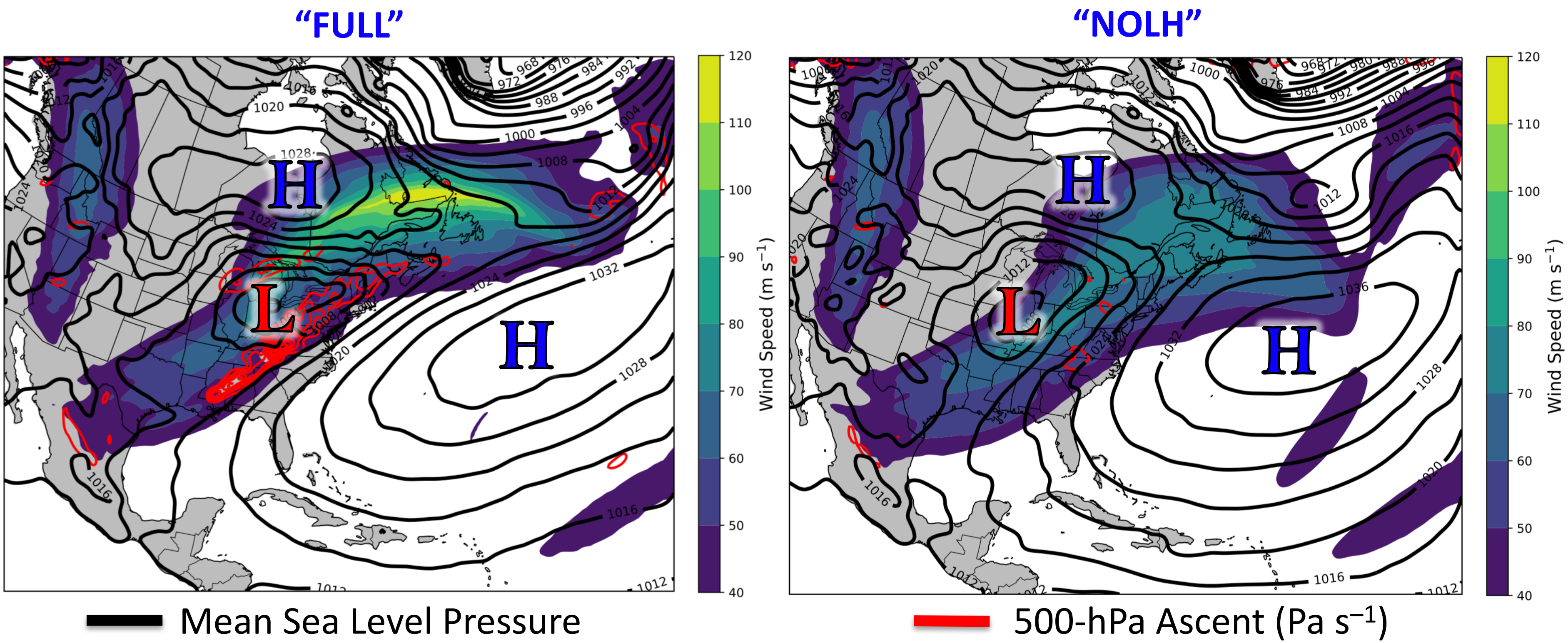

- Maximum 250-hPa wind speed is ~40 m s^{-1} weaker in "NOLH"
- Surface cyclone over the southern Great Lakes is weaker and located farther west in "NOLH"

WRF Simulations

1200 UTC 22 December 2013

"FULL" – "NOLH": 850-hPa Pot. Temp.

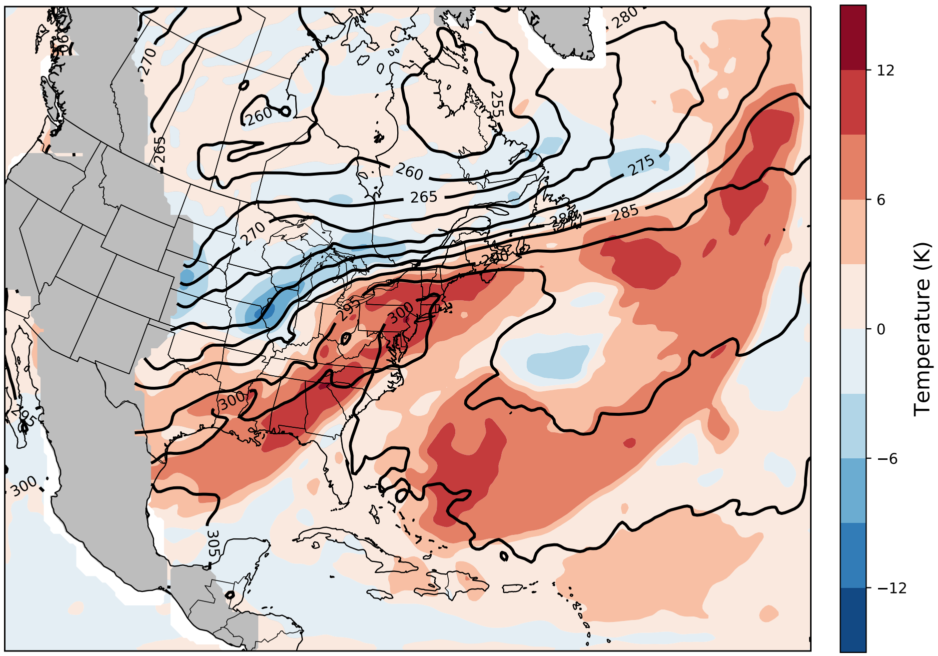

850-hPa "FULL" Pot. Temp. (K)

- The "FULL" simulation features a stronger lower-tropospheric temperature gradient than the "NOLH" simulation

WRF Simulations

1200 UTC 22 December 2013

"FULL" – "NOLH": 850-hPa Pot. Temp.

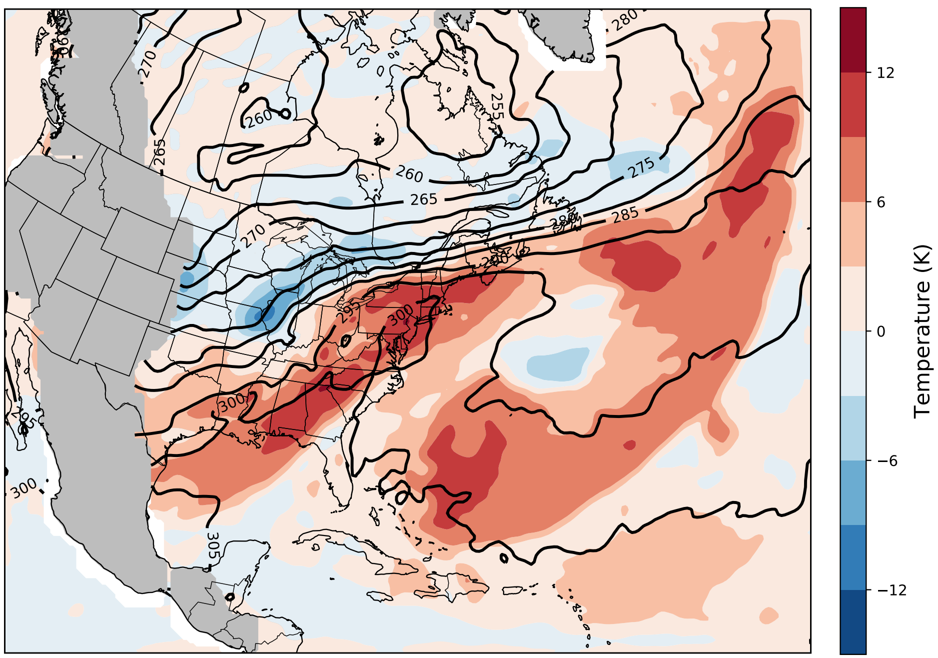

850-hPa "FULL" Pot. Temp. (K)

"FULL" – "NOLH": 250-hPa Height

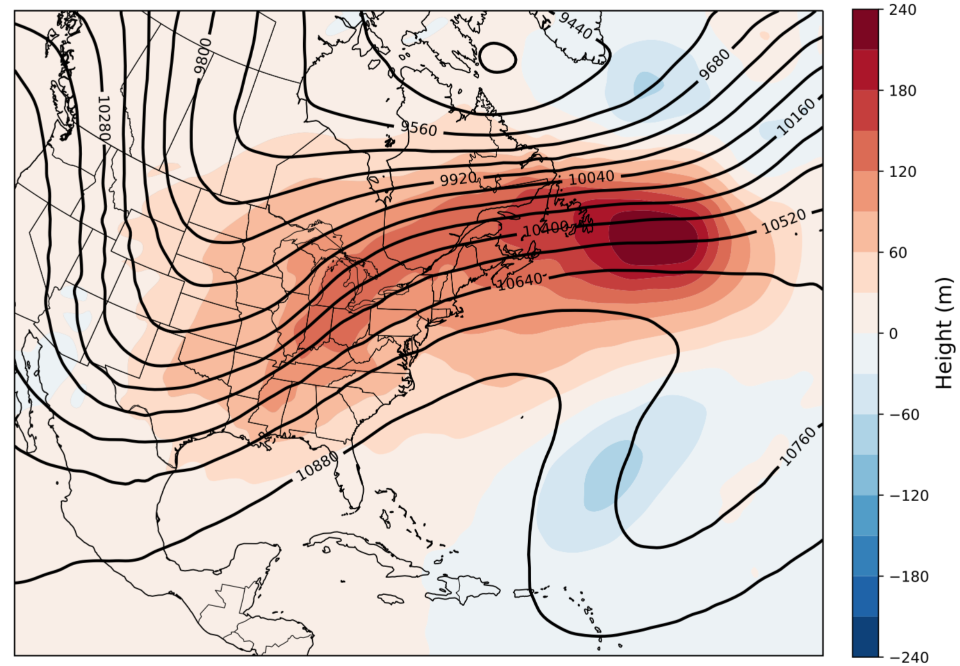

250-hPa "FULL" Height

- The "FULL" simulation features a stronger lower-tropospheric temperature gradient than the "NOLH" simulation
- The "FULL" simulation features larger geopotential heights and stronger flow curvature within the eastern North American ridge

WRF Simulations

1200 UTC 22 December 2013

“FULL” “NOLH”

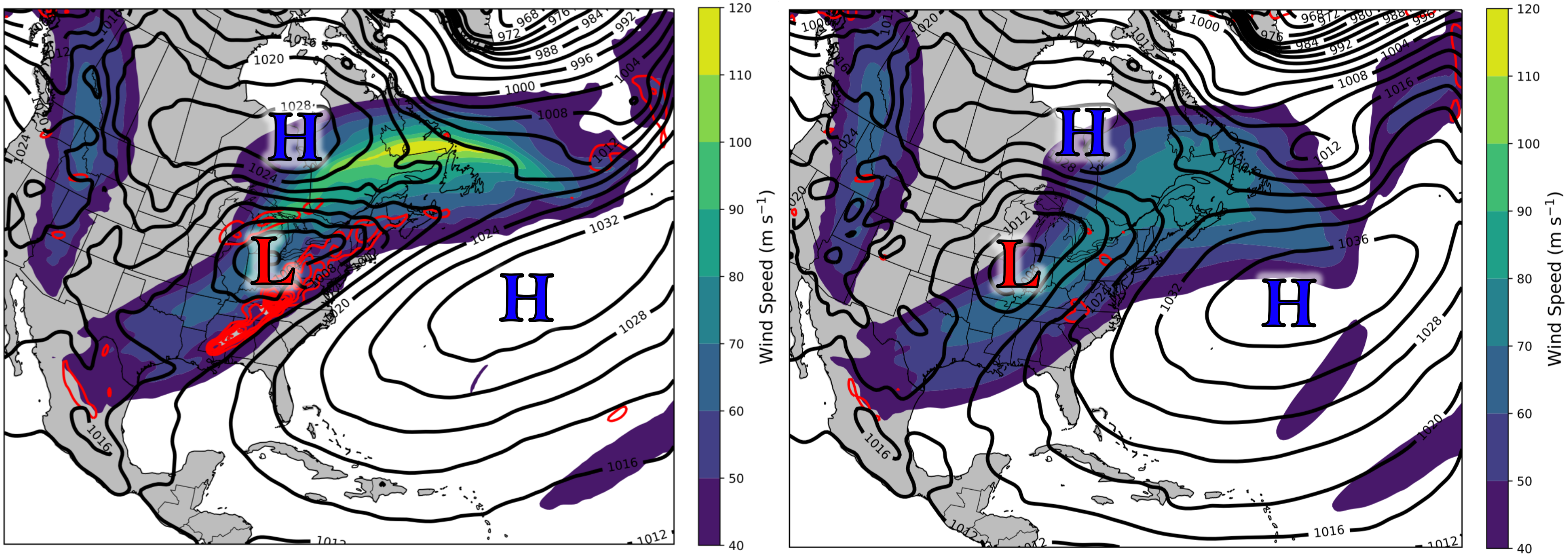

Mean Sea Level Pressure 500-hPa Ascent (Pa s^{-1})

- In the absence of latent heating, do the polar and subtropical jets become superposed?

WRF Simulations

1200 UTC 22 December 2013

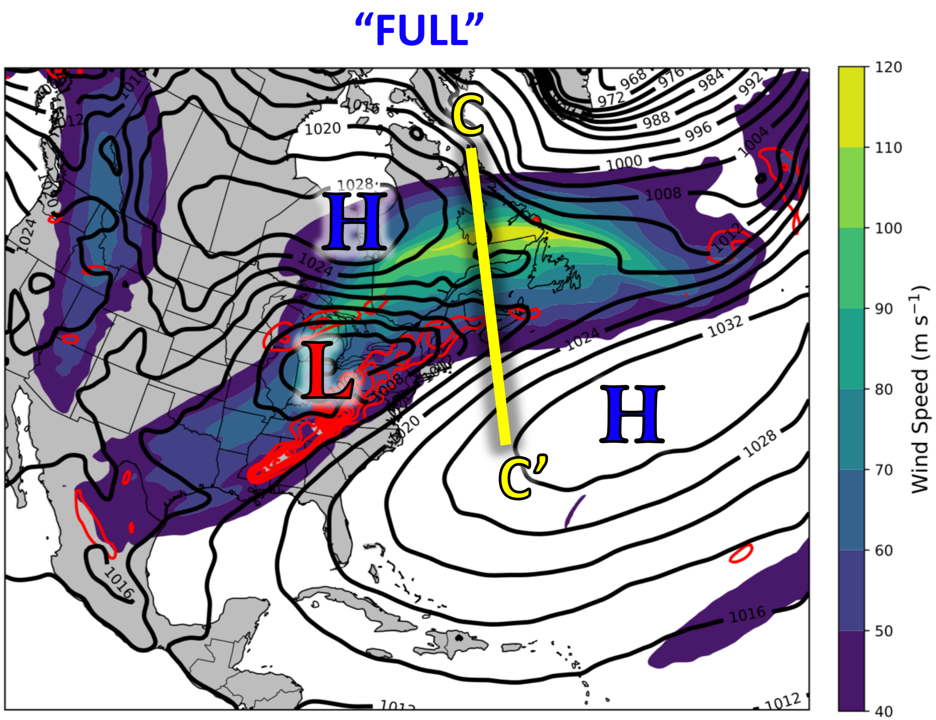

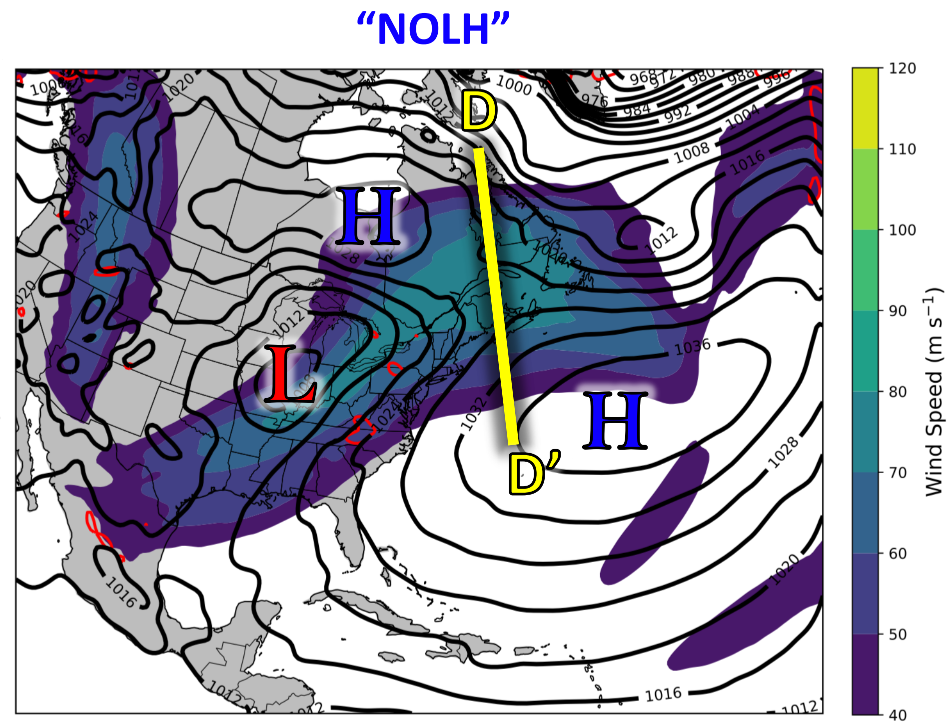

Mean Sea Level Pressure

500-hPa Ascent (Pa s^{-1})

- In the absence of latent heating, do the polar and subtropical jets become superposed?

WRF Simulations

1200 UTC 22 December 2013

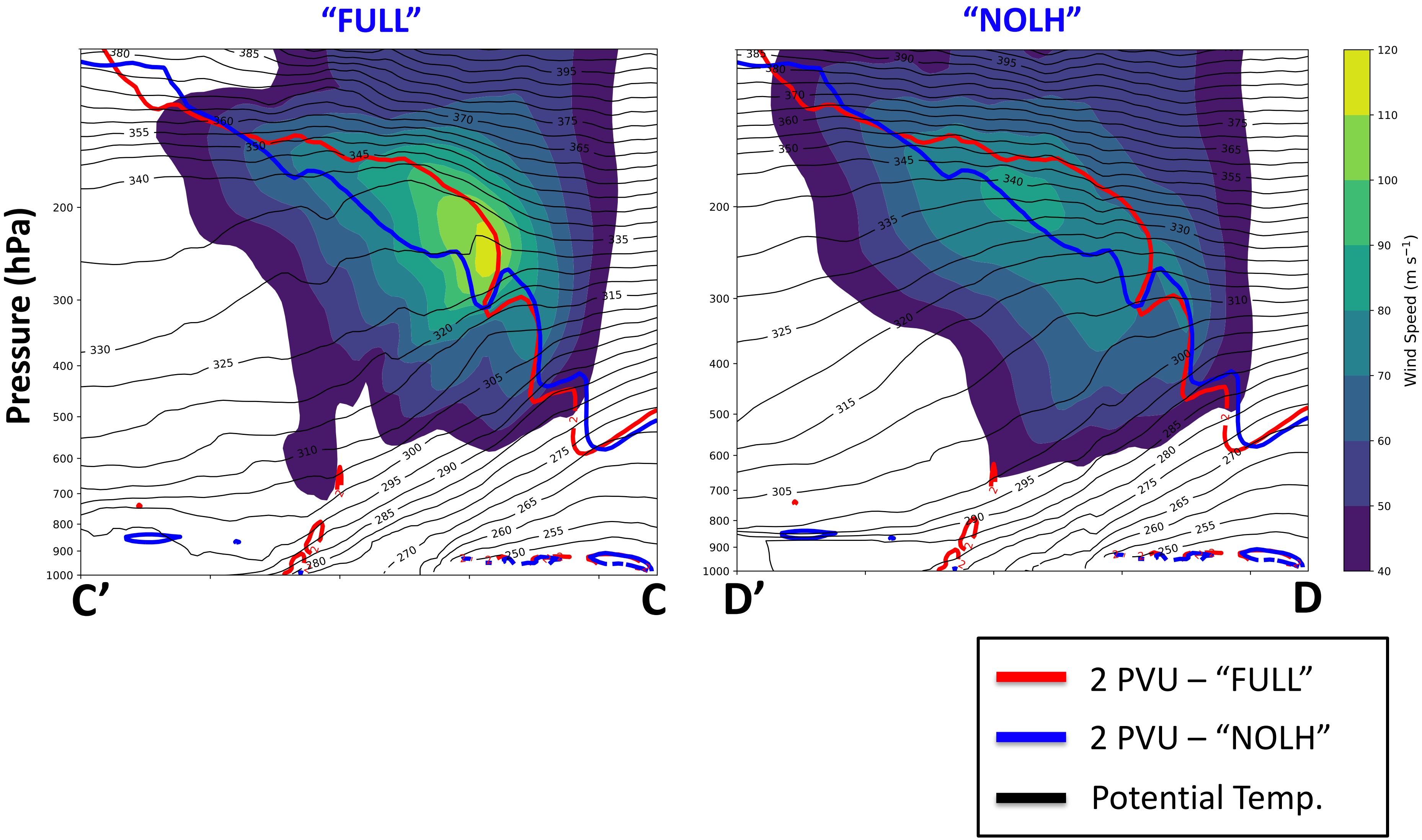

WRF Simulations

1200 UTC 22 December 2013

"FULL" **"NOLH"**

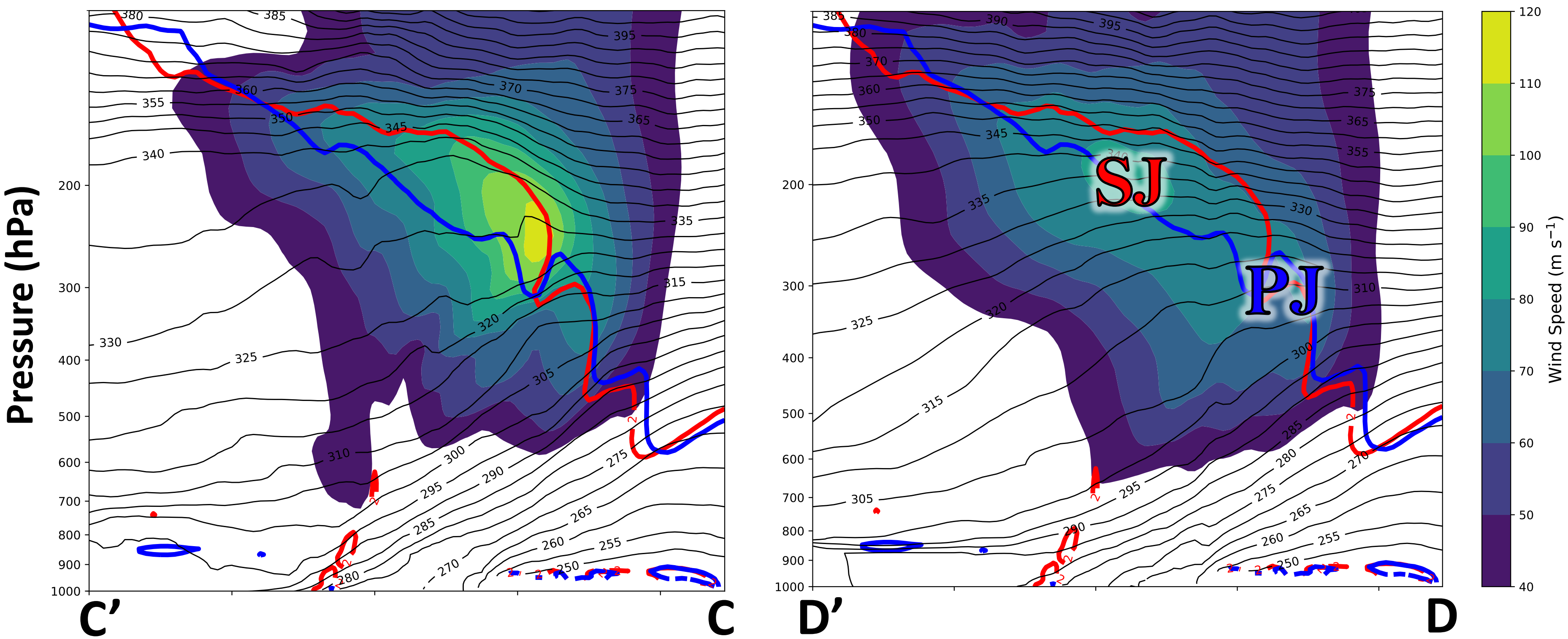

- 2 PVU – "FULL"
- 2 PVU – "NOLH"
- Potential Temp.

- The polar and subtropical jets do not superpose in the "NOLH" simulation

WRF Simulations

1200 UTC 22 December 2013

"FULL" "NOLH"

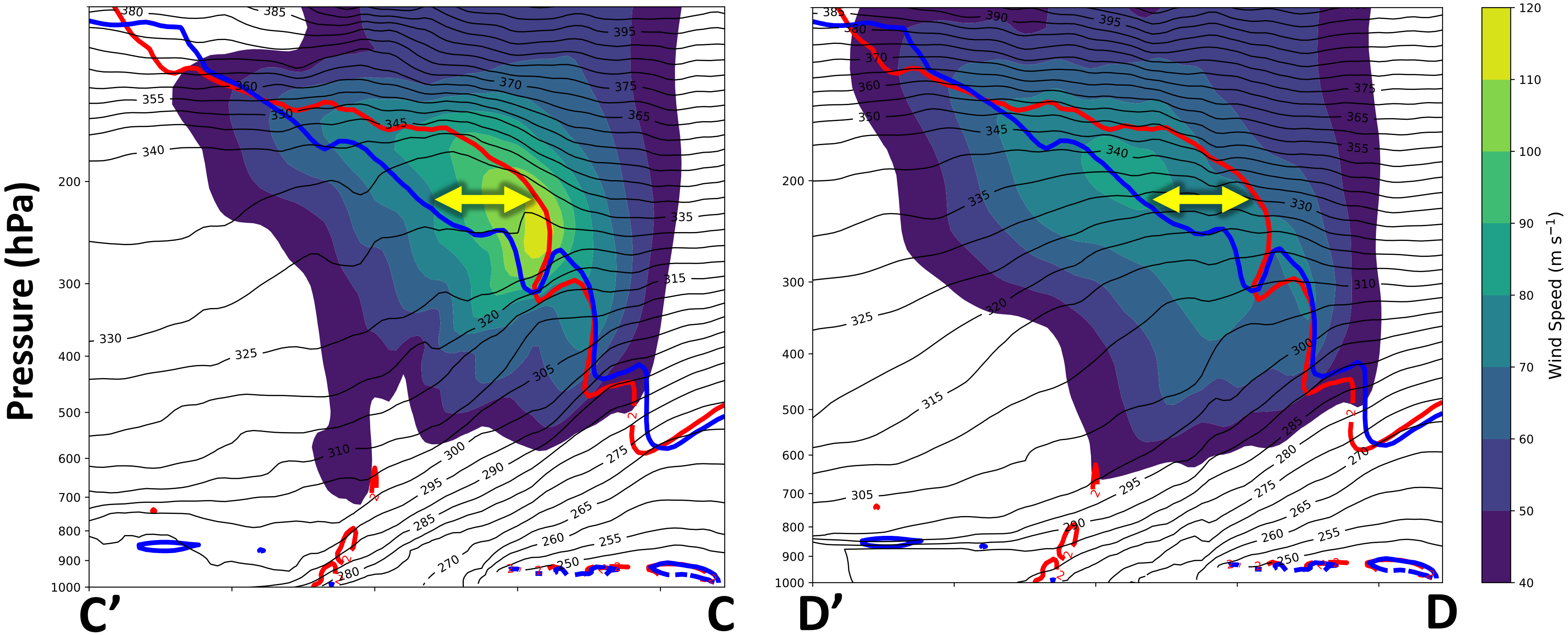

- The slope of the dynamic tropopause is markedly shallower in the "NOLH" simulation

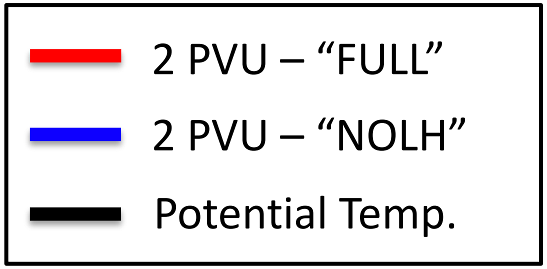

WRF Simulations

0600 UTC 22 December 2013

"FULL":
250-hPa PV Advection by Age. Wind

"NOLH":
250-hPa PV Advection by Age. Wind

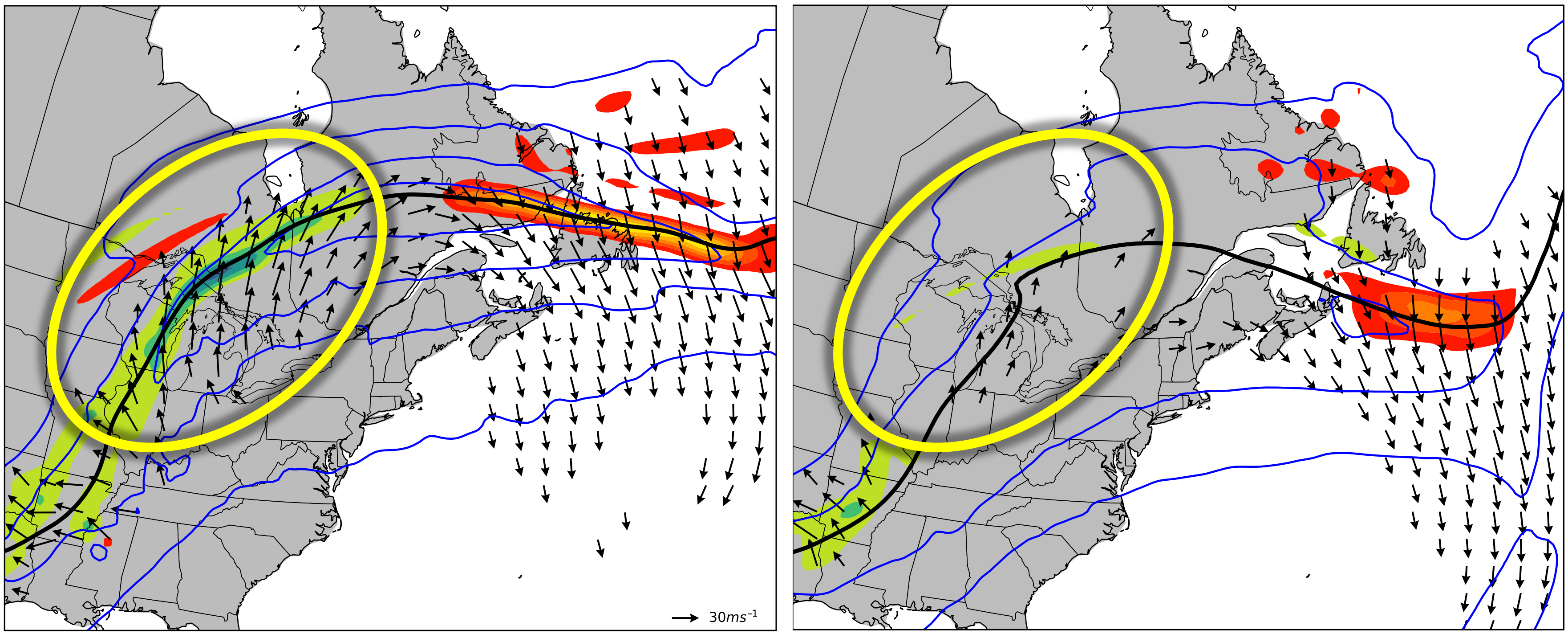

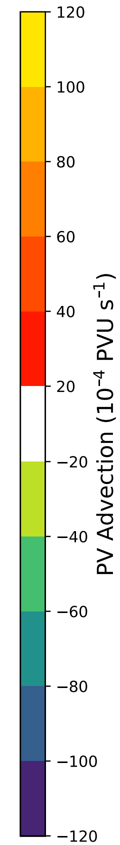

- Strong negative PV advection by the ageostrophic wind is diagnosed at the level of the dynamic tropopause on the western flank of the upper-tropospheric ridge in the "FULL" simulation

2 PVU
250-hPa Wind Speed

WRF Simulations

0600 UTC 22 December 2013

"FULL":
250-hPa PV Advection by Nondiv. Age. Wind

"NOLH":
250-hPa PV Advection by Nondiv. Age. Wind

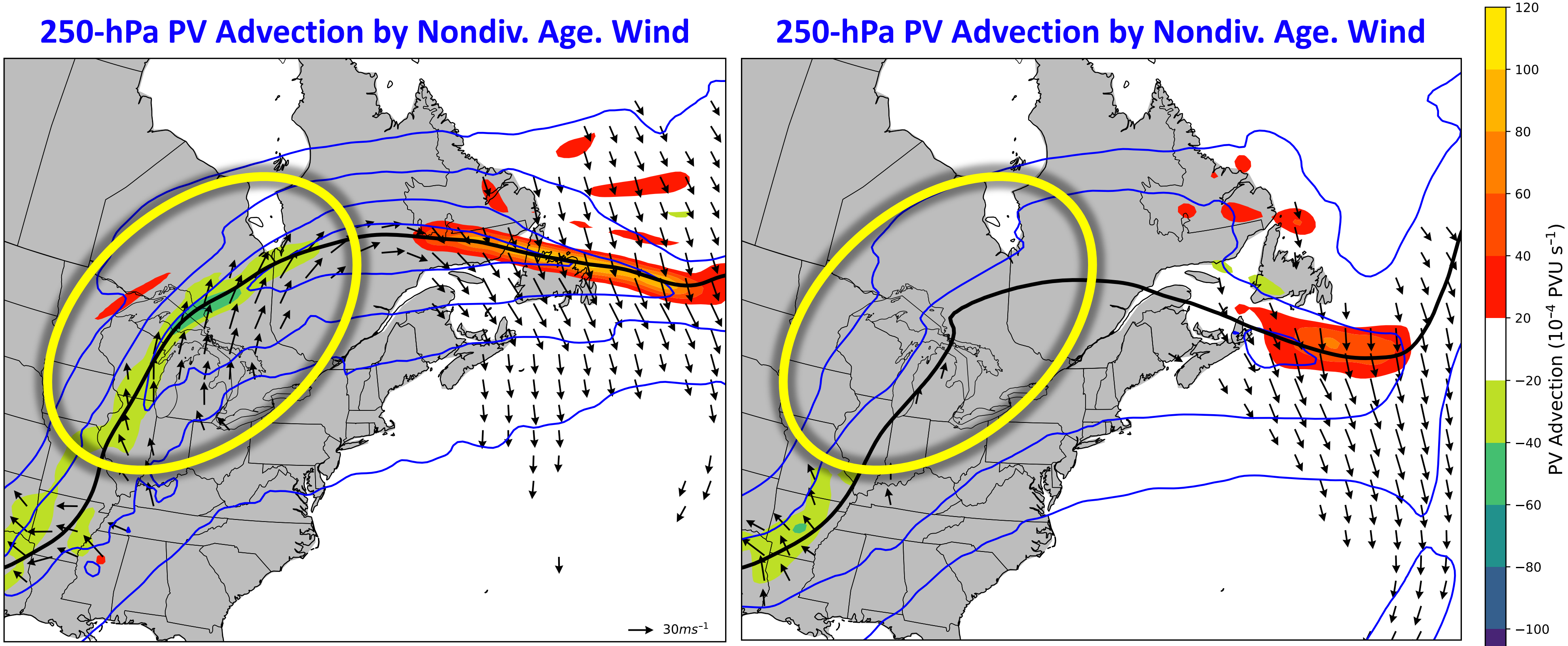

- Negative PV advection by the nondivergent component of the ageostrophic wind accounts for a large fraction of the PV advection by the full ageostrophic wind in the "FULL" simulation

2 PVU

250-hPa Wind Speed

WRF Simulations

0600 UTC 22 December 2013

“FULL”:
250-hPa PV Advection by Div. Age. Wind

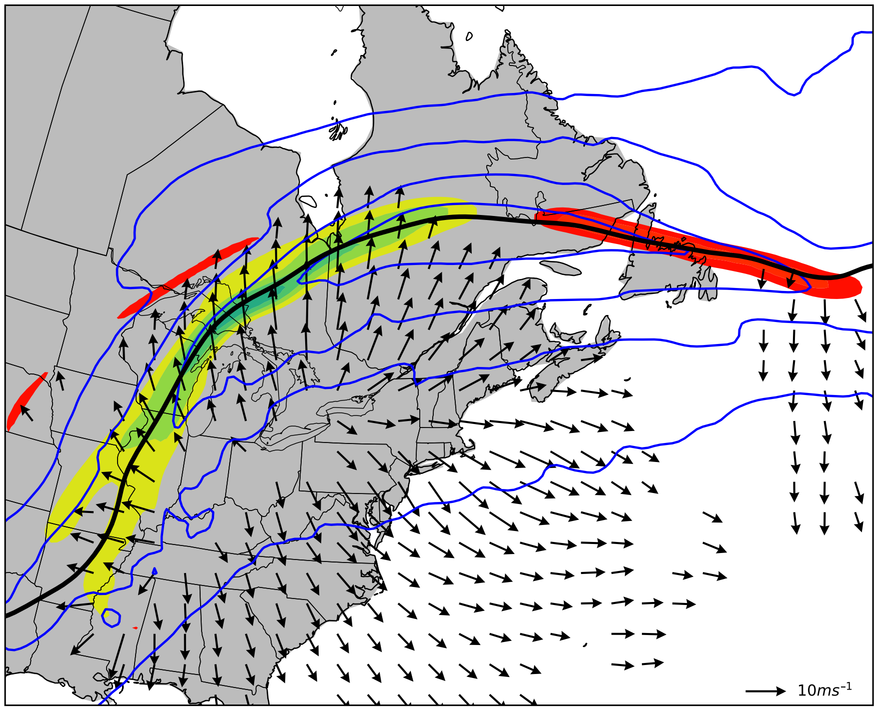

“NOLH”:
250-hPa PV Advection by Div. Age. Wind

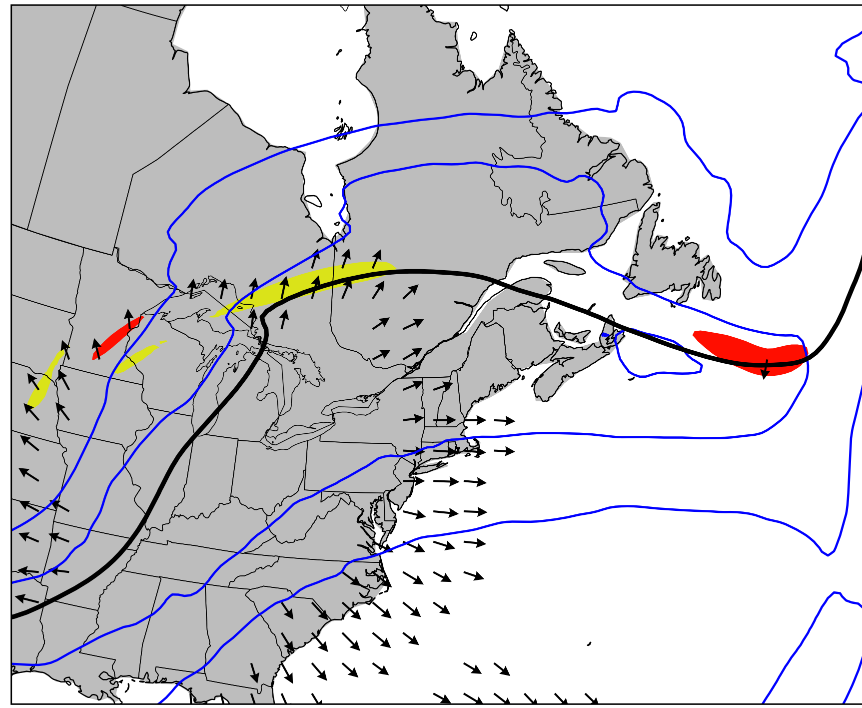

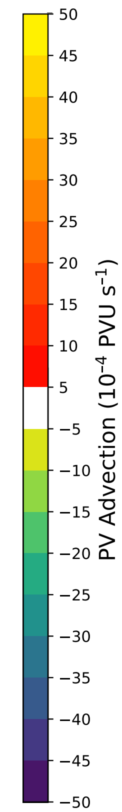

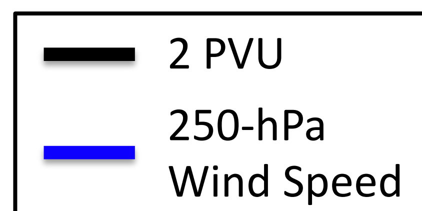

WRF Simulations

0600 UTC 22 December 2013

"FULL": 250-hPa PV Advection by Div. Age. Wind

"NOLH": 250-hPa PV Advection by Div. Age. Wind

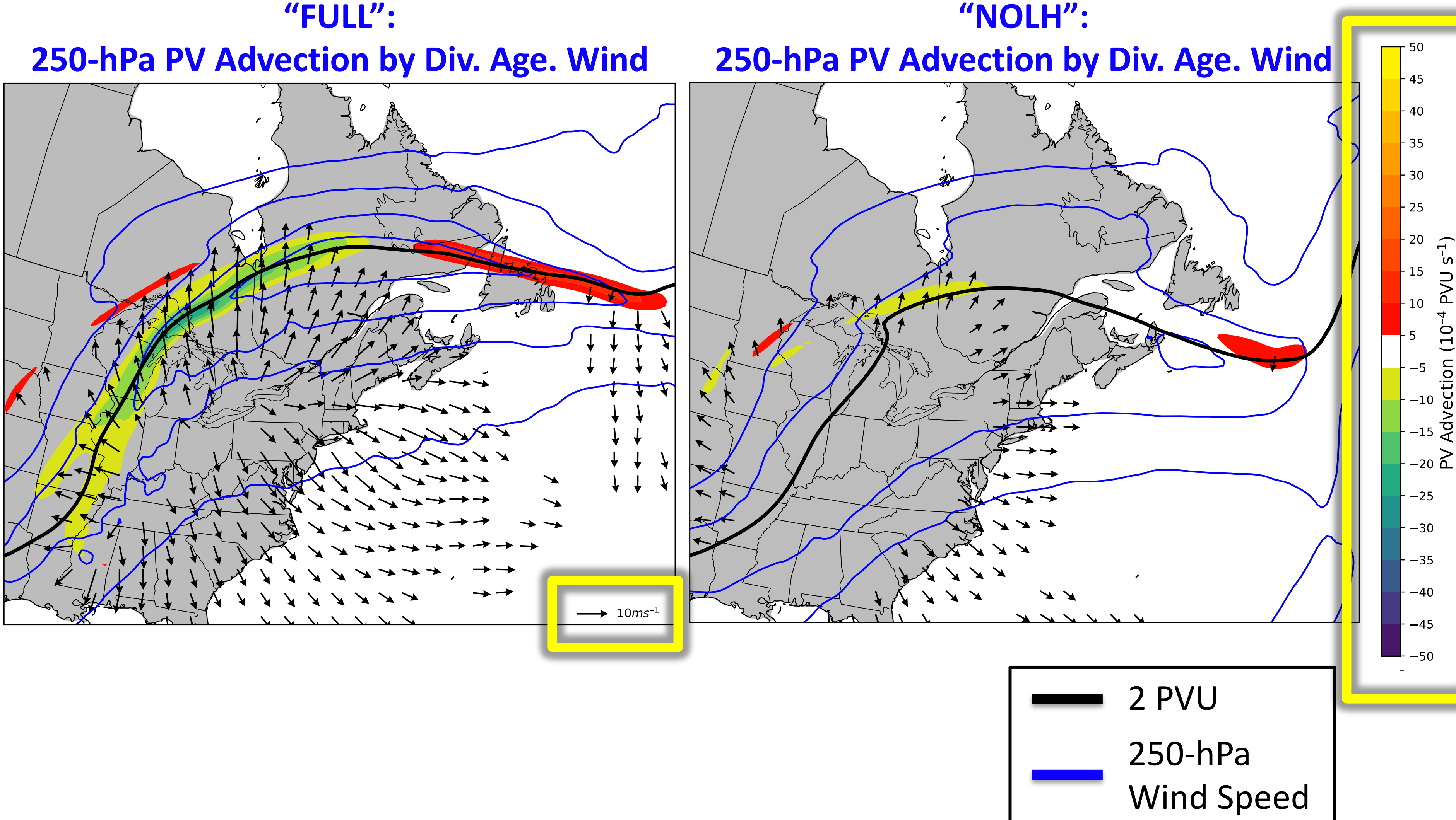

WRF Simulations

0600 UTC 22 December 2013

"FULL": 250-hPa PV Advection by Div. Age. Wind | **"NOLH": 250-hPa PV Advection by Div. Age. Wind**

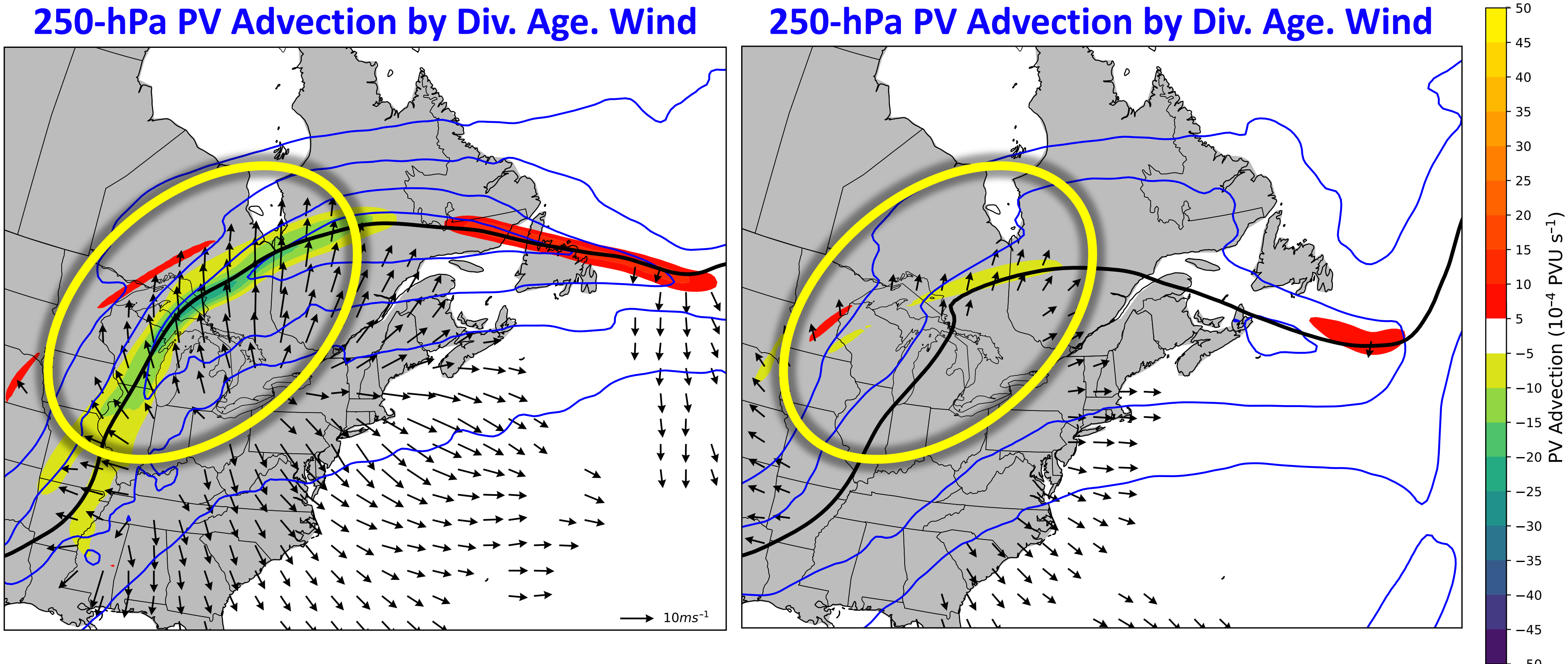

- Negative PV advection by the divergent component of the ageostrophic wind is substantial on the western flank of the upper-tropospheric ridge in the "FULL" simulation

2 PVU

250-hPa Wind Speed

Summary

- Latent heating plays an important role during the development of “subtropical dominant” jet superposition events
- The omission of latent heating during a WRF simulation (“NOLH”) of a subtropical dominant jet superposition event from December 2013 results in a double-jet structure
- The presence of strong negative PV advection by the ageostrophic wind at the level of the dynamic tropopause facilitates the formation of a jet superposition in the “FULL” simulation
- The results from this study have important implications for the subsequent evolution of the downstream large-scale flow pattern over the North Atlantic

Summary

- Latent heating plays an important role during the development of "subtropical dominant" jet superposition events
- The omission of latent heating during a WRF simulation ("NOLH") of a subtropical dominant jet superposition event from December 2013 results in a double-jet structure
- The presence of strong negative PV advection by the ageostrophic wind at the level of the dynamic tropopause facilitates the formation of a jet superposition in the "FULL" simulation
- The results from this study have important implications for the subsequent evolution of the downstream large-scale flow pattern over the North Atlantic

Questions: andrew.c.winters@colorado.edu

Supplementary Slides

References

Cavallo, S. M., and G. J. Hakim, 2010: Composite structure of tropopause polar cyclones. *Mon. Wea. Rev.*, **138,** 3840–3857.

Pyle, M. E., D. Keyser, and L. F. Bosart, 2004: A diagnostic study of jet streaks: Kinematic signatures and relationship to coherent tropopause disturbances. *Mon. Wea. Rev.*, **132,** 297–319.

Saha, S. and co-authors, 2014: The NCEP Climate Forecast System Version 2. *J. Climate*, **27,** 2185–2208

Skamarock, W. C., J. B. Klemp, J. Dudhia, D. O. Gill, D. M. Barker, M. G Duda, X.-Y. Huang, W. Wang, and J. G. Powers, 2008: A Description of the Advanced Research WRF Version 3. NCAR Tech. Note NCAR/TN-475+STR, 113 pp.

Winters, A. C., and J. E. Martin, 2017: Diagnosis of a North American polar/subtropical jet superposition employing piecewise potential vorticity inversion. *Mon. Wea. Rev.*,**145**, 1853-1873.

Winters, A. C., D. Keyser, L. F. Bosart, and J. E. Martin, 2019: Composite synoptic-scale environments conducive to North American polar–subtropical jet superposition events. *Mon. Wea. Rev*., **147,** [in review]

February 2019 Case

February 2019 Case

0600 UTC 20 February 2019

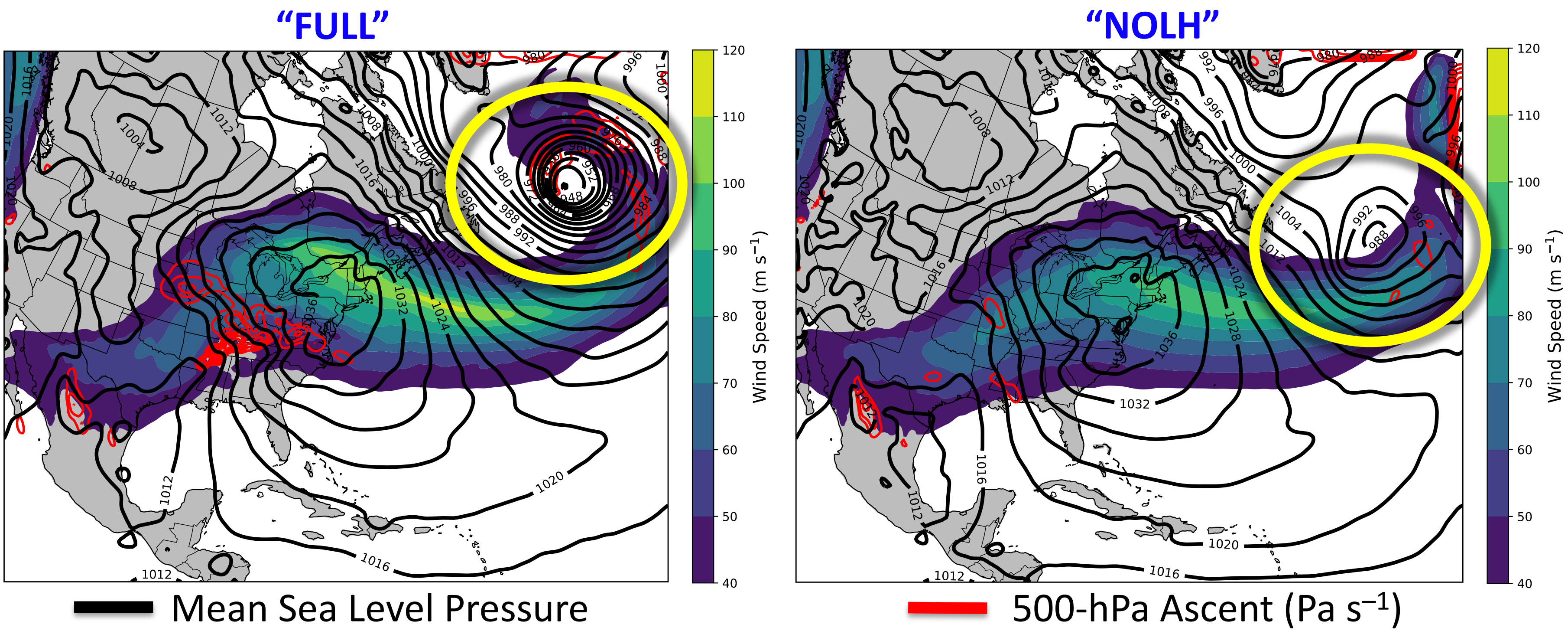

- Maximum 250-hPa wind speed is ~10–20 m s^{-1} weaker in "NOLH"
- Surface cyclone over the North Atlantic is ~40 hPa weaker in "NOLH"

WRF Simulations

1200 UTC 22 December 2013

"FULL" – 250-hPa Nondivergent Age. Wind

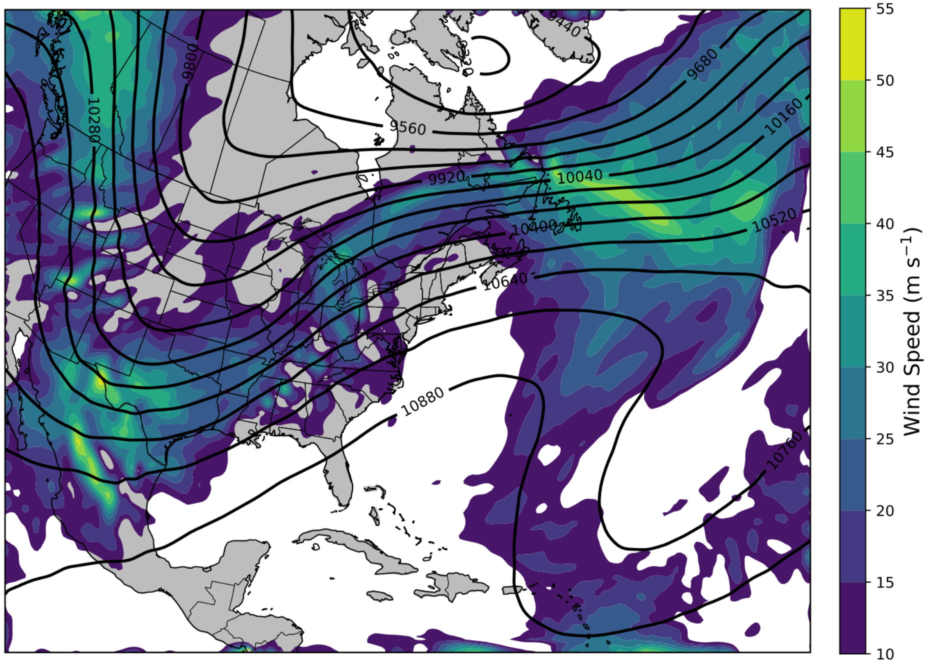

250-hPa Height: "FULL"

"NOLH": 250-hPa Nondivergent Age. Wind

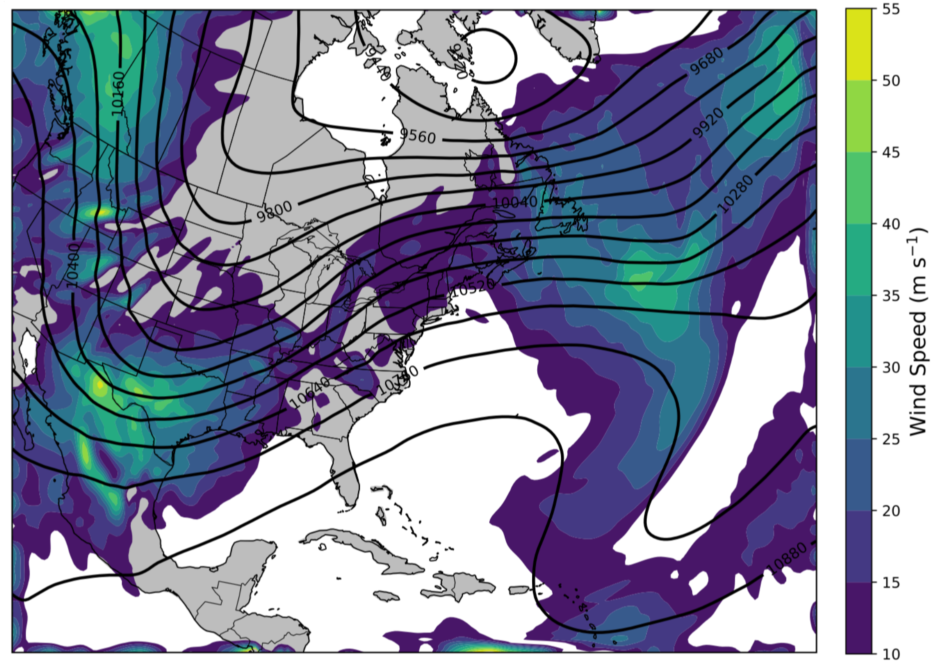

250-hPa Height: "NOLH"

- A substantial fraction of the difference in jet wind speeds between the two simulations can be attributed to the nondivergent component of the ageostrophic wind

WRF Simulations

1200 UTC 22 December 2013

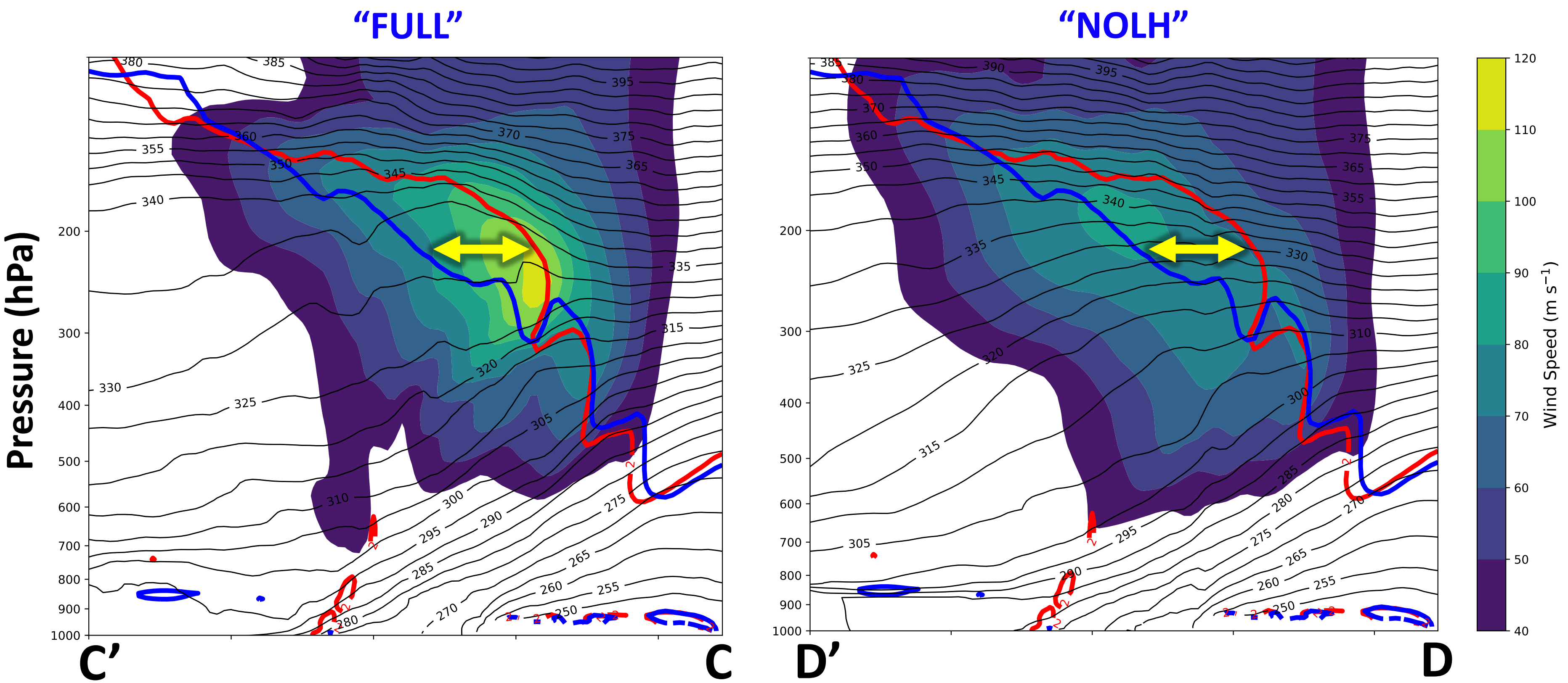

- The difference in the slope of the tropopause between the two simulations is due to marked differences in negative PV advection by the ageostrophic wind at the level of the dynamic tropopause

2 PVU – "FULL"
2 PVU – "NOLH"
Potential Temp.

Composite Characteristics

Jet Superposition Event Characteristics

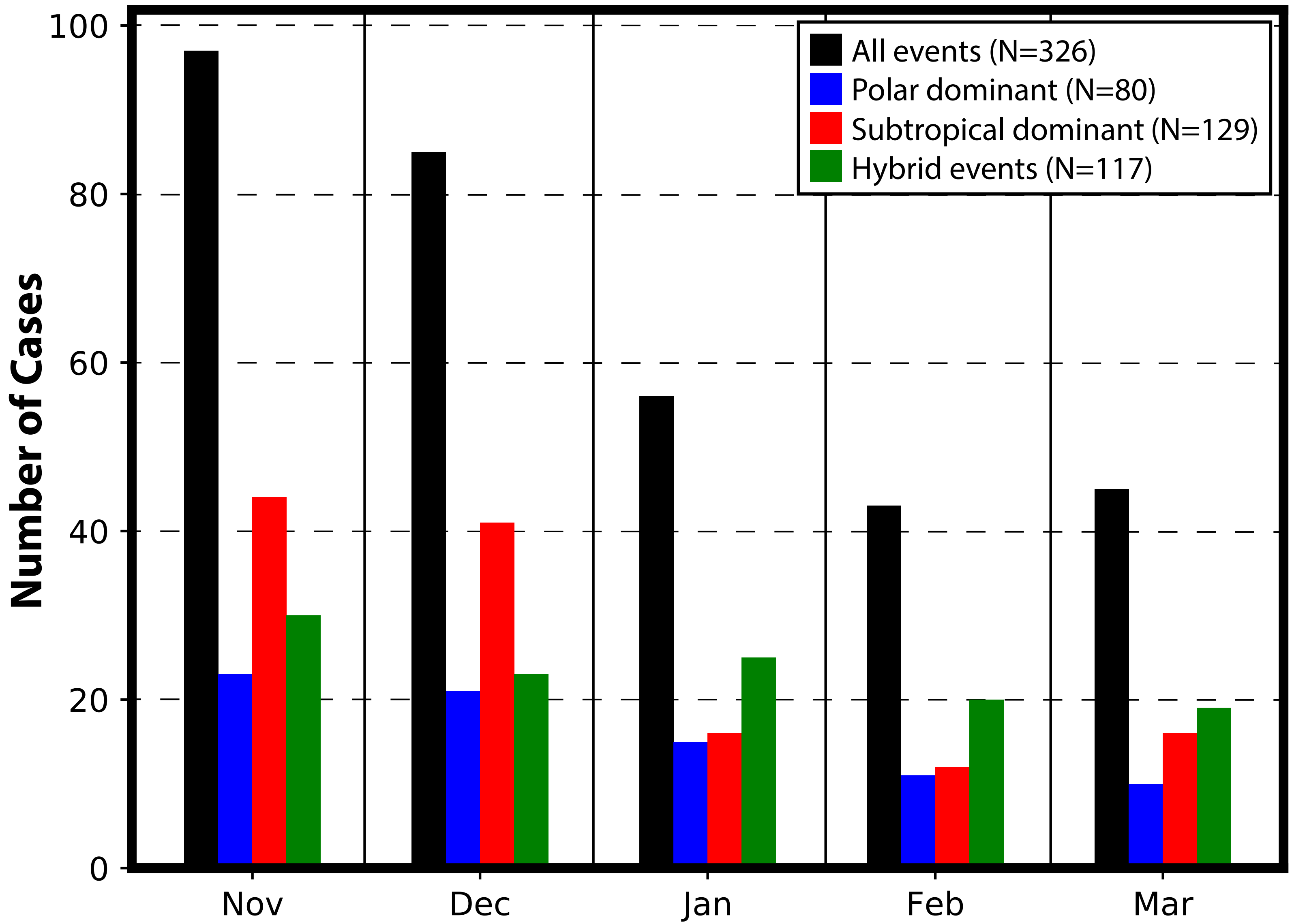

Jet Superposition Event Composites

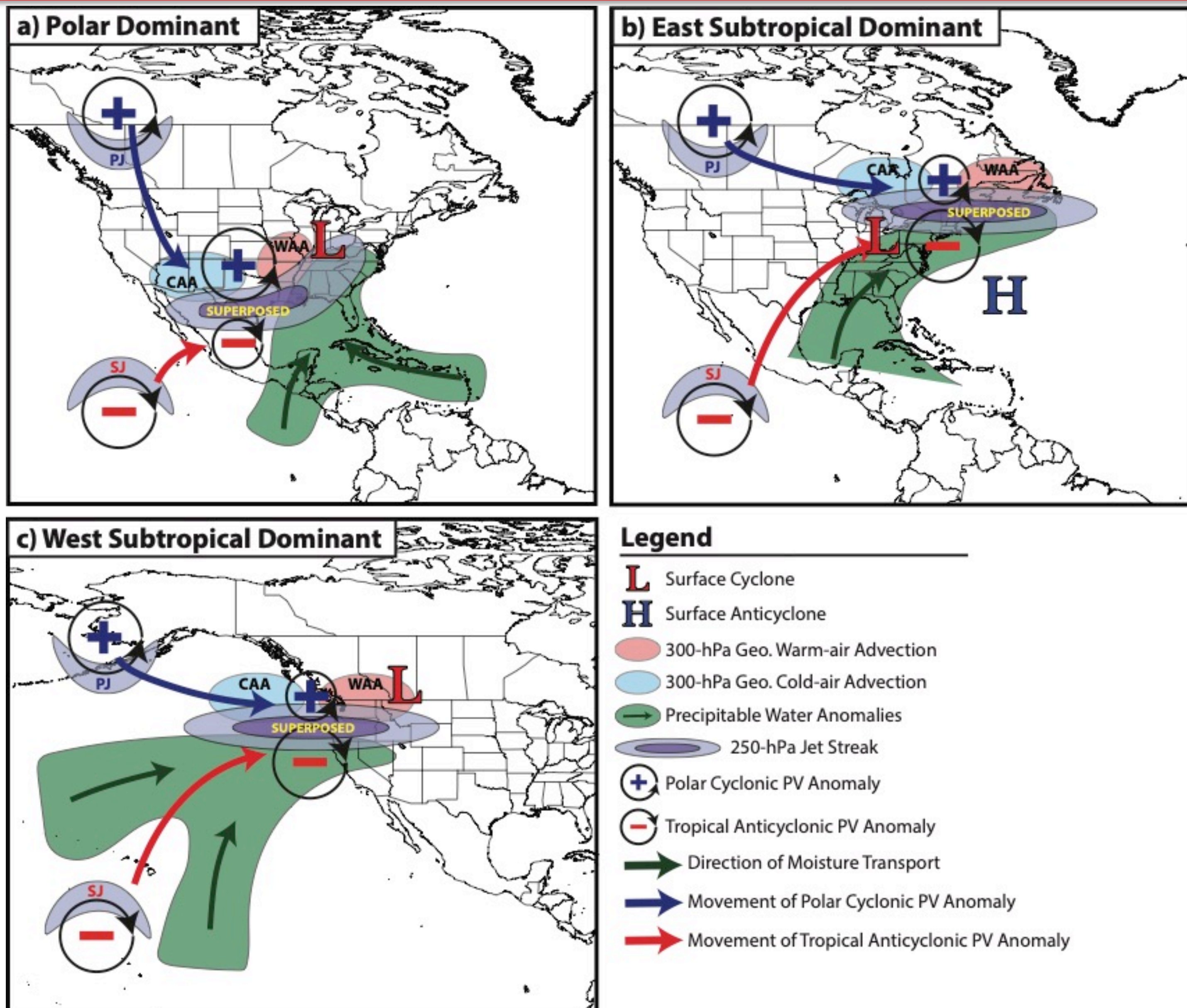

Downstream Consequences

North Atlantic Oscillation: 5 Days After Jet Superposition

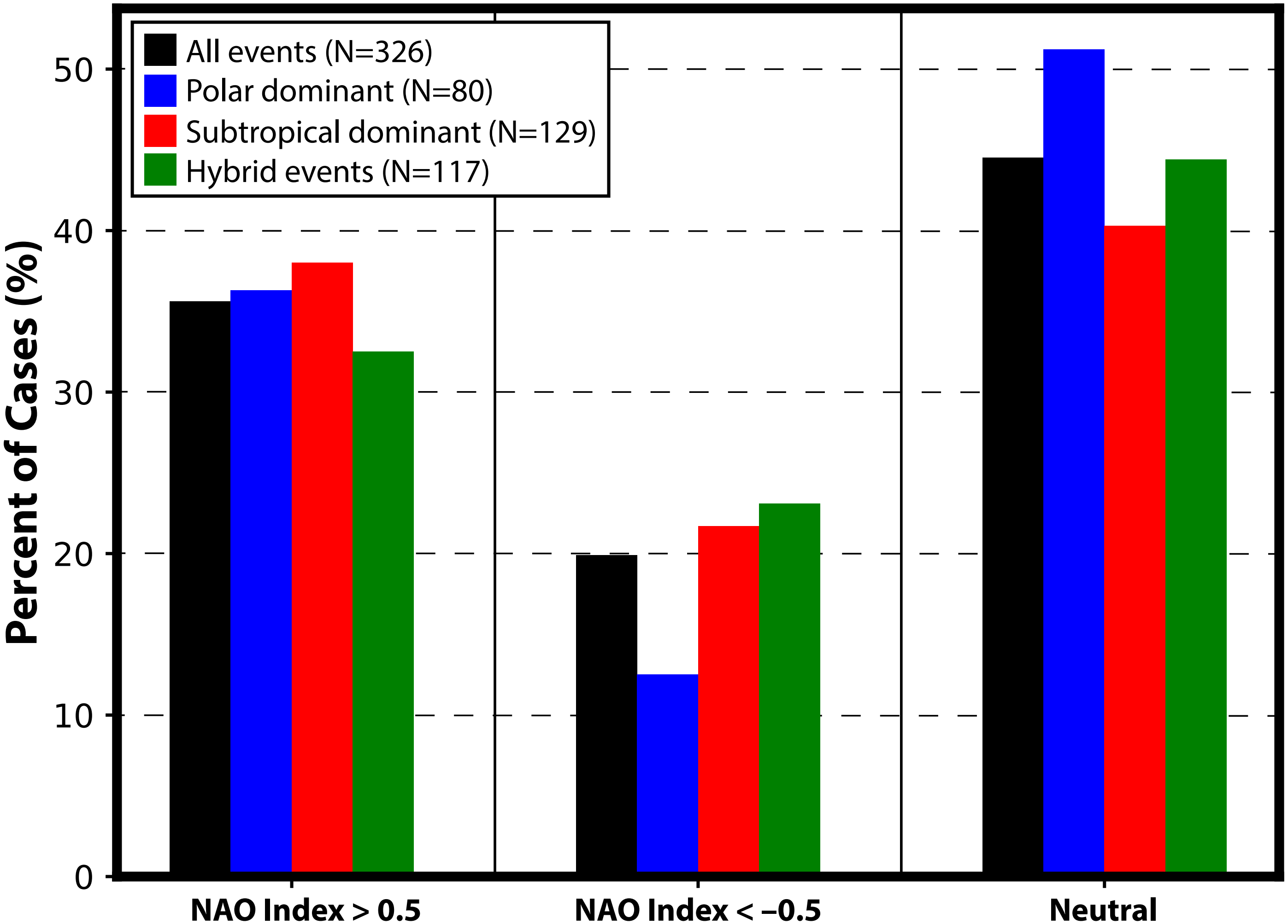

All Events ΔNAO
+0.11

Ave. Polar Dominant ΔNAO
+0.15

Ave. Subtropical Dominant ΔNAO
+0.13

Ave. Hybrid ΔNAO
+0.07

Background Material

Background

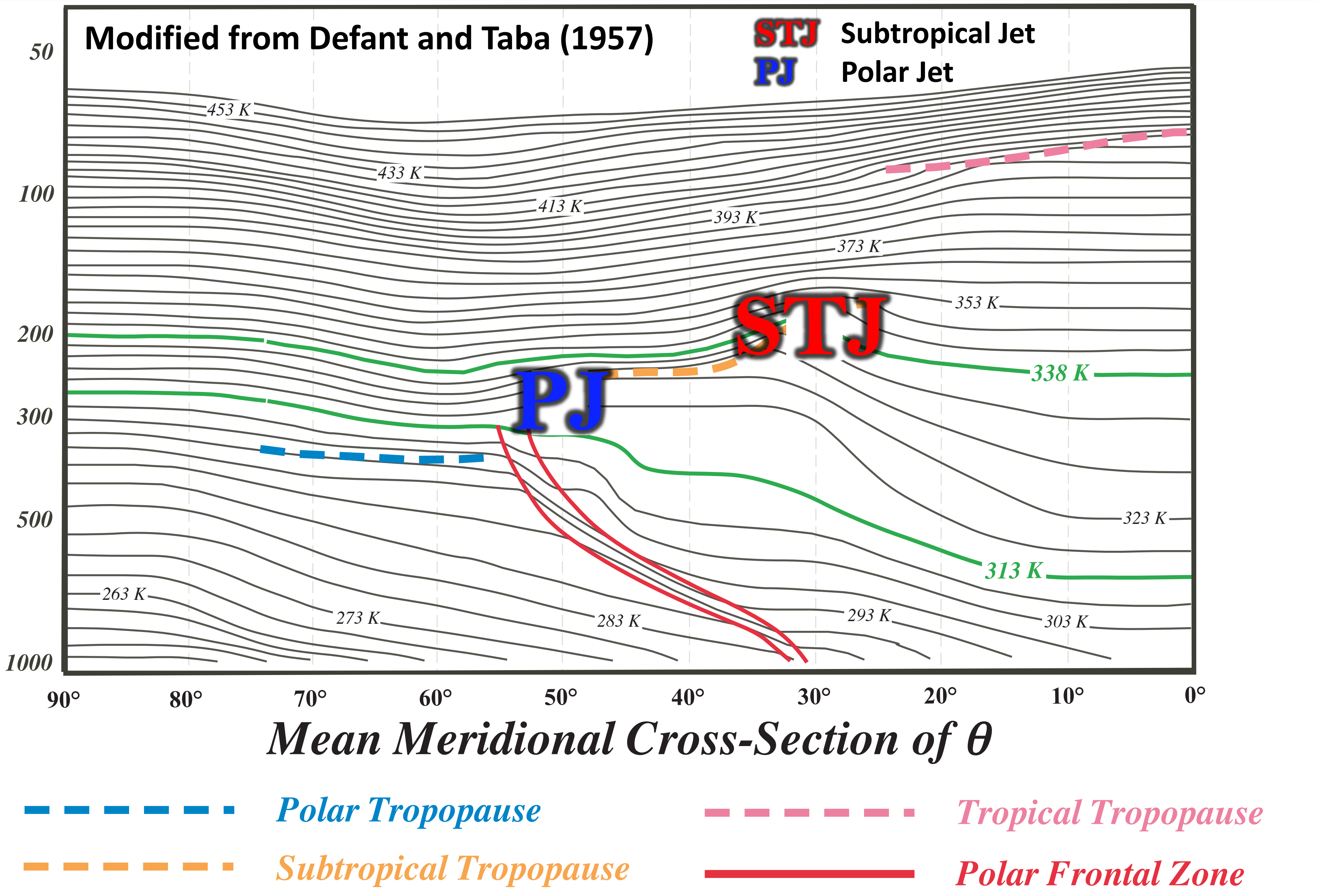
Modified from Defant and Taba (1957)
STJ Subtropical Jet
PJ Polar Jet
50
100
200
300
500
1000
453 K
433 K
413 K
393 K
373 K
353 K
338 K
323 K
313 K
303 K
293 K
283 K
273 K
263 K
STJ
PJ
90°
80°
70°
60°
50°
40°
30°
20°
10°
0°
Mean Meridional Cross-Section of θ
Polar Tropopause
Tropical Tropopause
Subtropical Tropopause
Polar Frontal Zone

Background

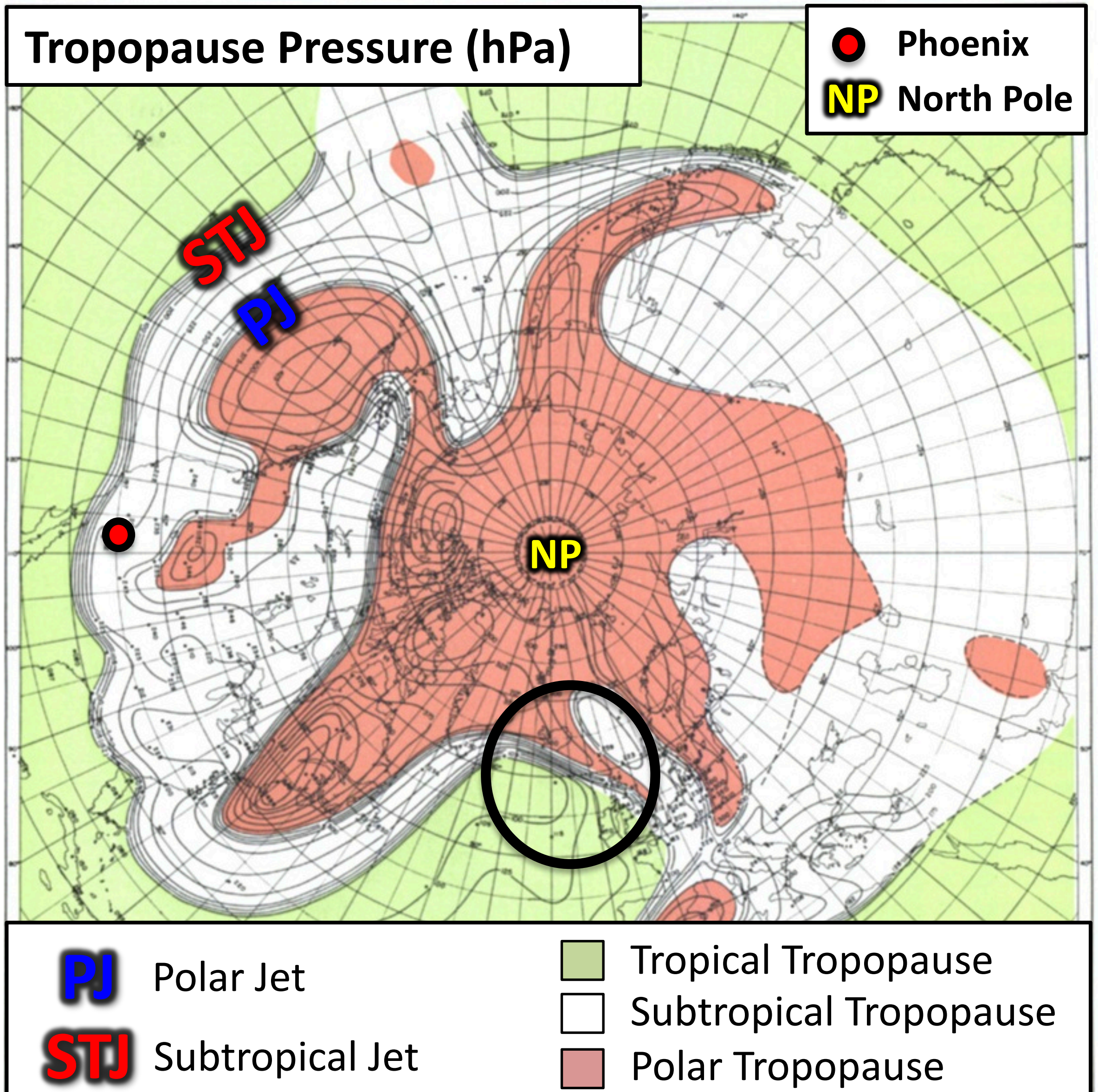

Maps of tropopause pressure help to identify the location of the jets.

While each jet occupies its own climatological latitude band, substantial meanders are common.

Occasionally, the latitudinal separation between the jets can vanish resulting in a vertical **jet superposition**.

Modified from Defant and Taba (1957)

Background

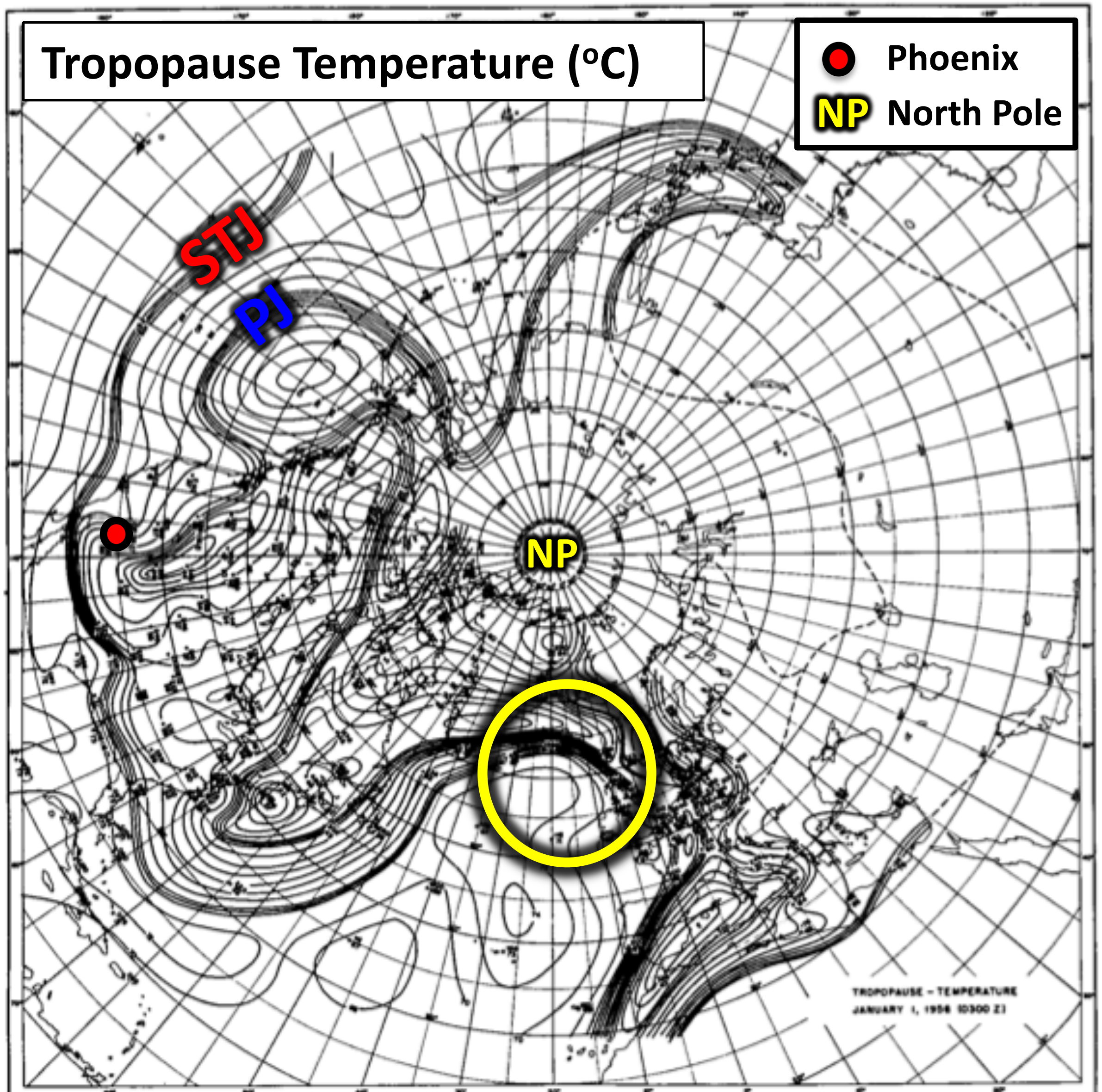

The pole-to-equator baroclinicity is combined into a much narrower zone of contrast in the vicinity of a jet superposition.

Intensified frontal structure is often attended by a strengthening of the superposed jet's transverse circulation.

Modified from Defant and Taba (1957)

Background

Christenson et al. (2017) highlight three locations that experience the greatest frequency of jet superpositions:

1) Western Pacific

2) North America

3) Northern Africa

Climatological frequency of Northern Hemisphere jet superposition events per cold season (Nov–Mar) 1960–2010

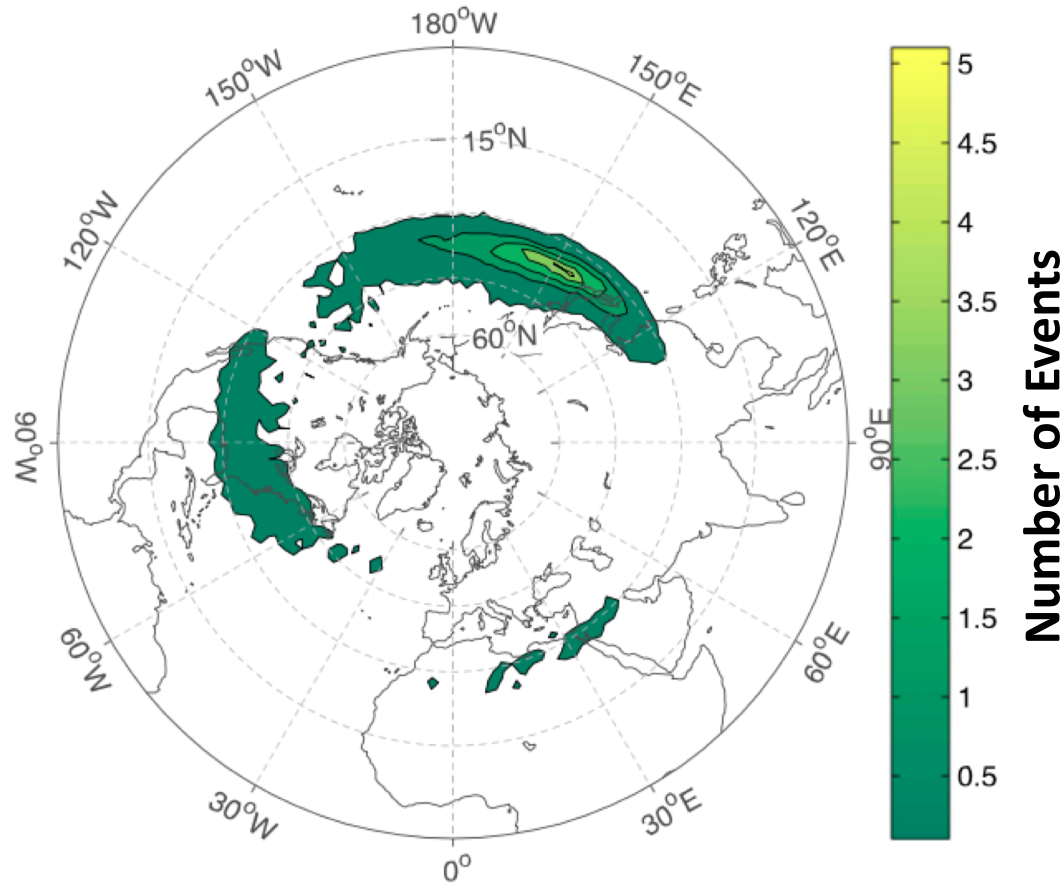

Christenson et al. (2017)

Jet Superpositions and High-Impact Weather

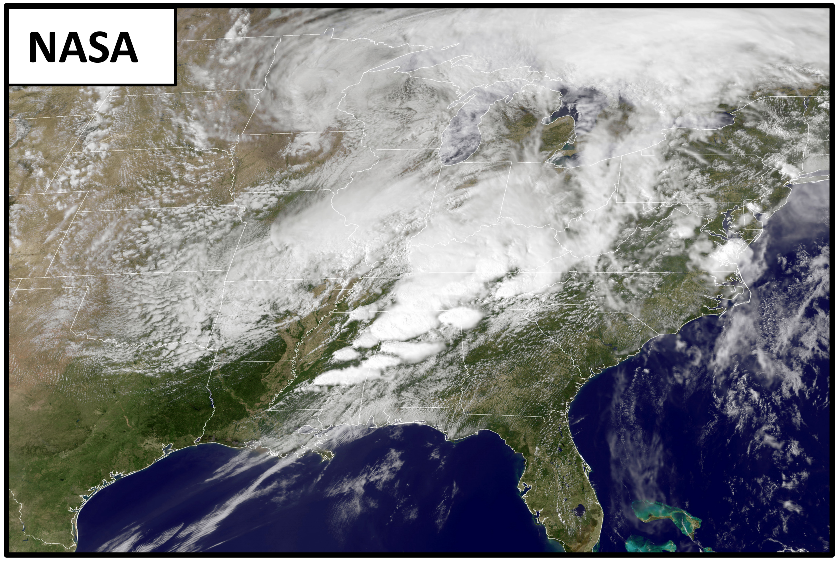

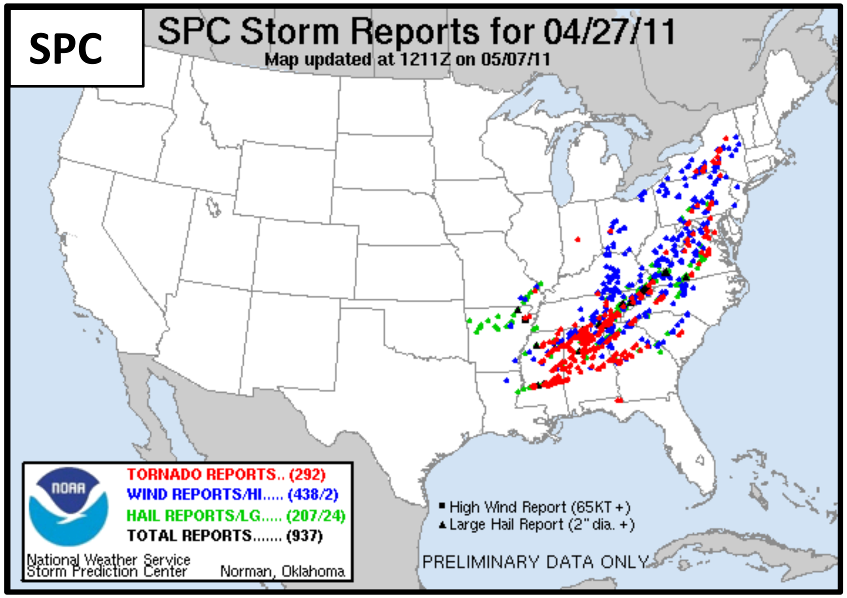

Jet superpositions can be an element of high-impact weather events

1–3 May 2010 Nashville Flood

- Jet superposition enhanced the poleward moisture transport via its ageostrophic circulation (Winters and Martin 2014; 2016).

18–20 December 2009 Mid-Atlantic Blizzard

- Jet superposition was associated with a rapidly deepening East Coast cyclone (Winters and Martin 2016; 2017).

26 October 2010: Explosive Cyclogenesis Event

- Jet superposition over the West Pacific preceded the development of an intense Midwest U.S. cyclone.

25–28 April 2011 Tornado Outbreak

- Jet superposition occurred over the West Pacific prior to the outbreak (Knupp et al. 2014; Christenson and Martin 2012).

Ageostrophic Transverse Jet Circulations

Traditional four-quadrant model

Geo. cold-air advection (CAA) along the jet axis promotes **subsidence** through the jet core

Geo. warm-air advection (WAA) along the jet axis promotes **ascent** through the jet core

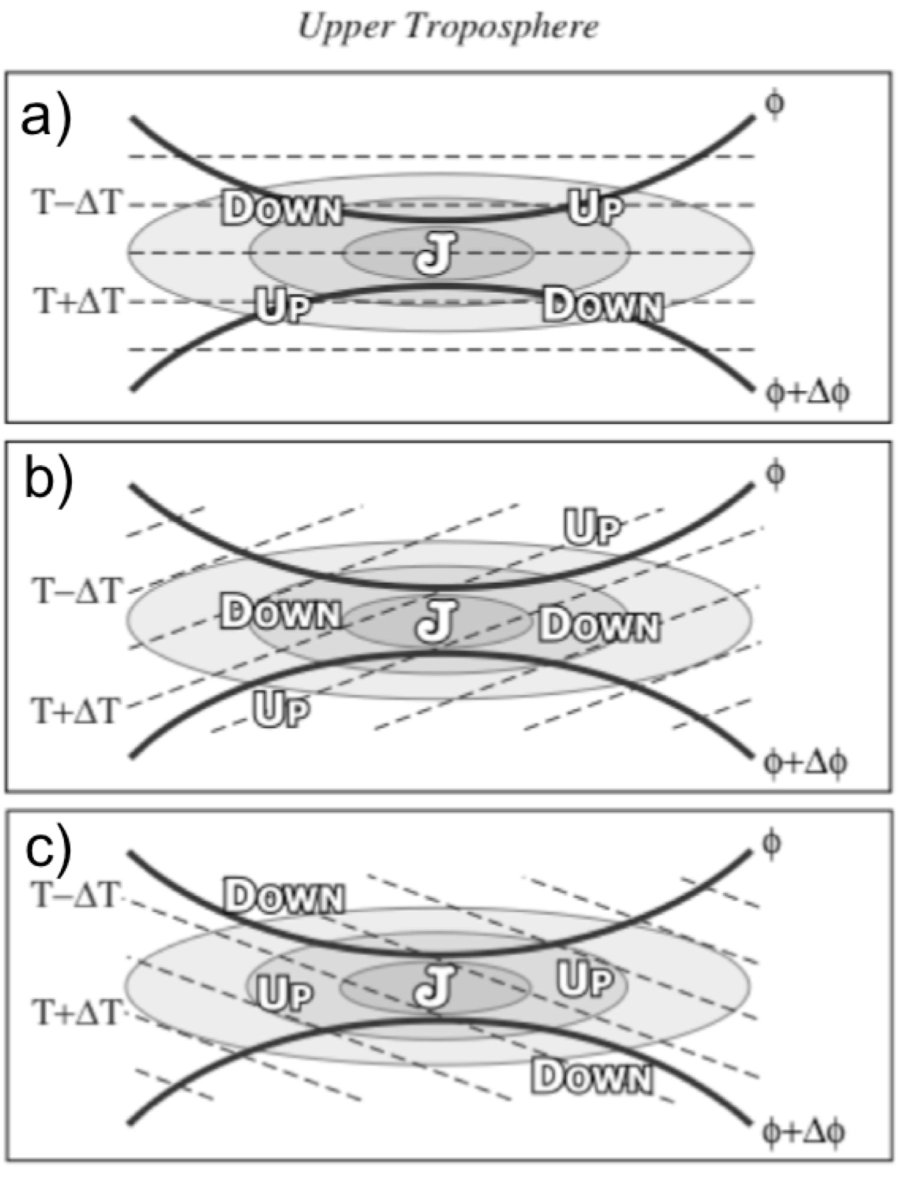

Lang and Martin (2012)

Background

Insight into how the tropopause can be restructured from a PV perspective can be found by consulting Wandishin et al. (2000)

Two processes can account for "foldogenesis":

1) **Differential vertical motions** can vertically steepen the tropopause.

2) **Convergence** or a **vertical shear** can produce a differential horizontal advection of the tropopause surface.

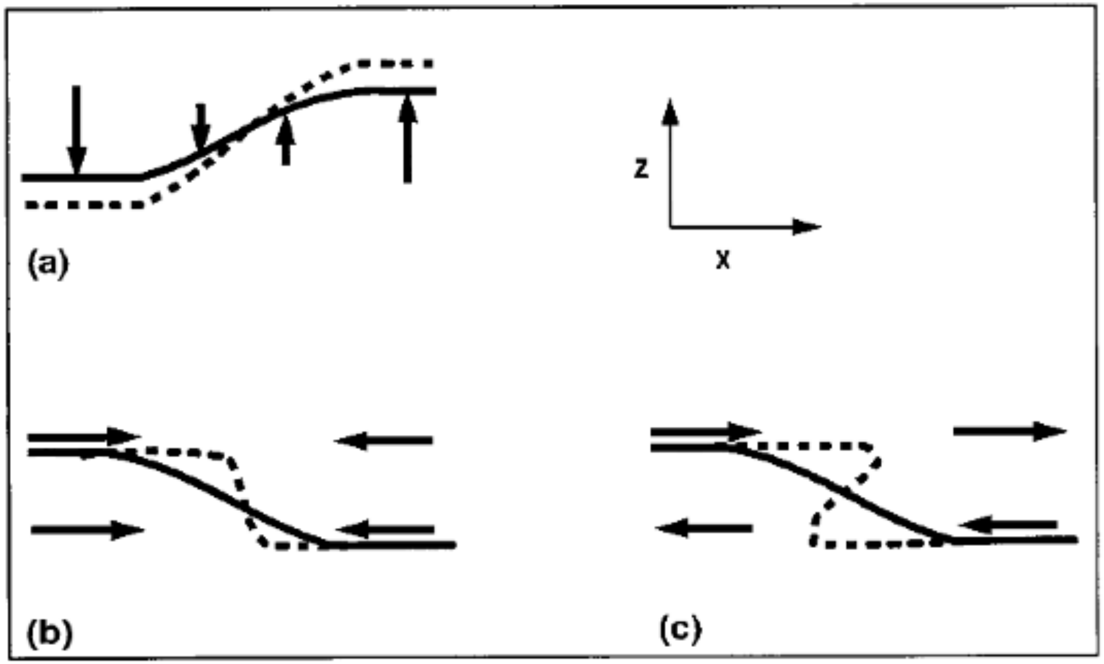

Wandishin et al. 2000

These same mechanisms are also likely to play an important role in superpositions.

Jet Identification

Jet Superposition Event Classification

1. Determined the mean position of the 2-PVU contour on the 320-K and 350-K surfaces at each analysis time in the CFSR.
2. Compared the position of the jet superposition centroid at the start of each event against the climatological position of the 2-PVU contour.

- **Polar Dominant**

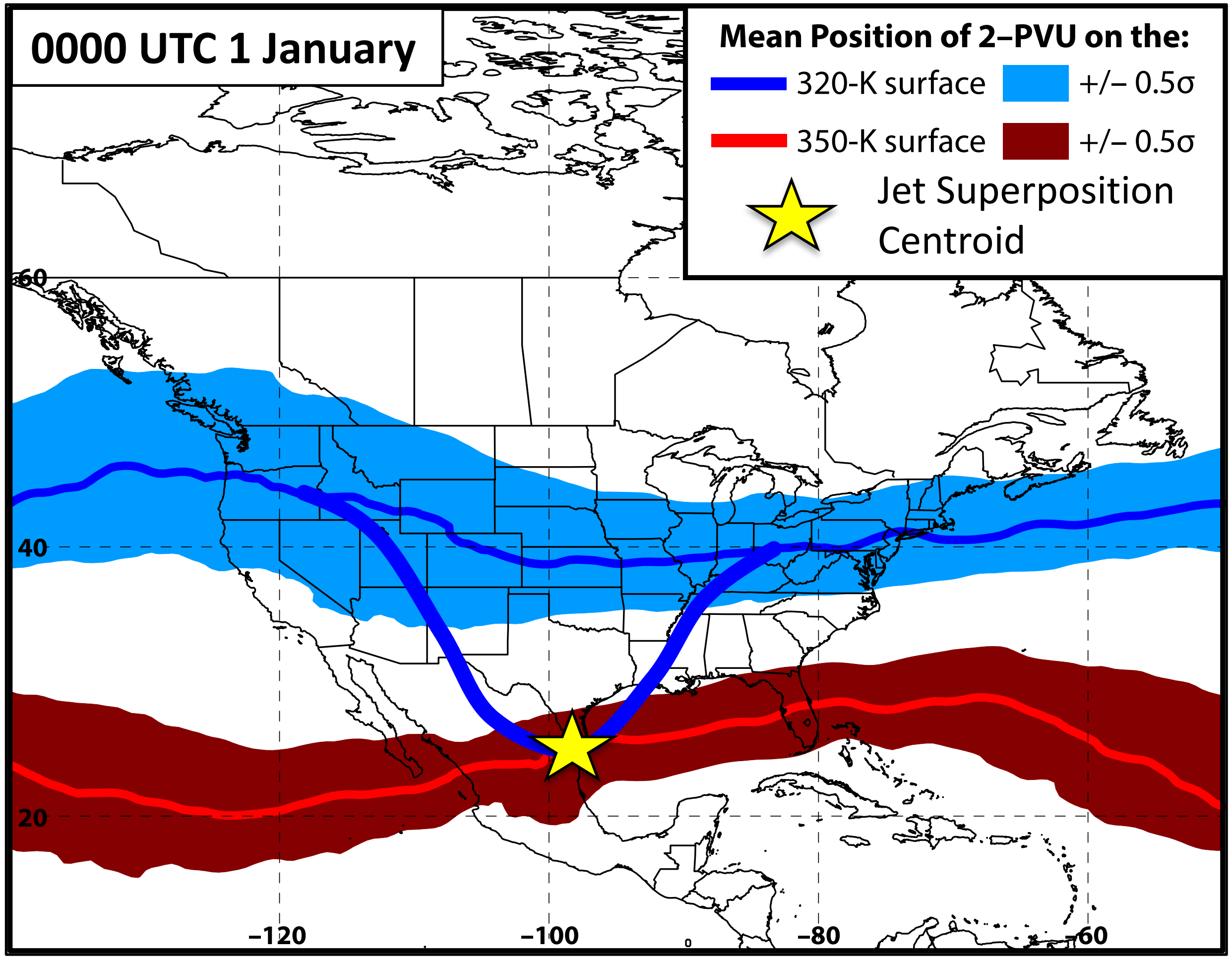

Jet Superposition Event Classification

1. Determined the mean position of the 2-PVU contour on the 320-K and 350-K surfaces at each analysis time in the CFSR.

2. Compared the position of the jet superposition centroid at the start of each event against the climatological position of the 2-PVU contour.

- Polar Dominant
- **Subtropical Dominant**

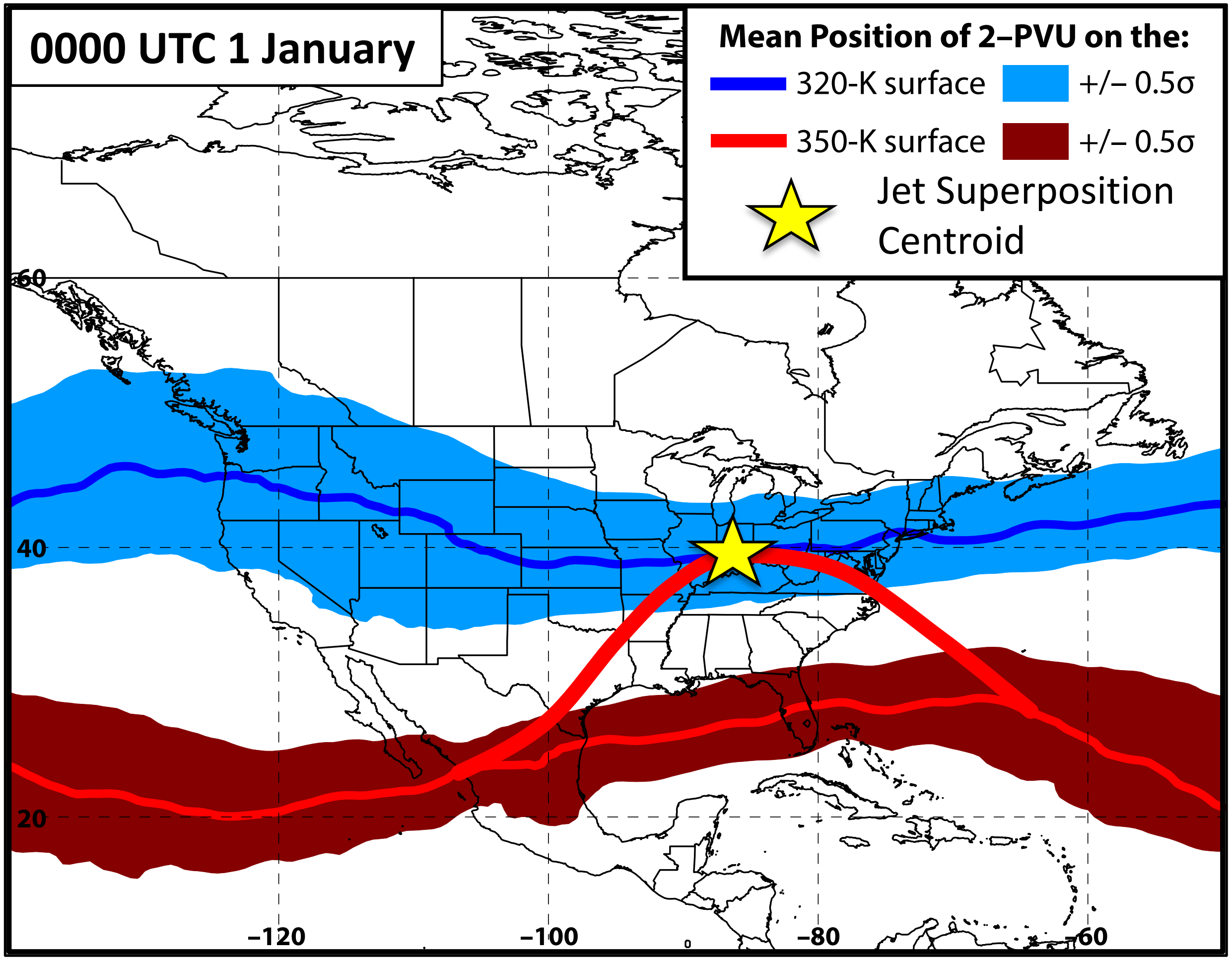

Jet Superposition Event Classification

1. Determined the mean position of the 2-PVU contour on the 320-K and 350-K surfaces at each analysis time in the CFSR.

2. Compared the position of the jet superposition centroid at the start of each event against the climatological position of the 2-PVU contour.

- Polar Dominant
- Subtropical Dominant
- **Hybrid**

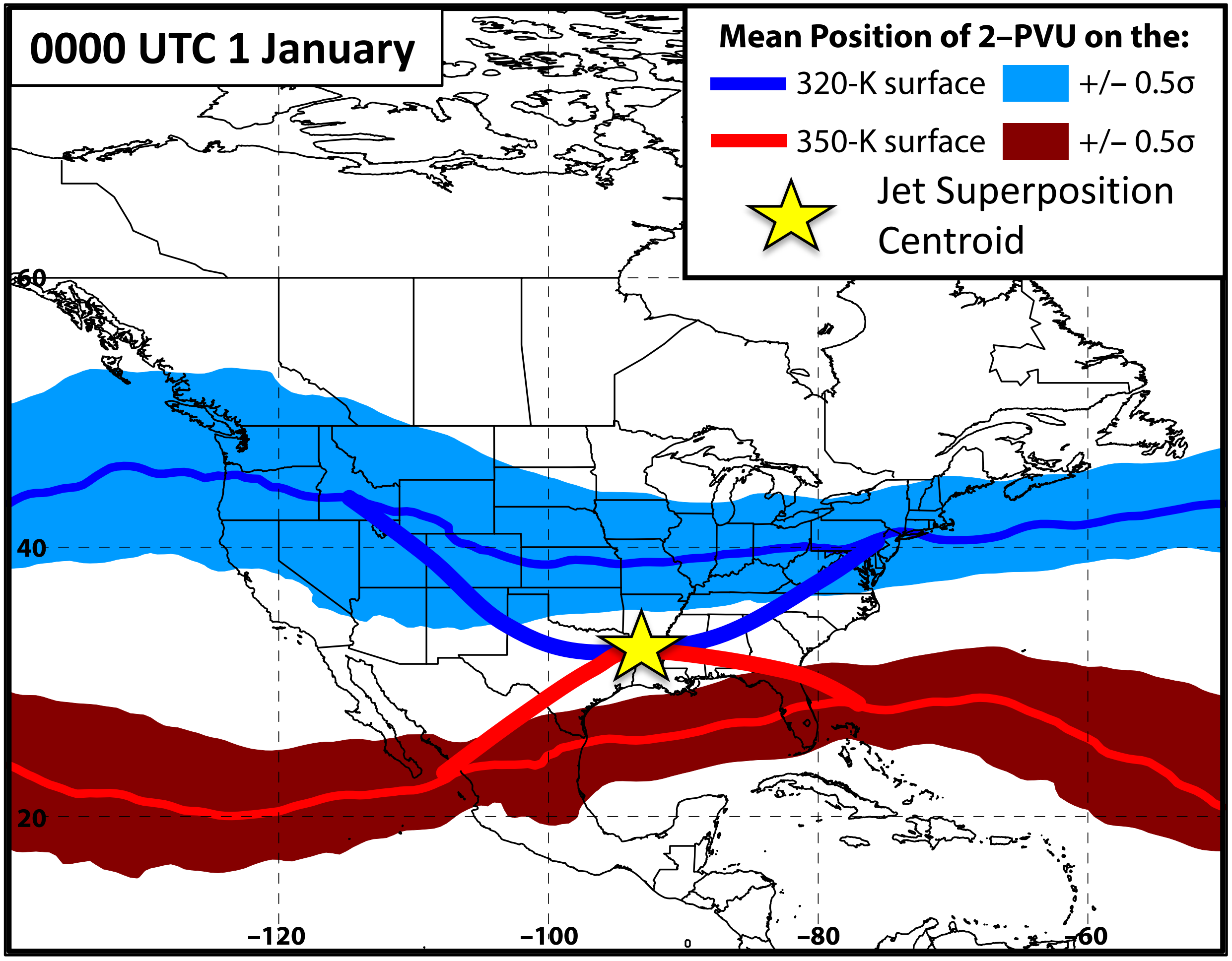

Jet Superposition Event Identification

0000 UTC 27 April 2010

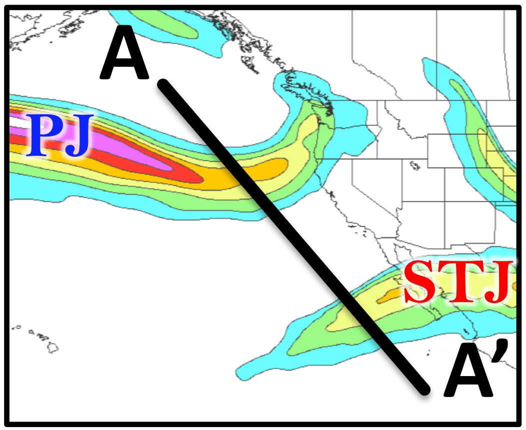

250-hPa wind speed

Isolated grid points over North America in the CFSR (Saha et al. 2014) characterized by polar and subtropical jets during Nov–Mar 1979–2010.

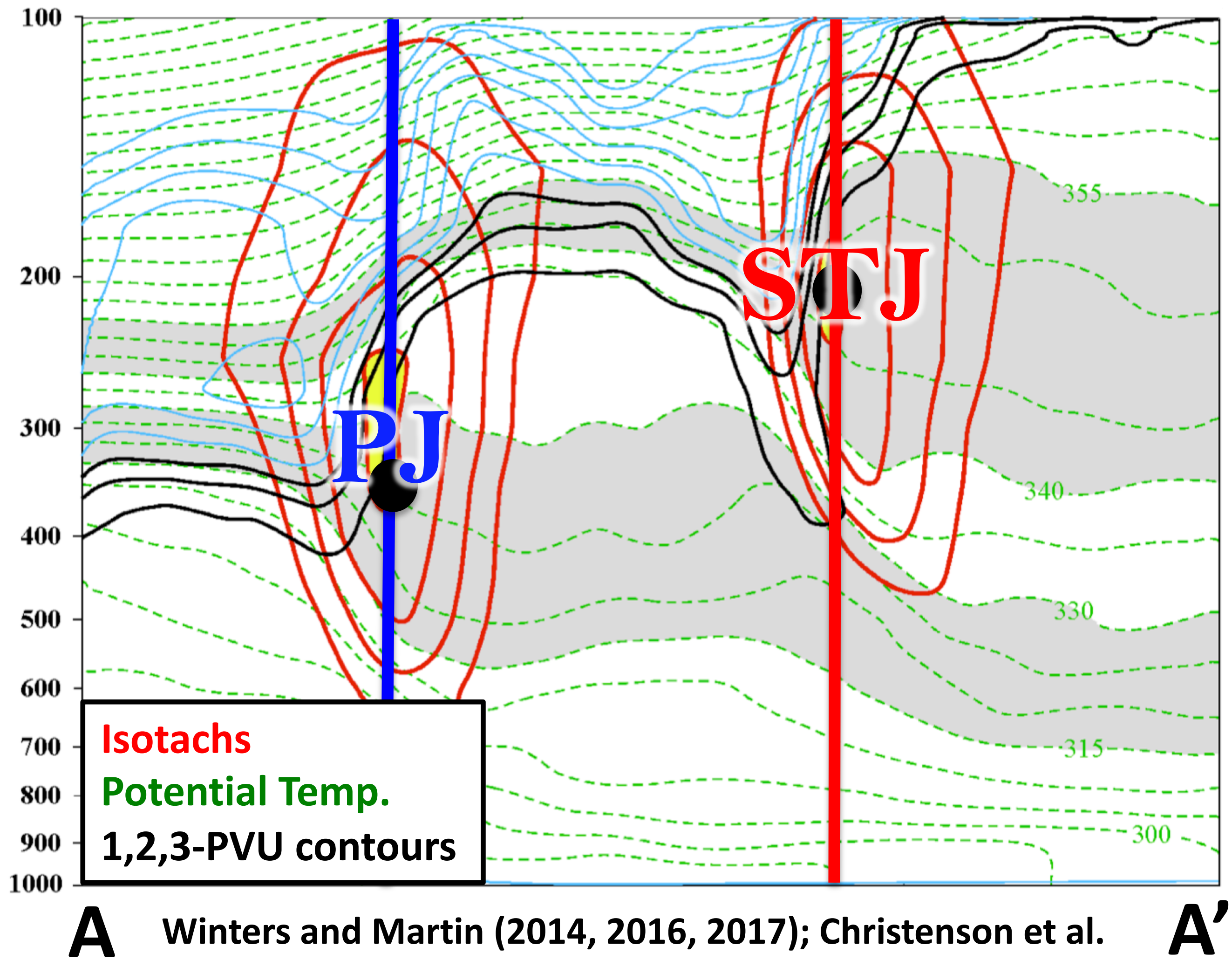

Winters and Martin (2014, 2016, 2017); Christenson et al. (2017); Handlos and Martin (2016)

Jet Superposition Event Identification

0000 UTC 27 April 2010

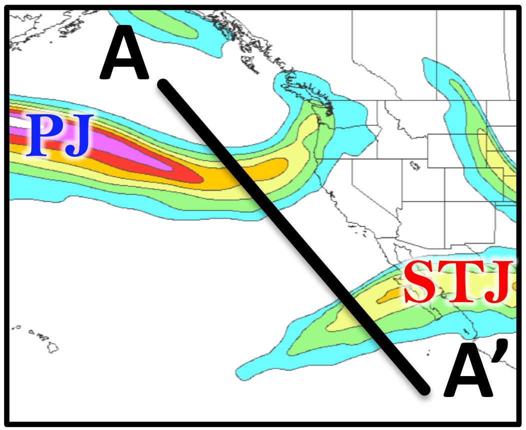

250-hPa wind speed

Isolated grid points over North America in the CFSR (Saha et al. 2014) characterized by polar and subtropical jets during Nov–Mar 1979–2010.

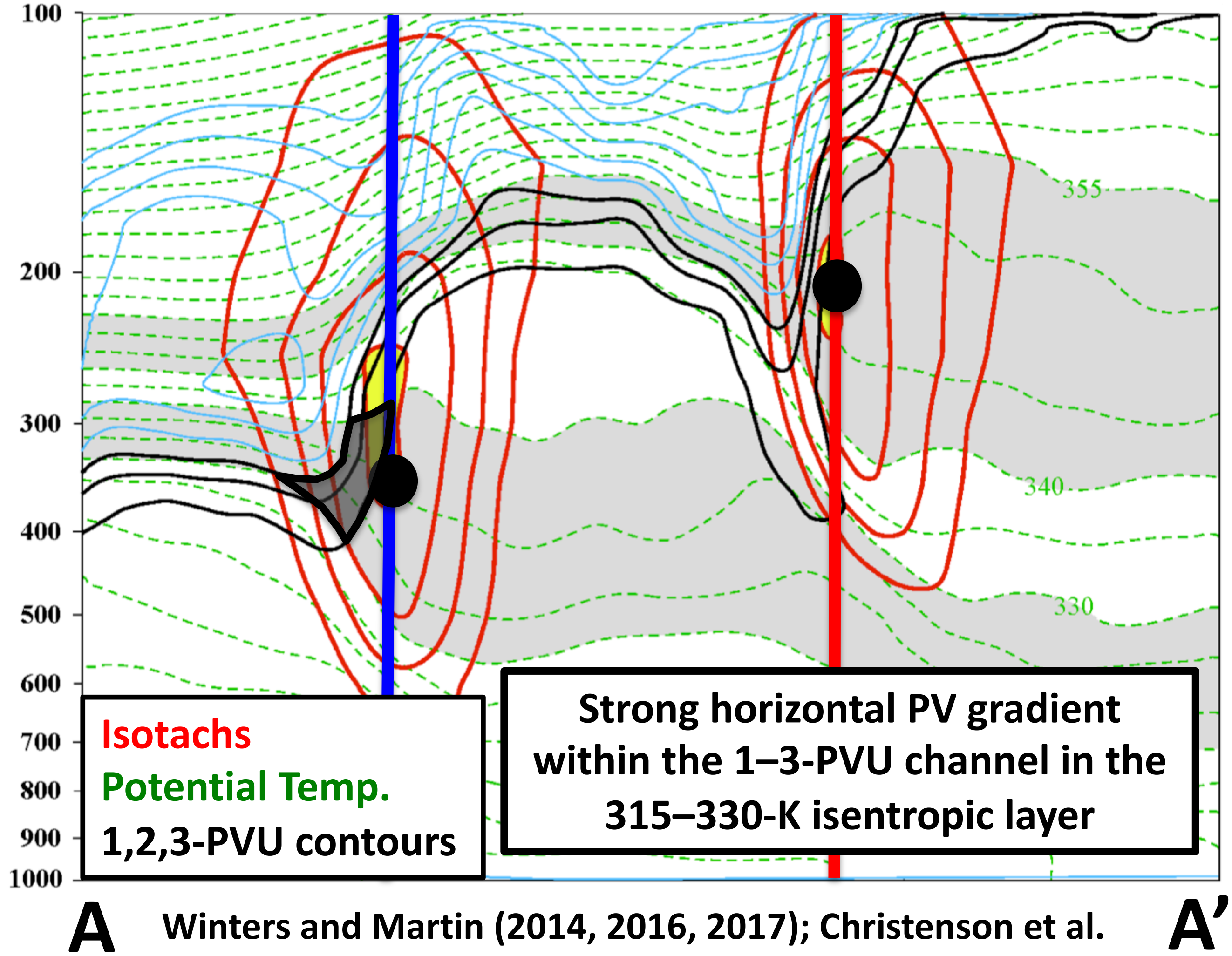

Winters and Martin (2014, 2016, 2017); Christenson et al. (2017); Handlos and Martin (2016)

Jet Superposition Event Identification

0000 UTC 27 April 2010

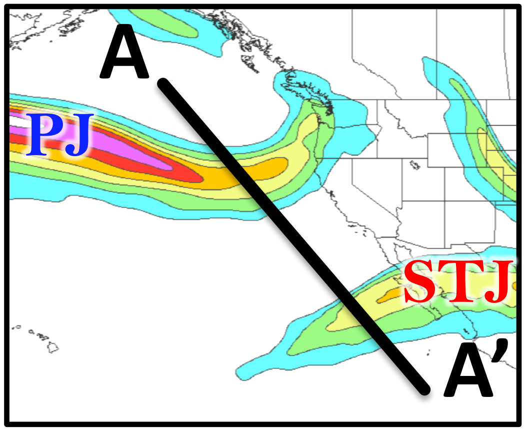

250-hPa wind speed

Isolated grid points over North America in the CFSR (Saha et al. 2014) characterized by polar and subtropical jets during Nov–Mar 1979–2010.

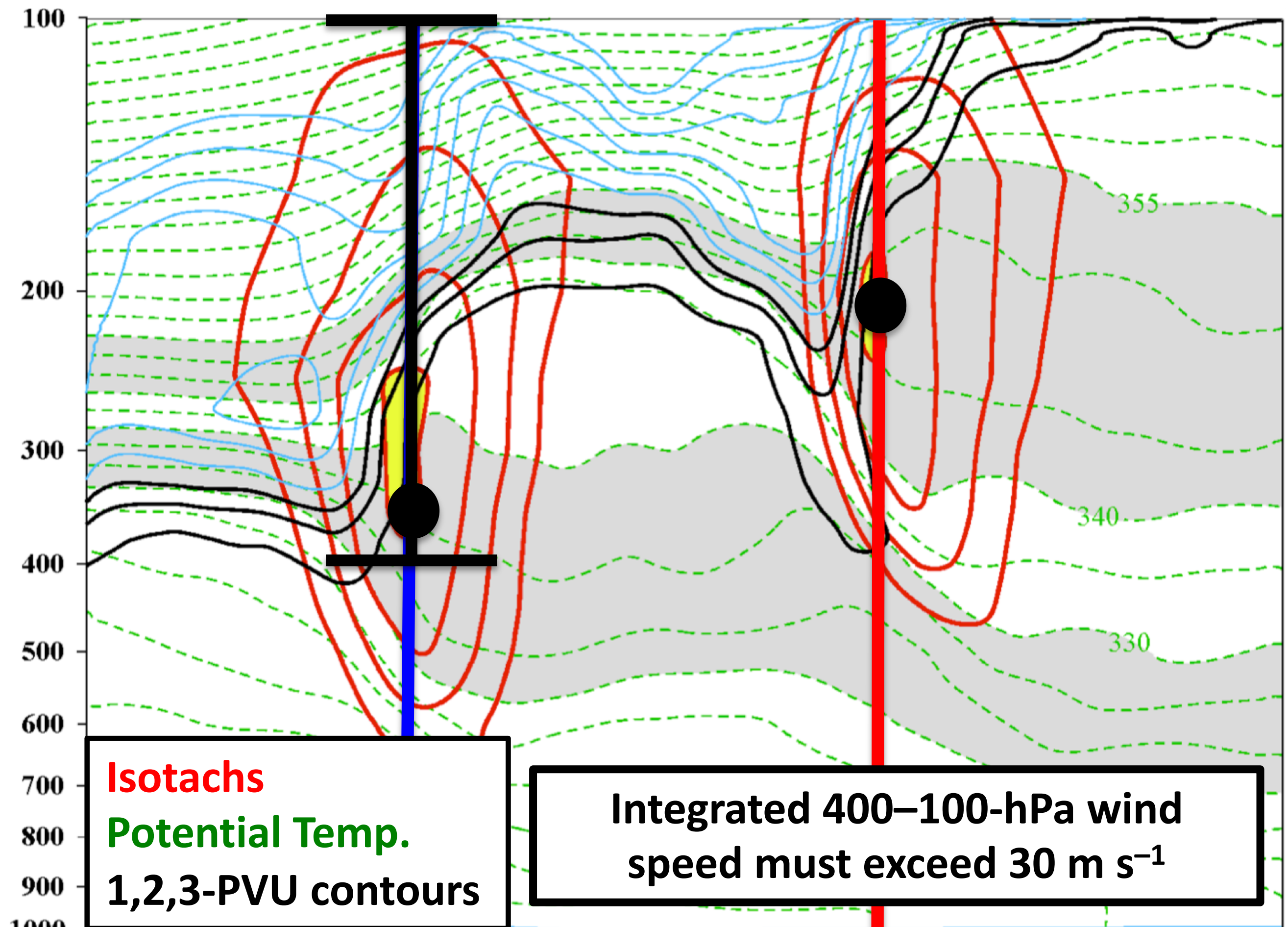

A Winters and Martin (2014, 2016, 2017); Christenson et al. (2017); Handlos and Martin (2016) A’

Jet Superposition Event Identification

0000 UTC 27 April 2010

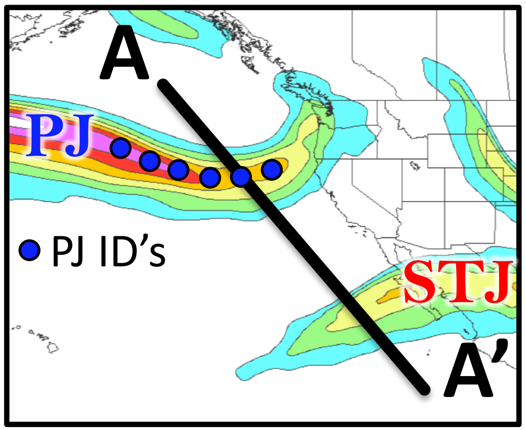

250-hPa wind speed

Isolated grid points over North America in the CFSR (Saha et al. 2014) characterized by polar and subtropical jets during Nov–Mar 1979–2010.

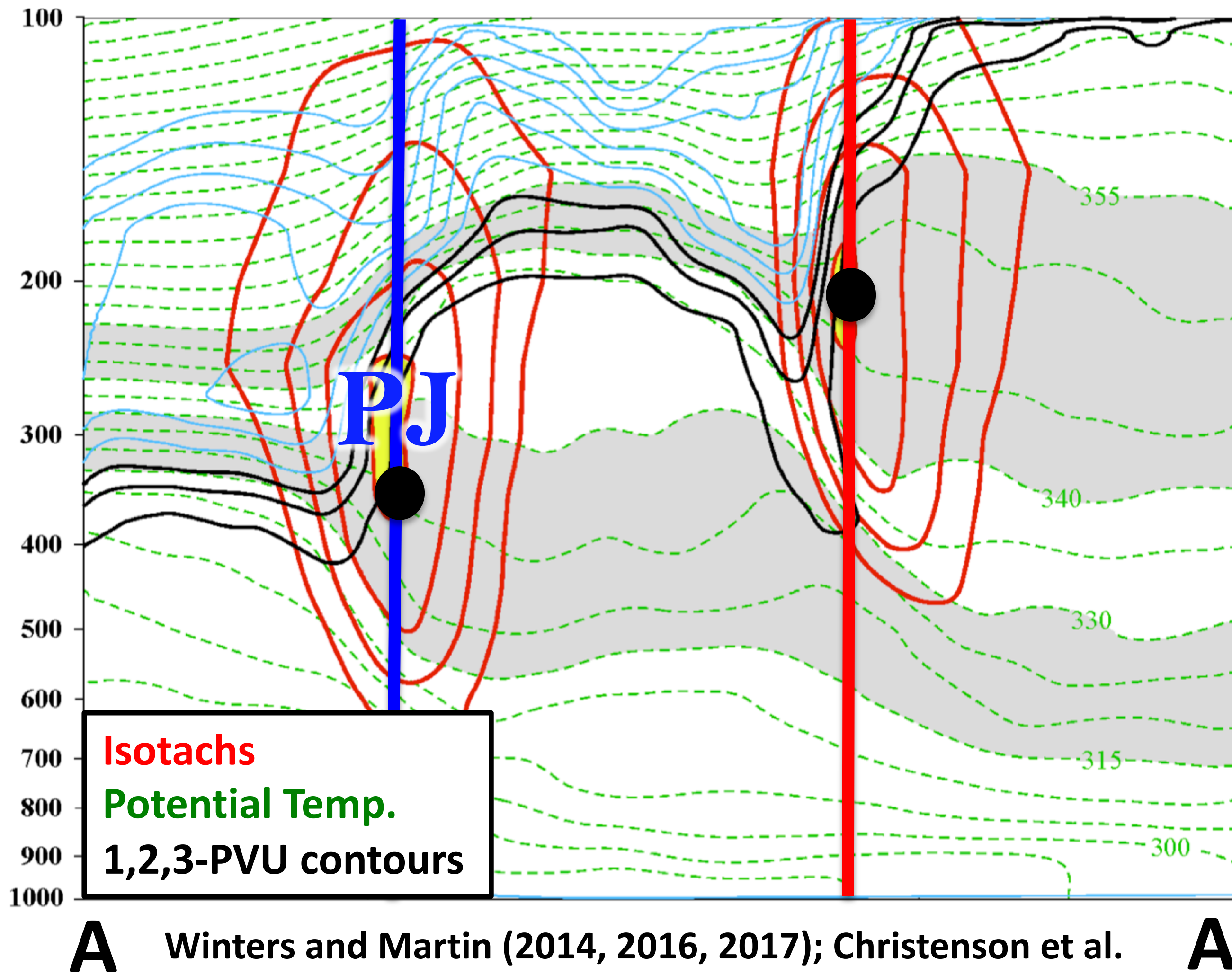

Winters and Martin (2014, 2016, 2017); Christenson et al. (2017); Handlos and Martin (2016)

Jet Superposition Event Identification

0000 UTC 27 April 2010

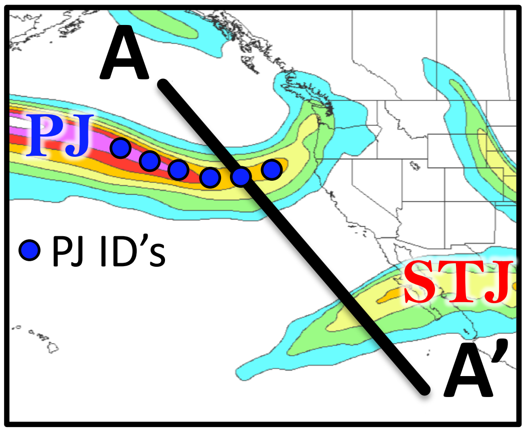

250-hPa wind speed

Isolated grid points over North America in the CFSR (Saha et al. 2014) characterized by polar and subtropical jets during Nov–Mar 1979–2010.

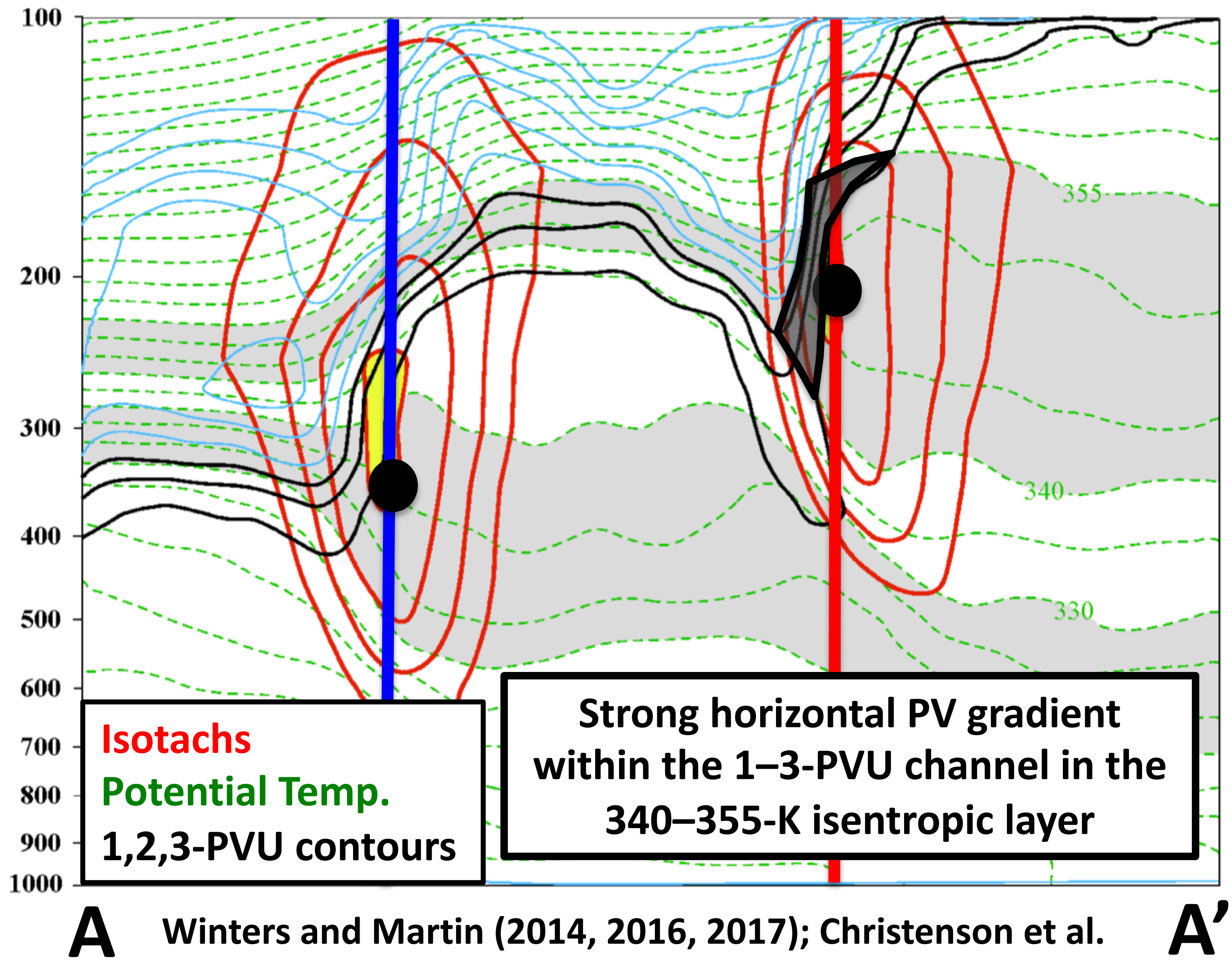

Winters and Martin (2014, 2016, 2017); Christenson et al. (2017); Handlos and Martin (2016)

Jet Superposition Event Identification

0000 UTC 27 April 2010

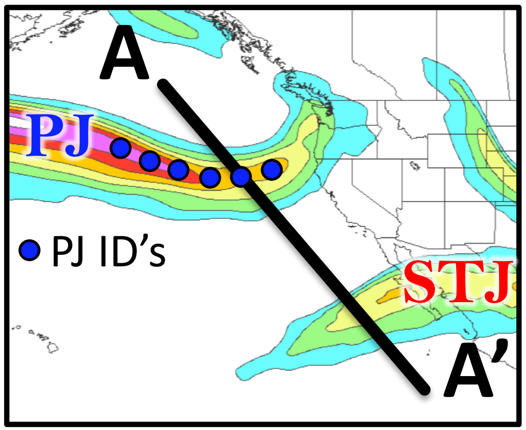

250-hPa wind speed

Isolated grid points over North America in the CFSR (Saha et al. 2014) characterized by polar and subtropical jets during Nov–Mar 1979–2010.

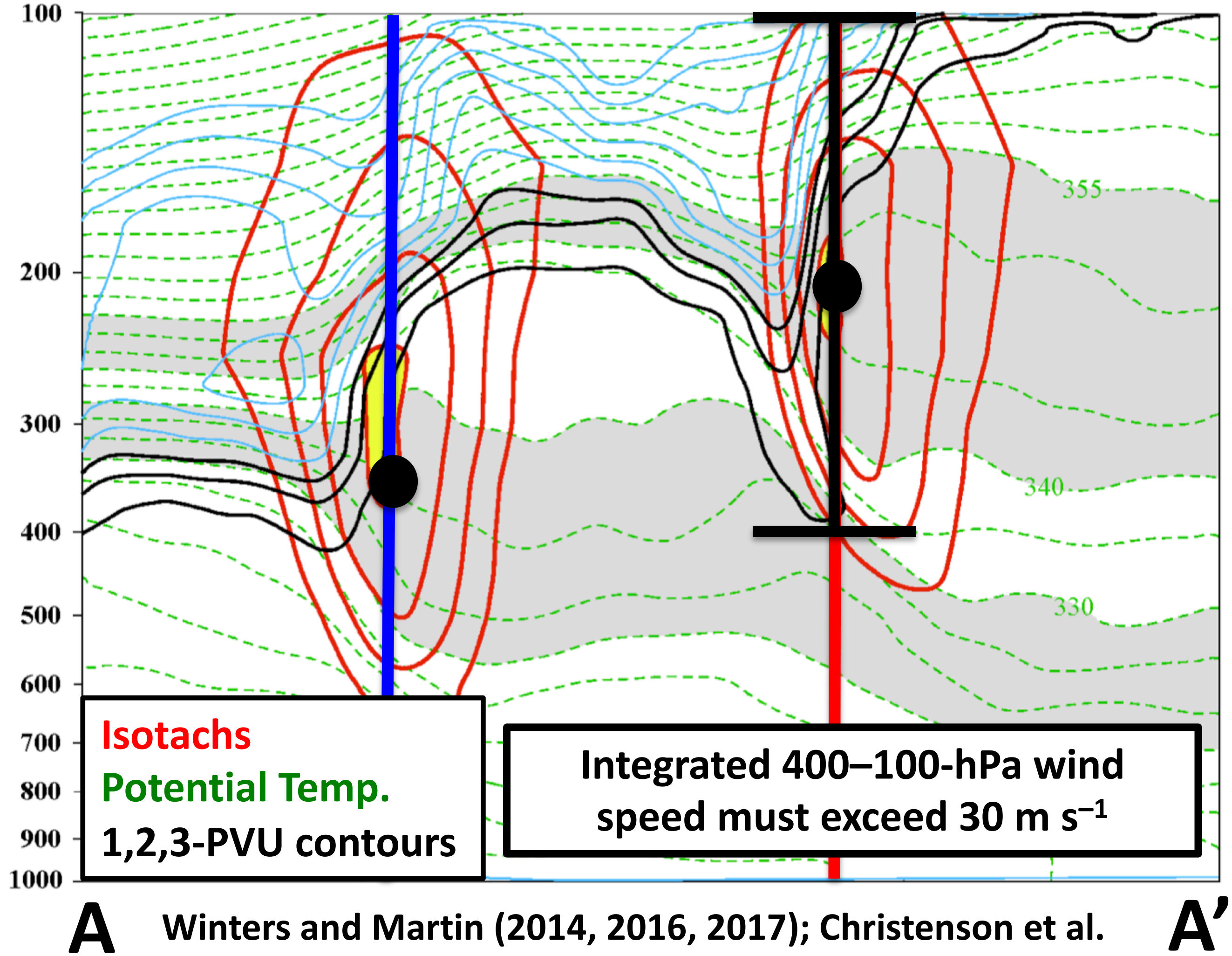

Winters and Martin (2014, 2016, 2017); Christenson et al. (2017); Handlos and Martin (2016)

Jet Superposition Event Identification

0000 UTC 27 April 2010

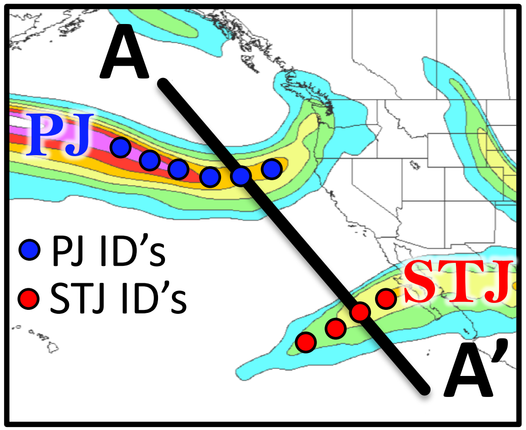

250-hPa wind speed

Isolated grid points over North America in the CFSR (Saha et al. 2014) characterized by polar and subtropical jets during Nov–Mar 1979–2010.

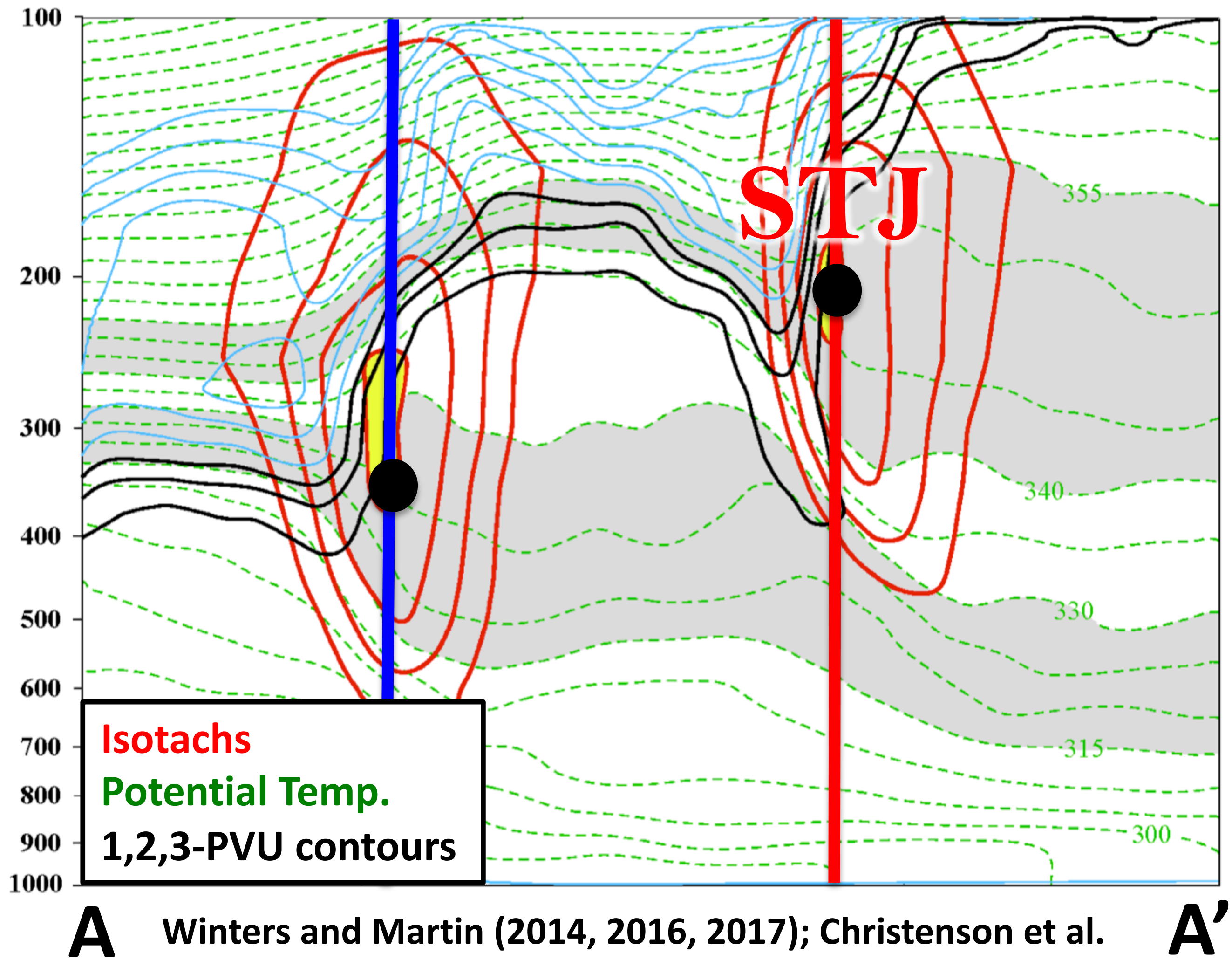

Winters and Martin (2014, 2016, 2017); Christenson et al. (2017); Handlos and Martin (2016)

Jet Superposition Event Identification

0000 UTC 24 October 2010

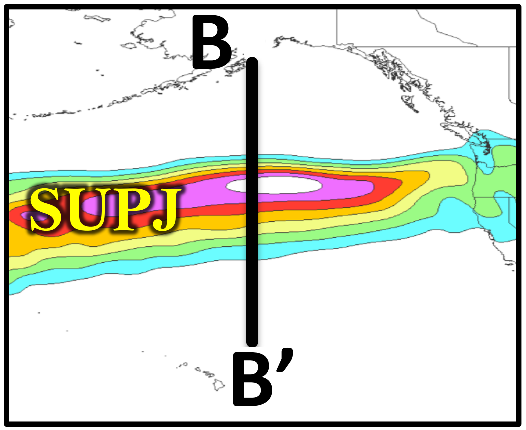

250-hPa wind speed

Isolated grid points over North America in the CFSR (Saha et al. 2014) characterized by a jet superposition during Nov–Mar 1979–2010.

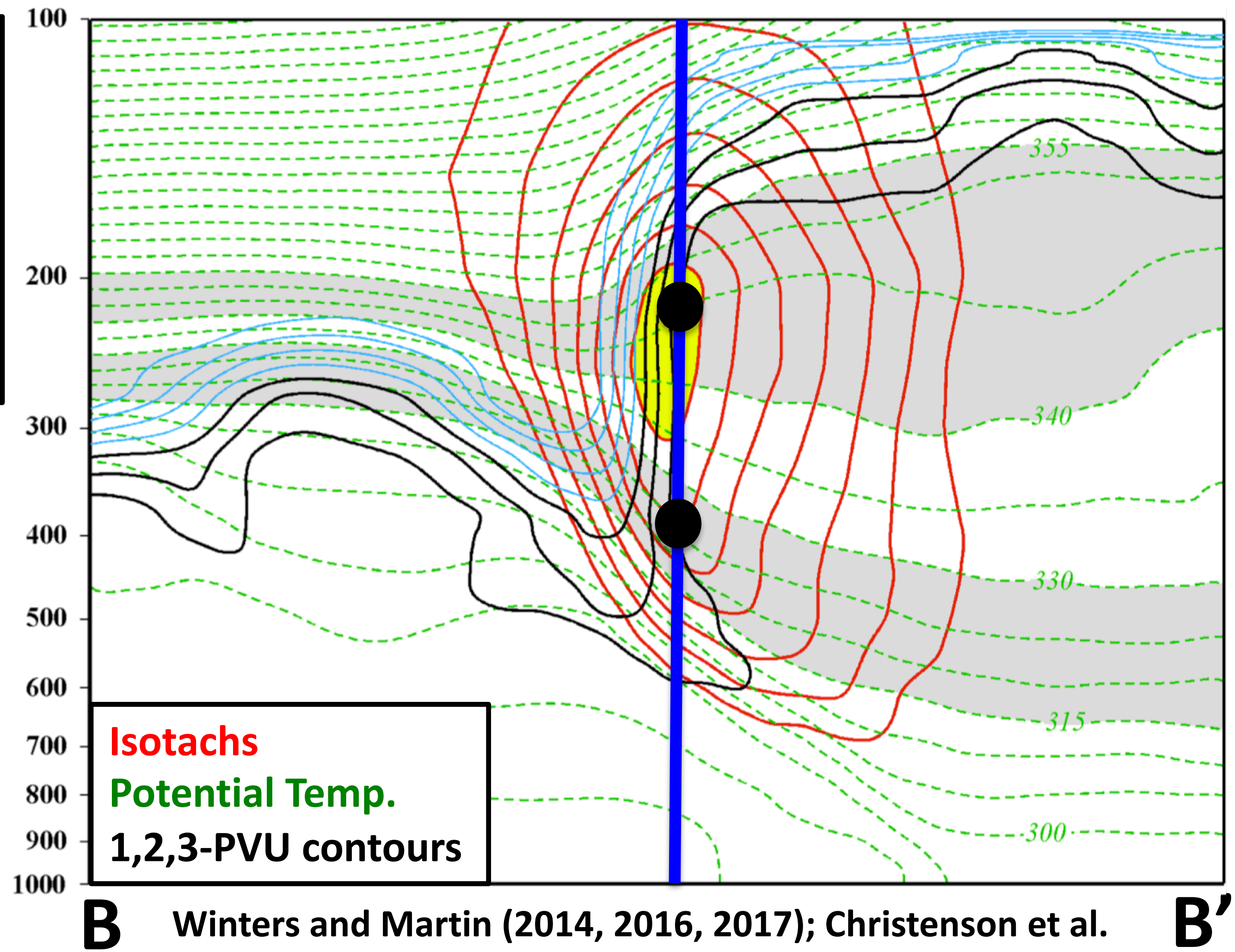

Winters and Martin (2014, 2016, 2017); Christenson et al. (2017); Handlos and Martin (2016)

Jet Superposition Event Identification

0000 UTC 24 October 2010

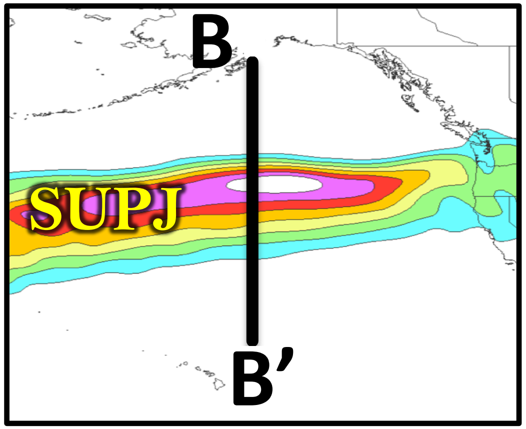

250-hPa wind speed

Isolated grid points over North America in the CFSR (Saha et al. 2014) characterized by a jet superposition during Nov–Mar 1979–2010.

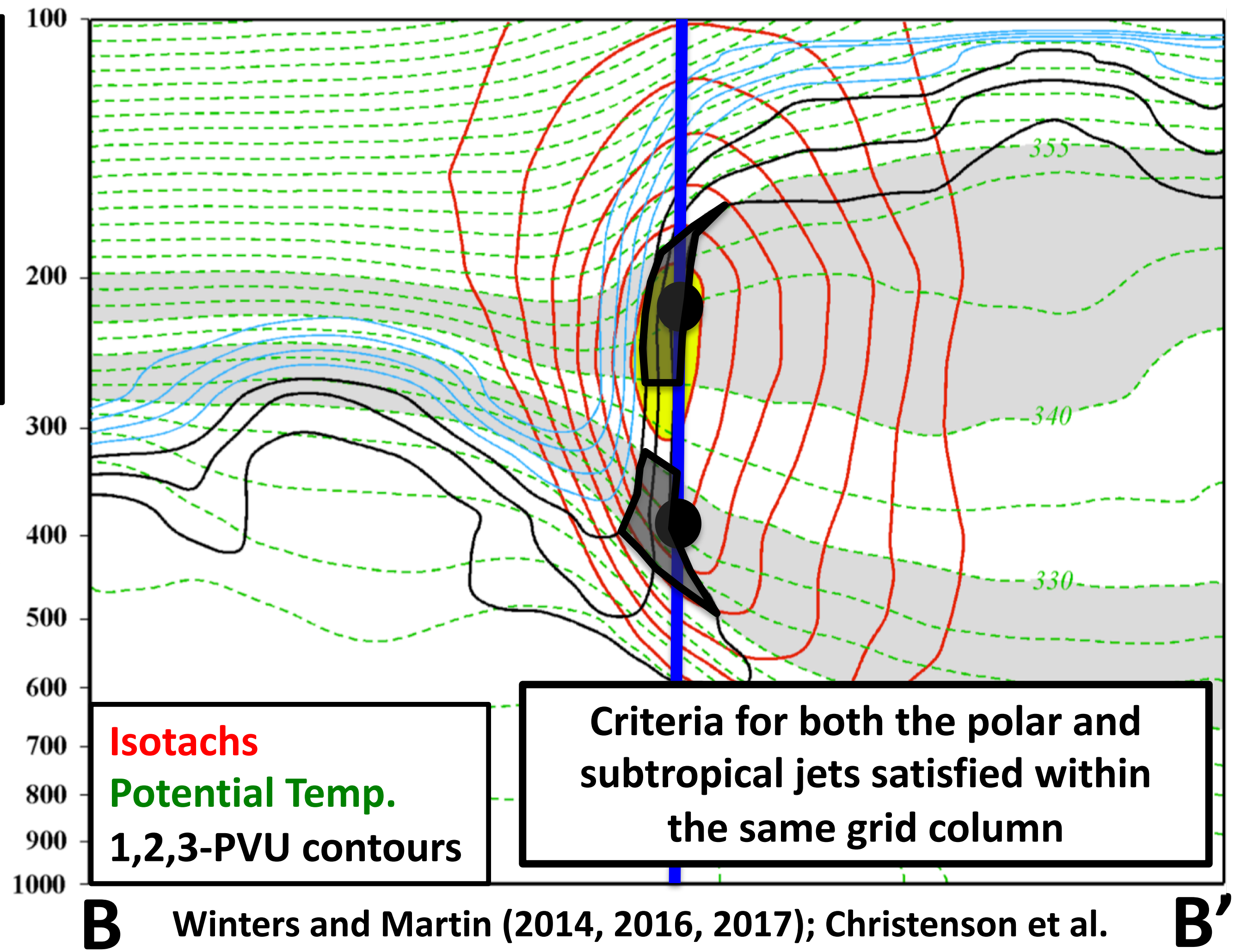

Winters and Martin (2014, 2016, 2017); Christenson et al. (2017); Handlos and Martin (2016)

Jet Superposition Event Identification

0000 UTC 24 October 2010

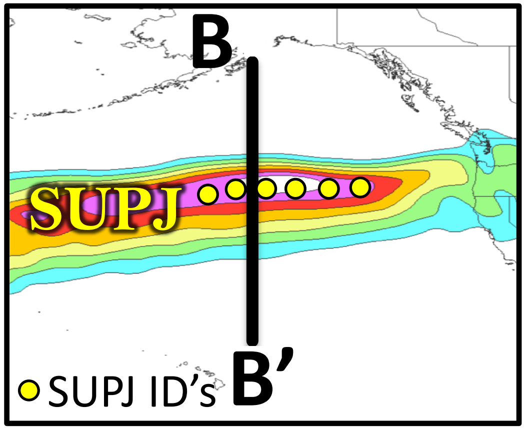

250-hPa wind speed

Isolated grid points over North America in the CFSR (Saha et al. 2014) characterized by a jet superposition during Nov–Mar 1979–2010.

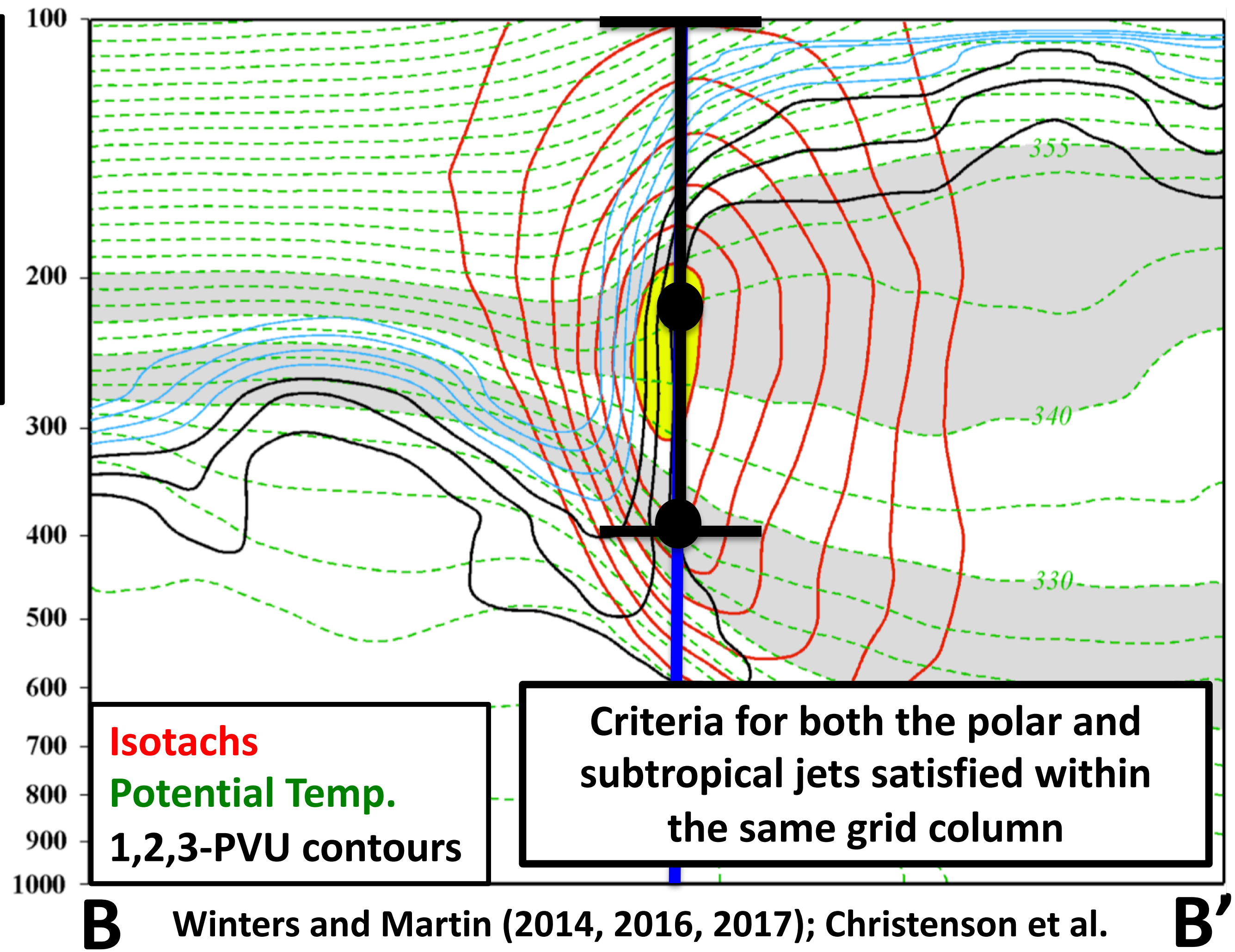

Winters and Martin (2014, 2016, 2017); Christenson et al. (2017); Handlos and Martin (2016)

Background

Christenson et al. (2017)

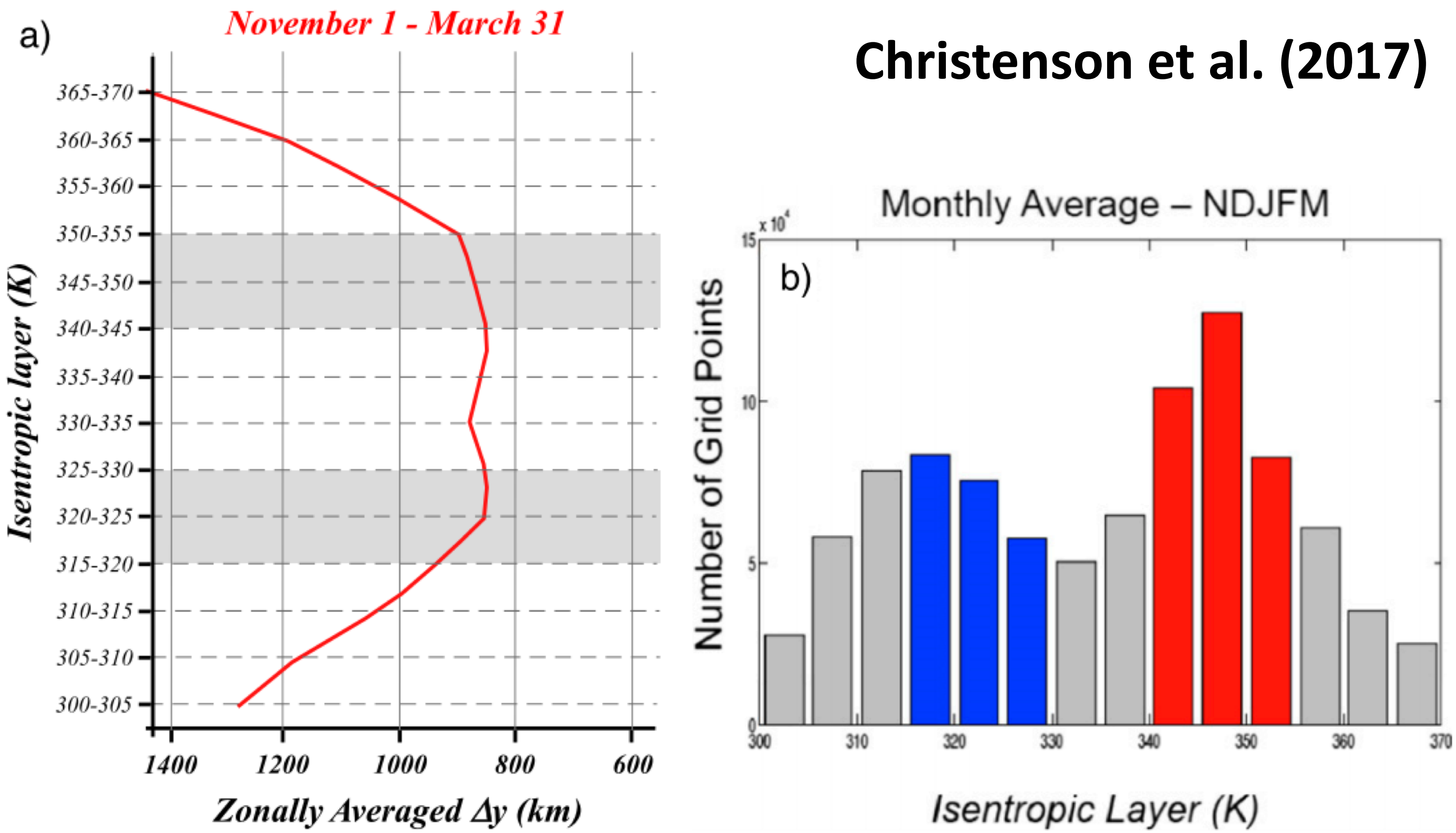

FIG. 2. (a) Cold season average of zonally averaged Δ*y* (km) for 5-K isentropic layers ranging from 300–305 to 365–370 K. The 315–330- and 340–355-K layers are highlighted in light gray shading. (b) The average frequency of occurrence of grid points with a maximum wind speed value within the 5-K isentropic layers along the abscissa per cold season. The 315–330- and 340–355-K layers are shaded in blue and red, respectively.

Jet Superposition Event Identification

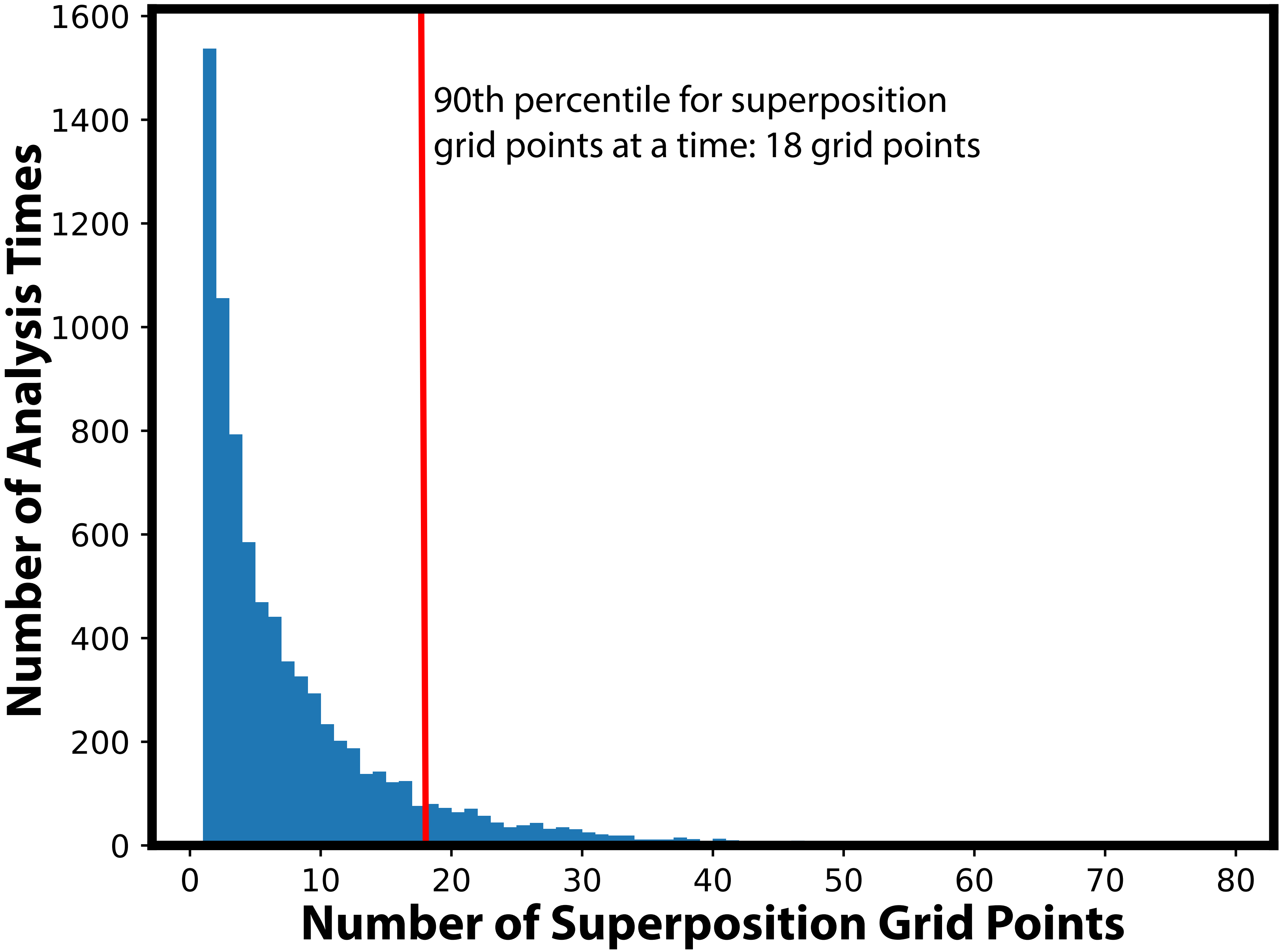

Jet Superposition Event Identification

Sample Jet Superposition Centroid Calculation

Calculated the centroid of each jet superposition based on all valid grid points at a particular analysis time.

To calculate the centroid, there must exist a group of 18 superposition grid points, of which no superposition grid point is >1000 km away from another superposition grid point.